ADHESIVE COMPLEX COACERVATE INSPIRED BY THE SANDCASTLE WORM AS A SEALANT FOR FETOSCOPIC DEFECTS

by

Sarbjit Kaur

A dissertation submitted to the faculty of
The University of Utah
in partial fulfillment of the requirements for the degree of

Doctor of Philosophy

Department of Materials Science and Engineering

The University of Utah

May 2015

The University of Utah Graduate School

STATEMENT OF DISSERTATION APPROVAL

The dissertation of **Sarbjit Kaur**

has been approved by the following supervisory committee members:

Russell J. Stewart	, Chair	**7/23/2014** Date Approved
Dinesh K. Shetty	, Member	**7/23/2014** Date Approved
Vladimir Hlady	, Member	**7/23/2014** Date Approved
Jules J. Magda	, Member	**7/23/2014** Date Approved
Dmitry Bedrov	, Member	**10/21/2014** Date Approved
Taylor Sparks	, Member	**10/15/2014** Date Approved

and by **Feng Liu**, Chair/Dean of

the Department/College/School of **Materials Science and Engineering**

and by David B. Kieda, Dean of The Graduate School.

ABSTRACT

Inspired by the Sandcastle Worm, biomimetic of the water-borne adhesive was developed by complex coacervation of the synthetic copolyelectrolytes, mimicking the chemistries of the worm glue. The developed underwater adhesive was designed for sealing fetal membranes after fetoscopic surgery in twin-to-twin transfusion syndrome (TTTS) and sealing neural tissue of a fetus in aminiotic sac for spina bifida condition.

Complex coacervate with increased bond strength was created by entrapping polyethylene glycol diacrylate (PEG-dA) monomer within the cross-linked coacervate network. Maximum shear bond strength of ~ 1.2 MPa on aluminum substrates was reached. The monomer-filled coacervate had complex flow behavior, thickening at low shear rates and then thinning suddenly with a 16-fold drop in viscosity at shear rates near 6 s^{-1}. The microscale structure of the complex coacervates resembled a three-dimensional porous network of interconnected tubules. This complex coacervate adhesive was used in vitro studies to mimic the uterine wall-fetal membrane interface using a water column with one end and sealed with human fetal membranes and poultry breast, and a defect was created with an 11 French trocar. The coacervate adhesive in conjunction with the multiphase adhesive was used to seal the defect. The sealant withstood an additional traction of 12 g for 30–60 minutes and turbulence of the water column without leakage of fluid or slippage. The adhesive is nontoxic when in direct contact with human fetal membranes in an organ culture setting.

A stable complex coacervate adhesive for long-term use in TTTS and spina bifida application was developed by methacrylating the copolyelectrolytes. The methacrylated coacervate was crosslinked chemically for TTTS and by photopolymerization for spina bifida. Tunable mechanical properties of the adhesive were achieved by varying the methacrylation of the polymers. Varying the amine to phosphate (A/P) ratio in the coacervate formation generated a range of viscosities. The chemically cured complex coacervate, with sodium (meta) periodate crosslinker, was tested in pig animal studies, showing promising results. The adhesive adhered to the fetal membrane tissue, with maximum strength of 473 ± 82 KPa on aluminum substrates. The elastic modulus increased with increasing methacrylation on both the polyphosphate and polyamine within the coacervate. Photopolymerized complex coacervate adhesive was photocured using Eosin-Y and treiethanolamine photoinitiators, using a green laser diode. Soft substrate bond strength increased with increasing PEG-dA concentration to a maximum of ~90 kPa. The crosslinked complex coacervate adhesives with PEG networks swelled less than 5% over 30 days in physiological conditions. The sterile glue was nontoxic, deliverable through a fine cannula, and stable over a long time period. Preliminary animal studies show a novel innovative method to seal fetal membrane defects in humans, *in utero*.

This dissertation is dedicated

to my Mother and sisters, Manpreet Kaur and Harjit Kaur,

and to all the Women who have inspired me to be here today.

TABLE OF CONTENTS

ACKNOWLEDGEMENTS

The research work of this dissertation was carried out with Dr. Russell J. Stewart with the Department of Biomedical Engineering from September 2009 to June 2014.

I want to give my hearty gratitude to my thesis advisor and committee chair Dr. Russell J. Stewart for his tremendous support and guidance throughout this process. He is an outstanding scientist and inspiring mentor. I am fortunate to have the opportunity to work with him on this project. He has continued to push me and has helped me grow academically and personally. I thank him for such significant research.

I want to thank our wonderful collaborators at the Texas Fetal Center, University of Texas Houston, Dr. Ramesha Papanna, Dr. Lovepreet K. Mann, and Dr. Kenneth J. Moise, for their kind support and companionship throughout this project. They have been gracious and hosted the animal studies that have been conducted. Thank you for expanding my scope of expertise and making such strong contributions to this work. I also would like to thank Dr. Robert H. Byrd, Dr. Edwina J. Popek, and Dr. Scheffer C. G. Tseng for contributing to the fetal studies.

Additionally I want to extend my gratitude to my committee members Dr. Vladimir Hlady, Dr. Dinesh Shetty, Dr. Taylor Sparks, Dr. Dmitry Bedrov, and Dr. Jules J. Magda for their guidance, support, and advice.

I would also like to thank my group members: Hui Shao, Ching-shun Wang, Mahika Weerasekare, Achille Mayelle Bivigou-Koumba, and Oscar V. Jasklowski. They have

helped me with every small question and provided support, advice, and emotional support and strength.

I would like to thank Dr. Raymond A. Cutler for being such an amazing mentor in my life. His firm belief in me and giving me the opportunity to do my first research project has helped me grow tremendously in the field of science. I have learned so much about doing research from him and am obliged and humbled by his work ethics. I am grateful for the knowledge he instilled in me, and it will guide me in the future.

Lastly, I want to thank my family and friends, without whom this all would not be possible, my parents, who have shown me that anything is achievable by working hard, my dear sisters Manpreet Kaur and Harjit Kaur, for always standing by my side through thick and thin and never giving up on me. They have helped me get back up after every failure and challenge that I faced throughout my life. My family has been the foundation to what I am today; without them I wouldn't be here. I want to thank my dear friends who have supported me and motivated me to get my PhD done. Thank you to all the inspirational friends and mentors who make me what I am today.

CHAPTER 1

INTRODUCTION

This chapter is an introduction to complex coacervate adhesives, inspired by the sandcastle worm, for the repair of fetal defects. The inspiration behind this work, the Sandcastle Worm, is thoroughly covered. The concepts that are key to this thesis are covered by explaining the complex coacervation. The formation of the synthetic underwater adhesive complex coacervate is discussed. The motivation behind this work comes from lack of adhesives to seal soft tissues, specifically for sealing defects in environments where adhesives have to be applied under aqueous conditions, like in utero. Research for this thesis is based on developing a synthetic complex coacervate adhesive for sealing fetal defects for two applications: Twin-Twin transfusion Syndrome and Spina Bifida, which represents a model for other fetal defect repair. An outline of this thesis is given at the end of this chapter.

1.1 Adhesives

Adhesives can be defined as materials that can join two surfaces together upon application and resist its separation [1]. Many terms like glue, cement, paste, etc., can be used interchangeably to define adhesives. Adhesion is a property often used to signify attraction between surfaces or particles. Adhesion forces itself to operate across the interface due to molecular van der Waals forces, dipole-dipole interactions, hydrogen

bonding, or covalent bonding [2]. The materials joined by the adhesive are known as substrates.

Adhesives have been around for centuries to glue materials together. One of the first adhesives dates back 200,000 years ago, using birch-bark-tar glue to fasten spear stone flake to a wooden shaft in Italy [3]. It is not until the last century, however, that the advances in adhesion and adhesives have been made. A major component playing a key role in these advances is the material developments of synthetic polymers in the 20th century. These materials have balance properties that allow them to adhere to other materials and transmit loads or forces between the two substrates [1]. Increasing demands in applications has spurred the research and development of specific adhesive formulations.

1.1.1 Soft Tissue Adhesives

An advance in adhesive technologies in all fields and applications has led to its use in medicine. Sutures and mechanical fixations were primarily used to bind tissue and bone together and still continue to be used in many areas today. Although a lot of progress has been made over the past decade in medicine, a suture is still the conventional method to close skin incisions. Alternative methods for soft tissue repair over the years have led to the development of soft tissue adhesives. Adhesives for tissue repair can replace sutures in many cases as well as limit their use. Gluing has many advantages because its fast and uncomplicated technique causes very little damage to the surrounding tissue [4]. A homogenous load is distributed between the bonding tissues. They are especially useful in applications where suturing is difficult, whether by location or the type of tissue that is being repaired. Using an adhesive also helps in sealing the

wound to prevent any leakage of fluid.

1.1.2 Underwater Adhesives

Since our body is mostly made up of water, maintaining adhesion underwater is a major challenge. A soft tissue adhesive must be able to bind the tissue together with adequate strength, be nontoxic, and maintain its integrity until wound healing occurs. Getting adequate strength for biological environments is a difficult task to accomplish for many bioadhesives. Synthetic adhesives used today are normally designed for dry applications and perform poorly in the presence of water [5]. They can have high strength to start out with but will eventually fail due to poor interfacial adhesion in watery environments [6–8]. Therefore, a good underwater adhesive must have robust interfacial adhesion to wet surfaces, without any surface preparation, while depositing the adhesive under water, with controlled solidification [5]. A suitable soft tissue adhesive must be able to overcome binding tissue surfaces in wet environments, maintain their strength over time, and be nontoxic.

1.2 Sandcastle Worm Inspired

We can learn a lot from Nature. We are inspired by our surroundings and adapt from them. There are many solutions we can derive to our modern day problems by observing natural phenomena. From a material scientist's perspective, a wide variety of materials with different functions serve as a source of inspiration [9]. Taking these materials from observation to in-depth analysis leads to bioinspired materials.

To tackle the underwater adhesion problem, marine organisms (like mussels, barnacles, and sandcastle worms) are being studied. These organisms secrete a liquid

protein adhesive, which adheres to all types of wet surfaces, whether organic or inorganic [10]. Intrigued by these natural organisms, scientists have developed biomimetic underwater adhesives for strong adhesion to biological tissue [11–13]

The sandcastle worm (*Phragmatopoma Californica*, *P-Cal*) is important to our research. This organism is unique in that it is able to bind dissimilar materials together under seawater in a single step without much surface preparation, with a self-contained mechanism to trigger a setting reaction, building a protective shell that it lives in [14]. The adhesive is secreted as a colloidal suspension with very low interfacial tension, which allows it to spread easily over the substrate while remaining very cohesive and not dispersing into the ocean [13]. Despite all the turbulent forces, temperature changes, and fluctuating salinities taking place in the ocean, the tubular structure that the worm builds does not fall apart [15]. The sandcastle worm cement represents the simplest permanent bioadhesive investigated to date [16]. Compared to mussels and barnacles, which directly attach themselves to the substrates, the sandcastle worm is mobile within the tube that it builds. Over the years these organisms have evolved workable materials solutions. By gaining knowledge and understanding of these natural phenomena, we are able to design and synthesize adhesives in wet environments [17]. Based on the basic chemistry of the natural worm glue, our synthetic complex coacervate adhesive is made.

1.2.1 Sandcastle Worm (*Phragmatopoma Californica*)

Phragmatopoma Californica (P. *californica*) is a marine polychaete that belongs to the family of sabellariids. P. *californica* (also called the sandcastle worm) lives along the coast of California. The sabellariids (known as tube-dwelling polychaetes) build massive reef-like mounds, consisting of tubes held together in honeycomb like

arrangements (Figure 1.1A and 1.1B). These tubular homes that the worm lives in almost resemble large-stone masonry [18].

Sabellariids are different than other shell-dwelling marines, such that that they gather mineral phases from the ocean and secrete a proteinaceous glue to bind the sand particles together [20], rather than making a complete mineralized shell [21]. The sandcastle worm has ciliated tentacles (Figure 1.1 C) that capture and transport food and particles from the ocean to its mouth [22]. They collect passing materials like sand grains, calcareous shells, or debris from water to bind. The food is ingested through the mouth, and the particles are evaluated for the right size, shape, composition, and surface chemistry at the building organ near the mouth. The unsuitable particles are cast away, and the suitable particles are pressed onto the existing tube in the best position to minimize any gaps in the structure [19]. Particles at the point of contact are spotted with glue and pressed into place. The worm wriggles the particle until the glue sets, taking approximately 20–30 sec [23]. Each worm builds the tube that it lives in for physical protection. A large colony of reef like structures is built by a coordinated effort, which affects the reef ecology [24]. The exact strength of these tubular structures is difficult to assess, but their location in these turbulent environments and the durability of the structure suggest a robust construction [13].

1.2.2 Sandcastle Worm Adhesive Structure

The sandcastle worm sets into a flexible leathery material with a structure of solidified foam, as shown in Figure 1.2 [20]. In the laboratory, the worm is given glass beads, which it uses to build a glass bead tube (Figure 1.2A). Its structure was analyzed using laser scanning confocal and atomic force microscopies. A porosity gradient was

(A) Photo courtesy of Dr. Jérôme Fournier.

Figure 1.1 Reef-building sabellariid tubeworms. A) Lateral growth of isolated dome-shaped colonies of S. alveolota (foreground) leads to fusion of colonies into a continuous tabular surface covering the beach. B) Closer view of a colony of P. *californica.* Each tube contains an individual worm. C) Left: P. *californica* removed from tubular shell. White bracket indicates parathorax region that contains the adhesive gland. Right: Zirconium oxide beads have been glued onto the anterior end of the natural tube. Arrow indicates the operculum [19]. Reprinted with permission from C. S. Wang, and R. J. Stewart, "Multipart Copolyelectrolyte Adhesive of the Sandcastle Worm, Phragmatopoma Californica (Fewkes): Catechol Oxidase Catalyzed Curing Through Peptidyl-DOPA," *Biomac.*, **14** [5] 1607–1617 (2013). Copyright 2013 American Chemical Society.

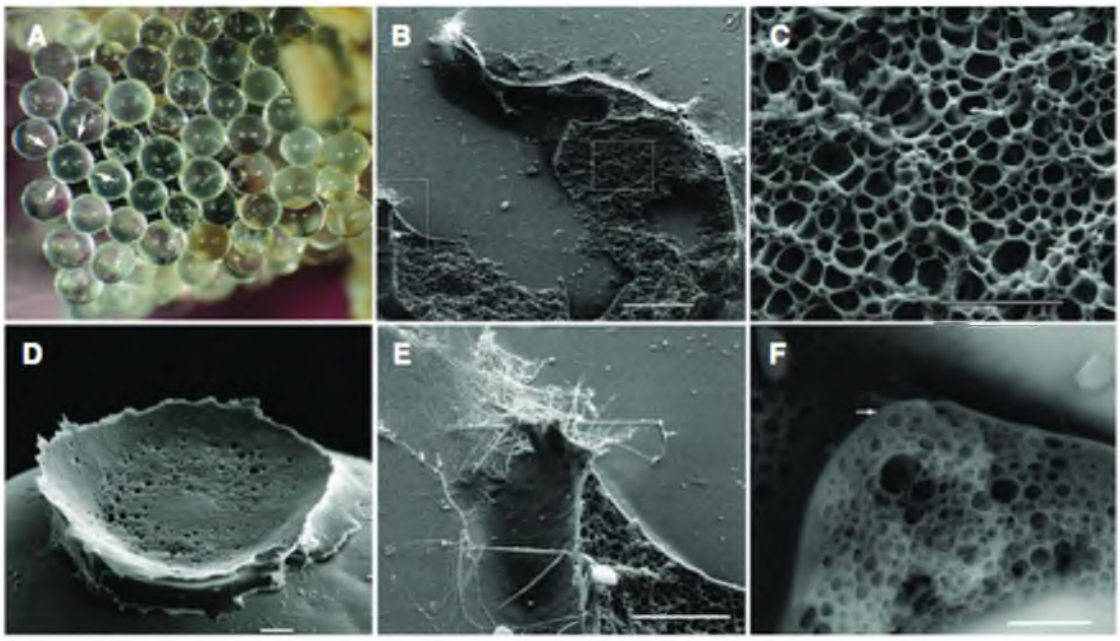

Figure 1.2 SEM of sandcastle adhesive. A) A tube of partially rebuilt with glass beads. The glue was applied only at four contact points (arrows); B) Sandcastle worms placed on coverslips glue glass beads to the surface. The glue fractured when the bead was pried away; C) The foamy interior in the right box in B; D) A spot of glue left on a glass bead, indicating liquid until set; E) Threads and nonporous skin layer on glue; F) Foamy interior imaged with backscattered electron detector. Distinct layers on the surface (arrow) and linking the pores are visible. Scale bar in (B and D) 50 μm; (C and E) 15 μm; F) 5 μm [26]. Springer, New York, and Biological Adhesive Systems, Editors J. V. Byern, I. Grunwalds, 2010, Morphology of the Adhesive System in the Sandcastle Worm, Phragmatopoma Californica, S. Wang, K. K. Svendsen, and R. J. Stewart, is given to the publication in which the material was originally published, by adding; with kind permission from Springer Science and Buisness Media.

observed with hardly any porosity on both the outside of the glue and the solid foam within the internal structure (Figure 1.2 B, C, D, E, & F). Showing 50% porosity down the center of the adhesive joint [23]. This was similar to the structure of the byssall adhesive plaques of the mussels. The foamy structure of the adhesive is very advantageous because it increases the adhesives elasticity and toughness (amount of energy that a material can absorb before failing) [25]. A foam packing material is more flexible and absorbs the dissipated energy, which decreases the amount of damage in the tube. The porous material saves the amount of adhesive used to glue the particles. The foam also serves as a cushion between the mismatched modulus of the rigid particles, linking the flexible cement that is key for binding various substrates [17]. These key properties play a big role in strengthening the joint by absorbing and dissipating strain energies. This gives the water-borne adhesive of the sandcastle worm a multiscale energy absorbing system that helps the worm deal with the turbulent environment of the ocean.

1.2.3 Sandcastle Worm Adhesive Composition

The composition of P. *californica* adhesive is known to be a proteinaceous, enriched with amino acids consisting of serine, glycine, lysine, and large amounts of 2,4-dihydroxyphenyl-L-alanine (DOPA) [18, 20, 27]. It is very similar in composition to the byssal adhesive of mussels [28–29], but much less complex. An amino acid and elemental analysis of the adhesive resulted in a mixture of three highly polar proteins Pc1, Pc2, and Pc3 with significant amounts of Ca^{2+} and Mg^{2+} [16, 18, 20]. Pc1 and Pc2 are positively charged proteins that are basic with pI > 9. The Pc1 protein consists of three residues, glycine (45 mol%), lysine (14 mol%), and tyrosine (19 mol%), and is highly repetitive and simple. The Pc2 is mostly histidine rich with lysine. Pc3 protein

exists in two variants (A, B) containing 4–13 serine residues with a single tyrosine residue. Because 95% of the serines in Pc3 are being phosphorylated, it is highly acidic, pI 0.5–1.5 [20]. This results in positively and negatively charged amino acids, with 30% phosphate sidechains and 10–20% amine sidechains in the worm's glue, as shown in Figure 1.3. Magnesium and calcium were other major components in the glue, with 4–5 times Mg to Ca and total cations to phosphate being a 1500 ppm ratio.

1.2.4 Sandcastle Worm Adhesive Curing

Many mechanisms come to play to solidify the worm glue. The glue initially sets in 30 sec followed by a covalent crosslinking that takes up to hours. First the initial set of the glue seems to be triggered by a pH change, from pH <6 inside the sandcastle worm, to pH > 8 when released into the seawater. The insolubility of polyphosphate and divalent cations Mg^{2+}/Ca^{2+} in seawater seem to suggest a pH triggering mechanism for the initial set [30].

The high amount of DOPA in the adhesive indicates that it readily undergoes oxidative covalent crosslinking. DOPA is known to be an adhesion promoter and facilitates solidification through di-DOPA, crosslinking in the byssal plaques of mussels [12]. The oxidation of DOPA occurs in alkaline sea water, giving rise to quinones that react further to crosslink adhesives proteins via aryl-aryl coupling (di-dopa formation) or possibly via Michael-type addition reaction with amine-containing protein residues [31–34]. This is also apparent when glue changes color, going from a whitish/clear appearance to a brownish coloring over time. DOPA is stable at pH 5 and converts to o-quinone at the pH approaches the pK_a (9.4).

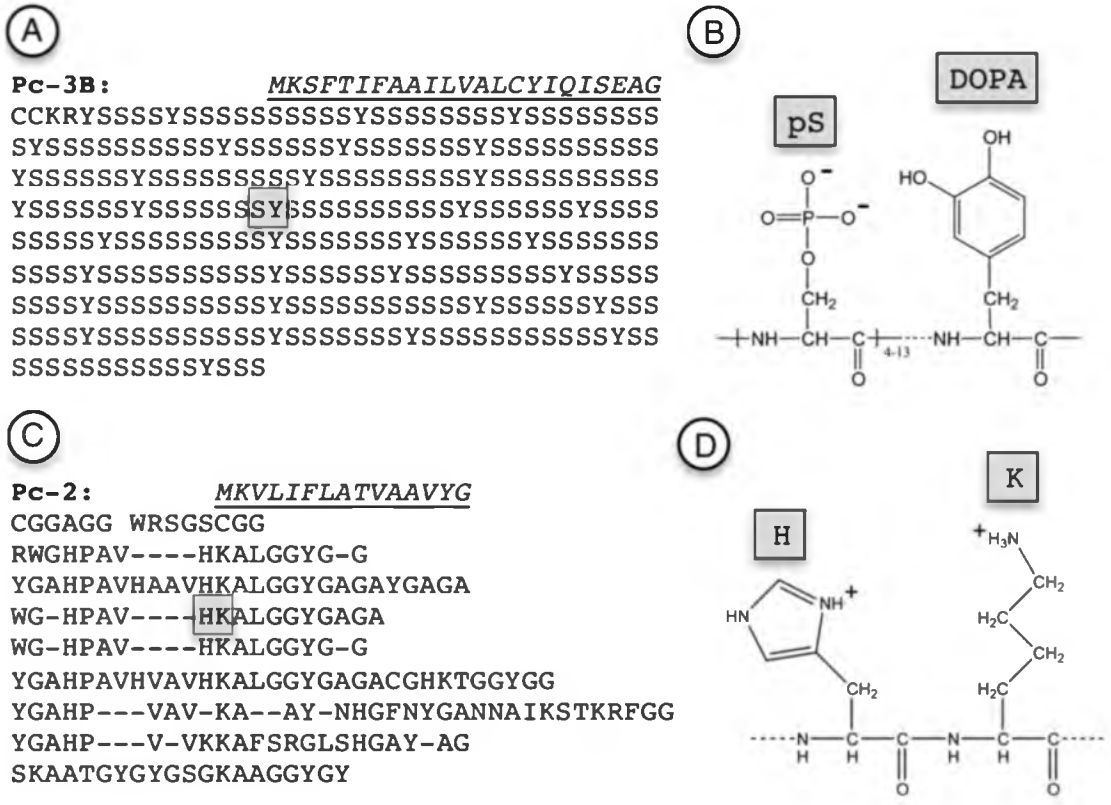

Figure 1.3 Representative glue protein sequences. A) Sequence of polyacidic Pc3B. B) The serine residues (S) are more than 95% phosphorylated on the hydroxyl sidechain. The tyrosines (Y) are hydroxylated into DOPA residues. C) Sequence of polybasic Pc2. D) Structure of histidine (H) and lysine (K) residues with amine sidechains.

1.3 Biomimetic Complex Coacervate Adhesive

1.3.1 Sandcastle Worm Adhesive Complex Coacervate Model

The compositions of the sandcastle worm adhesive, proteins consisting of oppositely charged polyelectrolytes at physiological pH, indicate a model based on complex coacervates [20]. This model explains the foamy structure, fluid character, low interfacial tension, and cohesive properties of the water-borne underwater adhesive of the sandcastle worm [20].

1.3.2 Complex Coacervate

In a colloidal system, separation of a liquid into two phases is called Coacervation [35]. The denser phase in the colloid is called the coacervate, while the other phase is the equilibrium solution. In the aqueous solution of two polymers, phase separation can occur if there is an electrostatic attraction. A complex coacervate is formed when coacervation occurs due to two oppositely charged colloids [36] (Figure 1.4). They could be positively and negatively charged macroions, such as polyelectrolytes, with balanced charges. The two phases coexist and are immiscible in solution. The coacervate phase, or the polymer-rich phase, is an isotropic liquid that contains amorphous particles that move relatively freely to each other. The second phase, known as the supernatant, is a very diluted phase. The two macroions are surrounded by a double layer, a region with increased concentration of counterions, with lower energy (the average distance between positive and negative charges is smaller than that between positives or between negatives), and low entropy (small ions have less translational freedom) [37]. When the two macroions mix, the double layer is destroyed and counterions are released in the form of salt, which shows that both the enthalpy and entropy of the system changes, thus driving the

A) B)

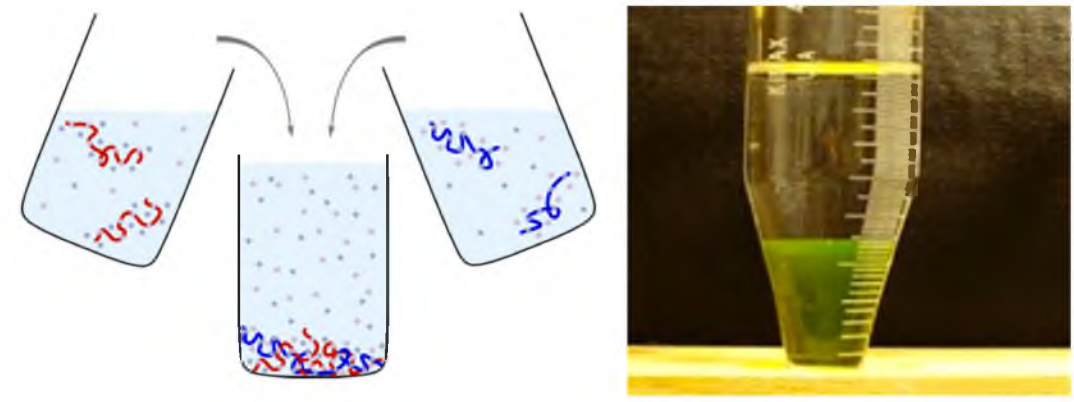

Figure 1.4 Complex Coacervate Formation. A) Mixing solution of polycation and polyanions can lead to associative phase separation and formation of complex coacervate [37]. B) Coacervate/supernatant after centrifugation of coacervate system: BSA-F (bovine serum albumin) + Poly(diallyldimethylammonium chloride), at pH 9.5 and I = 0.1 M NaCl [38].

coacervation [37].

Tiebackx [39] was the first to notice the coacervation phenomena in 1911. But it was Bungenberg de Jong [40] and Kruyt [41] who first systematically studied it on a gum arabic-gelatin coacervate, and named it complex coacervate. There are many theories and models, like Voorn-Overbeek theory [42–45] (gelatin/acacia coacervate), Veis-Aranyi "dilute phase aggregate model" [45] (albumin/gelatin coacervate), Nakajima-Sato Model [46], and Tainaka model [47–48], which have tried to explain the coacervate process. Burgess tried to compare and resolve a lot of contradictions that exist in coacervates [49]. The complex coacervate formation is dependent on molecular weights, concentrations, and ratio of two interacting polyions and on the ionic strength, pH, and temperature of the media [49]. All of the theories agree on the suppression of coacervation at high ionic strength. The random coil configuration of both polyions plays an important role. The Voorn-Overbeek theory studied the gelatin/acacia coacervates and explained that the electrical attractive forces tend to accumulate on charged polyions and the entropy effects tend to disperse these forces. The bundles of oppositely charged polyelectrolytes associate together due to these electrostatic forces to form a coacervate. The loops between polymers entrap water in the coacervate, which gives rise to entropy, which allows the number of possible macromolecule arrangements to occur. According to Voorn and Overbeek a random coil of the polyions is necessary, if the polymers were completely folded, no water could be entrapped, and coacervation would be unlikely. The distributive nature of electrostatic interaction allows for overall electrical neutrality in the coacervate, yet the molecules are free to move around in the liquid phase [49]. The Veis-Aranyi model considers coacervates a two-step process rather than a spontaneous

process. They explain upon mixing of oppositely charged polyions, aggregates of low configurational entropy form, in which "coacervate sols" rearrange to form the coacervate phase [49]. This rearrangement can take from hours to days and is driven by gain in configurational entropy upon the formation of randomly mixed concentrations of coacervate phase and dilution of aggregate phase.

Despite the contradictions all these theories could agree to the following about complex coacervates: complexes began to form before the phase separation occurs, even if there is an excess of one polyelectrolyte, the complex are only modestly charged, salt has a dissociating effect on the complexes, salt concentration is equal in the coacervate and supernatant phase, and in coacervate there is clear mobility of both polymers. By one polyelectrolyte carrying a positive and one carrying a negative charge restricts the complex coacervate formation occurring at a finite pH range. The coacervation phenomena are entropically driven. The coacervate and supernatant phases must be neutral or near neutrality, where this neutral complexes resembling gas-liquid separation in colloids. [50–51]

There are many reasons that contribute to the stability of complex coacervates. The coulomb attraction (ion pairing) and the entropy increase due to counterion release are major driving forces for the formation, which includes hydrophobic effect, hydrogen bonding, and hydration forces [52]. Coacervates have low interfacial tension in water (~ 0.0005 dynes/cm) and exhibit ~ 0° contact angles [41]. The interfacial tension is important and is directly related to interaction between the macroions. In comlex coacervate core micelles the interfacial tension drives the formation of micelles and can be used to predict the critical aggregation concentration [53]. The interfacial tension is

very sensitive to the added salt [54].

There are many examples and applications that the complex coacervates exist in, in nature as well as industry. DNA is packed into small volume of DNA-binding proteins, in both eukaryotic and prokaryotic cells. This DNA compaction is largely due to the electrostatic attraction between oppositely charged macroions [55]. This phase separation can also occur in polyelectrolytes and oppositely charged colloids like micelles [56], proteins [57], and dendrimers [58]. In industry, coacervates have found applications in protein purification [59], drug and enzyme immobilization [60], cosmetic formulations [61], pharmaceutical microencapsulation [62], and in trapping organic plumes [63–64].

The Pc1, Pc2, and Pc3 proteins of the sandcastle worm are water-soluble polyelectrolytes. If the worm secretes them sequentially, it would be risky to loose them by dilution into the surrounding seawater [20]. That is why the complex coacervate method was proposed as a model for the worm. Coacervates can absorb the water from wet surfaces, and with their low interfacial tension they tend to spread easily over wet surfaces [65].

1.3.3 Synthetic Analog: Complex Coacervate Adhesive

Inspired by the sandcastle worm a synthetic analog to the underwater adhesive is made. The P. *californica* adhesive is of particular interest to us because of its ability to bond to wet surfaces, versatility in bonding to various particle substrates, and its effectiveness at low mortar-to-filler weight ratios [66–67]. This water-borne glue is able to displace surface bound water from the substrates, which is a big insight into its strong interfacial adhesion properties [13]. Its ability to hold together a robust shell capable of holding strong high-energy environments makes it an intriguing model for biomimetic

adhesive [13].

The synthetic adhesive was formed by the method of complex coacervation of glue protein analogs of the sandcastle worm [13–14]. The oppositely charged Pc3 and Pc1 protein analog polymers were made, containing the phosphate and amine sidechains, using a similar ratio to that found in the worm (Figure 1.5). These proteins were easily copied with poly(meth)acrylates. The copolymers were water-soluble, inexpensive, and scalable. The Pc3B polymethacrylate also contained the catechol, as shown in Figure 1.5. When mixed under the set conditions, the aqueous polymer solutions condensed into a complex coacervate at neutral pH [13]. The complex coacervate adhesive was chemically crosslinked through the oxidation of DOPA by $NaIO_4$ to convert the catechol to dopaquinone [68].

This biomimetic complex coacervate adhesive was designed for gluing bone together. Our lab group was able to show that using the synthetic complex coacervate adhesive attained 40% strength of commercially available cyanoacrylate glue [13]. This water-borne adhesive has an advantage over other commercially available adhesives; our adhesive can be injectable under water and adheres to wet surfaces, whereas all glues fail under water eventually.

1.3.4 Multipart Copolyelectrolyte Model Sandcastle Worm Adhesive

Recent work on the sandcastle worm shows that complex coacervation may not be playing a role in the natural adhesive formation [19]. It would be difficult for the worm to preform and premix the complex coacervate before secretion. The worm glue, instead, is a multipart polyelectrolyte adhesive. The oppositely charged proteins are packaged separately in highly concentrated granules, which are mixed as they leave the building

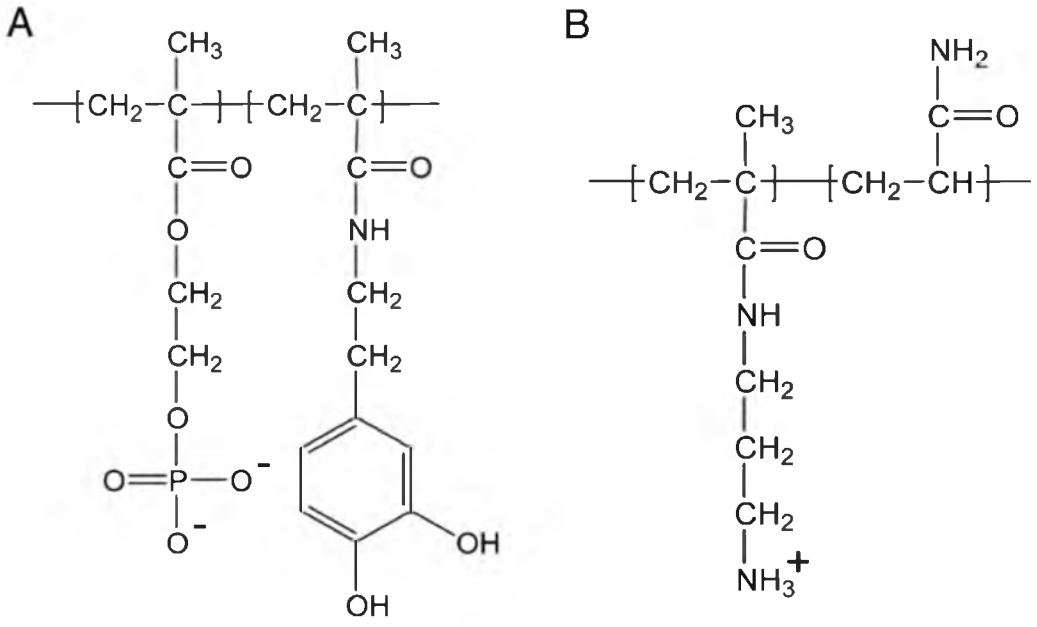

Figure 1.5 Synthetic analogs of glue proteins. A) of the Pc3B polymethacrylate analog copolymer. B) Structure of the polyamine analog copolymer. The analog polymers are random copolymers synthesized by free radical polymerization [30]. Reprinted from Advances in Colloid and Interface Science, 167 (1-2), R. J. Stewart, C. S. Wang, and H. Shao, Complex Coacervates as a Foundation for Synthetic Underwater Adhesives, 85–93, Copyright 2011, with permission from Elsevier.

organ and have a "burst" release effect once in contact with seawater. Homogeneous granules contain sulfated macromolecules and Pc2/Pc5 protein. The heterogeneous granules contain Pc3A and Pc3B proteins along with divalent cations, Pc1 and Pc4, with both granules containing DOPA. Once they leave the building organ, the proteins form solid foam and fully set within 30 sec. The sandcastle worm would not have enough time to form a complex coacervate it is more a multipart copolyelectrolytes.

1.4 Fetal Defects

The water-borne synthetic complex coacervate adhesive can be used in many fields of medicine. Adhering or binding soft tissues in wet environments is a major challenge. Most soft tissue adhesives are designed for dry applications that ultimately fail under water due to fluid in the joints. Applying the adhesive on wet surfaces and controlling its solidification is difficult. One such field where advanced soft tissue adhesive could be used in is gluing fetal tissue, *in utero*.

1.4.1 The Need for Fetal Tissue Adhesives

Increased use of ultrasound scanning since the 1980s has led to the early detection of fetal defects. Advanced medical diagnostic techniques are able to detect congenital malformations earlier in pregnancy. Early detection has given rise to a large number of treatments and interventions. Fetal surgery is one of those promising therapeutic options for number of congenital malformations [69], where the field has grown from a concept to a medical subspecialty today [70]. In the past 2 decades advances have been made in fetal surgical interventions and fetal therapy by nonoperative means [69]. Fetal imaging, diagnosis, and anesthesia have allowed fetal interventions to be a vital tool for patients

who would otherwise face morbidity and mortality [70]. This makes minimal access fetal surgery possible where the fetal condition determines the invasiveness of the surgery. This is possible with laparoscopic surgery and fetoscopy.

Fetal surgery, although very successful in a growing number of malformations, is limited in treatment due to conditions like preterm labor, chorionamniontic membrane separation, altered fetal homeostasis, and iatrogenic preterm premature rupture of the fetal membranes (iPPROM) [71]. Even in invasive procedure like fetoscopy, iPPROM is a big complication, resulting in amniotic fluid leakage. Fetoscopy is an endoscopic procedure during pregnancy that gives access to the fetus. Once the patient is diagnosed with iPPROM, the mother can barely carry the fetuses for longer than a few months [72]. In fetoscopic procedures there is a 6–45% rate where iatrogenic preterm premature rupture of the fetal membrane occurs [73]. All these associated risks involved give rise to morbidity and death, which compromises the expected benefits of such methods to begin with [73].

Many attempts have been made to close the ruptured fetal membranes but have been unsuccessful. The natural healing of human fetal tissue appears to be slow, if not absent, even in very small fetoscopic punctures. Histological studies after fetoscopic puncture defect of human membranes show no healing or growth in the tissue [74]. New innovative techniques to plug up the fetoscopic access site are being tested [75–76]. Intraamniotic injection at the puncture site of maternal platelets mixed with fibrin cryoprecipitate (amniopatch) has been successful, but the high platelets in the amniopatch has accounted for otherwise unexplained fetal deaths [77]. Dry collagen and gelatin plugs or liquid blood-derived sealants are being studied [78–79]. Cyanoacrylate adhesives, well

known for strong adhesion in surgical and traumatic wound repair [80], damaged the fetal tissue and disrupted the membrane structure [73, 81]. Commercially available Dermabond and Histoacryl adhesives were cytotoxic when in contact with fetal membranes [73]. Other PEG-based hydrogel polymers like SprayGel failed to bond to fetal membranes under wet conditions [73]. Adhesive that can glue in wet conditions, to plug the amniotic sac to prevent amniotic fluid leakage, and is biocompatible is needed. The iPPROM after a fetal surgery or invasive prenatal procedure is an unsolved clinical problem [73].

1.5 Aim of This Research

Adhesives for soft tissue repair, more so for sealing fetal defects, is needed. Bonding tissue is a major challenge in wet environments, and having something that adheres *in utero* and biocompatible is difficult. The aim of this research is to develop a bioadhesive, inspired by the sandcastle worm, to seal fetal defects, in particular designing the glue for the applications in two fetal conditions: twin-to-twin transfusion syndrome (TTTS) and spina bifida. The twin-to-twin transfusion syndrome is the unequal sharing of maternal blood in twin pregnancies. This syndrome requires fetoscopic laser surgery as one of its treatments, and an adhesive to plug the fetoscope-punctured membrane is needed. The second condition spina bifida is a congenital disorder, where the neural tissue of the fetus is exposed to the amniotic fluid causing neurological defects at birth. An adhesive patch to cover the neural tissue with a minimally invasive procedure, until birth, a more complex closure, can prolong a better outcome when the baby is born [82–83]. The objective of this work is to design a synthetic complex coacervate adhesive that can fit both of these applications, *in utero* repair. The bioadhesive has to be stable

and have the ability to be used in the practical application of the adhesive in these conditions.

1.5.1 Twin-to-Twin Transfusion Syndrome

Twin-to-twin transfusion syndrome (TTTS) is a condition that is diagnosed during pregnancy by ultrasound. In pregnancies of twins, one–third of twins are monozygotic (MZ), and three–fourths of the MZ twins have presence of monochorionic diamniotic (MCDA) [84]. Twin pregnancies of MCDA placenta are at a high risk of TTTS that affects about 8–10% of pregnancies [85–87]. Currently TTTS occurs in approximately 1–3 per 10,000 births [88]. With TTTS, the two fetuses have unequal sharing of the mothers blood, which leads to asymmetrical fetal growth and fetal mortality, if left untreated. They share a placenta that contains abnormal blood vessels, where the blood supply from one baby to another is disproportional. The donor twin fetus receives less blood, which slows down its growth, and the recipient twin has excess blood, causing too much strain on the heart of the fetus. TTTS is a progressive disease in which sudden deterioration can occur leading to death of the fetuses, risk of miscarriage, brain damage, and morbidity [89–90]. This condition is diagnosed normally in second trimester of the pregnancy. Fetoscopic laser ablation is an effective treatment for TTTS, where a laser through a fetoscope coagulates the blood vessels as shown in Figure 1.6.

The survival rates after fetoscopic laser surgery of TTTS are 50–70% [92]. The laser surgery for TTTS is a fetoscopic procedure with insertion of laser into the scope [70]. The risk of iPPROM is 10–30% procedure-associated fetal loss with laser [84, 93]. Sealing the defect site after fetoscopic laser ablation can reduce the perinatal morbidity and mortality. Although we are focusing on TTTS, designing the adhesive to seal the

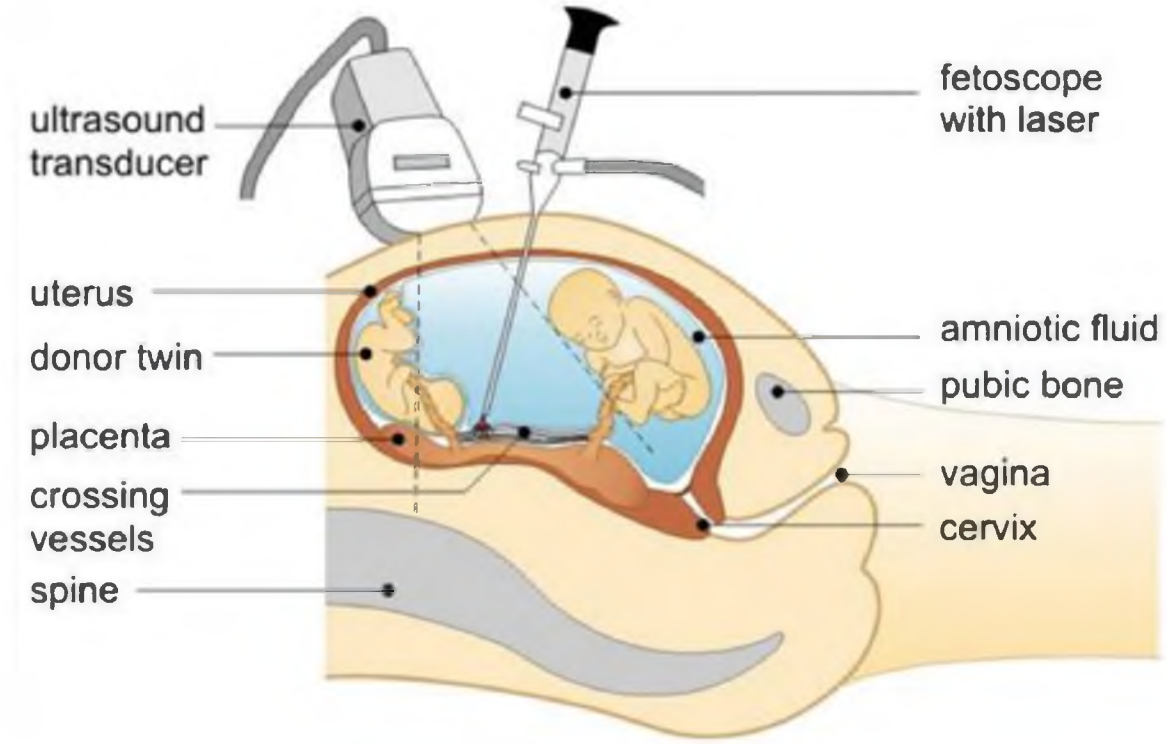

Figure 1.6 Fetoscopic laser ablation for twin-to-twin transfusion syndrome treatment [91]. Reprinted with permission from so+gi.

defect for this application can be a model sealing all fetal tissues for other conditions.

1.5.2 Spina Bifida

Spina Bifida, "split spine," is a developmental congenital disorder where the fetus neural tube is left unclosed, affecting 1,500 babies a year [94]. Myelomeningocele (MMC) is the most severe case of Spina Bifida (Figure 1.7), where the closure defect protrudes and bulges out of the posterior spinal column. The MMC is a severe malformation that can result in disability at birth and be a major challenge to fix in fetal repair [95]. The condition is detected 16 to 20 weeks of pregnancy. The exposed neural tissue undergoes progressive damage with advancing gestation age due to being in contact with amniotic fluid [96]. The fetus also develops a Chiari II condition of the brain, resulting in irreversible neurological impairments at birth, from the pressure disturbance and loss of cerebrospinal fluid [97]. At birth a number of defects result due to MMC: paraplegia, sphincter incontinence hydrocephalus, cranial nerve disturbances, respiratory problems, and death [98].

The treatment for MMC repair is challenging, with high risk of maternal and fetal morbidity and mortality. The surgical procedure could face difficulties like iPPROM, uterine rupture, maternal hemorrhage, and hysterectomy. The first intrauterine surgery repair of fetal myelomeningocele was performed on humans at Vanderbilt University Medical Center in Nashville, Tennessee, USA, in 1994 [100–101]. It was a very difficult and risky procedure, with a lot of research underway to improve the method of treatment [102]. The intrauterine surgery requires the defect to be closed in multilayer fashion, with neural dissection, dural closure, and suturing of the spinal cord, which increases the operating time as well [103]. Animal studies have shown that repair of neural tube defect

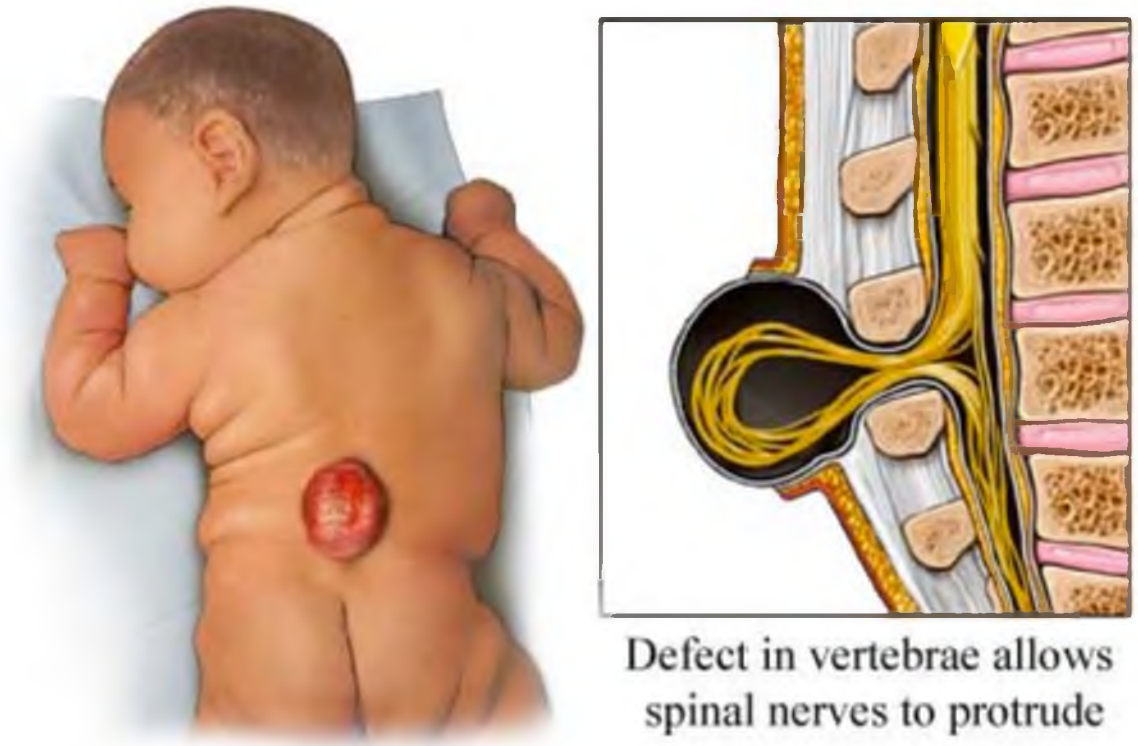

Figure 1.7 Illustration of a child with Myelomeningocele (MMC). [99] Reprinted with permission from so+gi.

in the womb could result in a less severe hindbrain and spinal cord injuries at birth [82, 83, 104]. The multilayer closure has been reported in fetoscopic repair, but the method is technically very demanding and time consuming [102]. Less invasive surgical technique that would just cover up the defect till birth, followed by a more complex MMC repair could be an effective treatment. An adhesive patch to cover up the defect through a minimally invasive method would be an ideal scenario for this application. Currently there is nothing out there that can adhere the patch under aqueous conditions to the spinal column of the fetus.

1.6 Outline of This Thesis

This thesis consists of research in developing a synthetic complex coacervate adhesive for sealing fetal defects *in utero*. The biomimetic adhesive is designed for two applications of TTTS and spina bifida. The research work consists of preliminary studies to prove that the synthetic complex coacervate adhesive can be used to seal fetal membranes, followed by a more in depth approach to making an adhesive composition that is more stable and used in practical applications and taking this adhesive from design and synthesis to animal studies.

In Chapter 2 a multiphase adhesive complex coacervate with increased bond strength was developed. Polyethylene glycol diacrylate was entrapped into the coacervate, creating a second polymer network via crosslinking, which helps aid in increased shear bond strength. The rheological flow behavior of the complex coacervate adhesive was extensively studied. Shear-thinning behavior without destructing the coacervate network is an important property for an injectable system.

In Chapter 3 the high bond strength adhesive was tested in conjunction with a

fetal membrane patch to model the adhesive as a potential sealant for fetoscopic procedures. The adhesive was tested with the in vitro model, mimicking the wall-fetal membrane. The cytotoxicity of the adhesive was tested with direct contact to human fetal membranes. This preliminary study was key in taking the adhesive to the next phase of animal studies.

In Chapter 4 a complex coacervate adhesive was developed using methacrylated polyphosphate and polyamine polymers. The synthesis methods used were explained. Aqueous polymerization and grafting methods were evaluated. Reversible Addition-Fragmentation Chain Transfer (RAFT) was used for polyamine polymer. The complex coacervate system was studied to tailor the properties to the application.

In Chapter 5 the mechanical properties of the methacrylated complex coacervate adhesive was tailored to the TTTS application. A chemically crosslinked coacervate adhesive was designed for this application. The crosslinking kinetics, bond strengths, and stability were studied. The sterile complex coacervate adhesive packets were prepared for the pig animal studies.

In Chapter 6 the mechanical properties of the methacrylated complex coacervate adhesive was tailored for the spina bifida application. A photocrosslinked coacervate adhesive patch was designed for this application. The crosslinking kinetics, bond strengths, and swelling behavior were studied. The sterile complex coacervate adhesive packets were prepared for sheep animal studies.

In the concluding chapter findings are summarized. The impact of our study and its contribution to soft tissue adhesives, more specifically fetal tissue adhesive is discussed. The future direction of this study is also discussed.

1.7 References

1. A. J. Kinloch, *Adhesion and Adhesives: Science and Technology*. Chapman and Hall, London, 1987.

2. N. M. Bikales, *Adhesion and Bonding*. Wiley-Interscience, New York, 1971.

3. P. A. Mazza, "A New Palaeolithic Discovery: Tar-hafted Stone Tools in a European Mid-Pleistocene Bone-bearing Bed," *J. Archaeol. Sci.*, **33** [9] 1310–1318 (2006).

4. A. Berg, F. Peters, and M. Schnabelrauch, *Biological Adhesive System: From Nature to Technical and Medical Application*. Edited by I. Grunwald, J. von Byern, Springer, New York, 2010.

5. R. J. Stewart, T. C. Ransom, and V. Hlady, "Natural Underwater Adhesives," *J. Polym. Sci. B Polym. Phys.*, **49** [11] 757–771 (2011).

6. A. V. Pocius, *Adhesion and Adhesive Technology: An Introduction*. 2nd ed. Hanser Gardner, Cincinnati, 2002.

7. P. J. Frantzis, "Durability of Adhesive Joints Made Underwater," *J. Mater. Civ. Eng.*, **20** [10] 635–639 (2008).

8. W. E. Cloete, and W. W. Focke, "Fast Underwater Bonding to Polycarbonate Using Photoinitiated Cyanoacrylate," *J. Adhes. Adhes.*, **30** [4] 208–213 (2010).

9. P. Fratzl, "Biomimetic Materials Research: What Can We Really Learn From Nature's Structural Materials?" *J. R. Soc. Inter.*, **4** [15] 637–642 (2007).

10. D. J. Crisp, G. Walker, G. A. Young, and A. B. Yule, "Adhesion and Substrate in Mussels and Barnacles," *J. Colloid Interface Sci.*, **104** [1] 40–50 (1985).

11. J. L. Dalsin, B. H. Hu, B. P. Lee, and P. B. Messersmith, "Mussel Adhesive Protein Mimetic Polymer for the Preparation of Nonfouling Surfaces," *J. Am. Chem. Soc.*, **125** [14] 4253–4258 (2003).

12. J. H. Waite, and X. Qin, "Polyphosphoprotein From the Adhesive Pads of Mytilus Edulis," *Biochem.*, **40** [9] 2887–2893 (2001).

13. H. Shao, K. N. Bachus, and R. J. Stewart, "A Water-borne Adhesive Modeled After the Sandcastle Glue of P. Californica," *Macromol. Biosci.*, **9** [5] 464–471 (2009).

14. H. Shao, and R. J. Stewart, "Biomimetic Underwater Adhesives With Environmentally Triggered Setting Mechanisms," *Adv. Mater.*, **22** [6] 729–733

(2010).

15. J. H. Waite, "Adhesion in Byssally Attached Bivalves," *Biol. Rev.*, **58** [2] 209–231 (1983).

16. H. Zhao, C. Sun, R. J. Stewart, and J. H. Waite, "Cement Proteins of the Tube-building Polychaete Phragmatopoma Californica," *J. Biol. Chem.*, **280**, 42938–42944 (2005).

17. T. J. Deming, "Mussel Byssus and Biomolecular Materials," *Curr. Opi. Chem. Bio.*, **3** [1] 100–105 (1999).

18. J. H. Waite, R. A. Jensen, and D. E. Morse, "Cement Precursor Proteins of the Reef-building Polychaete Phragmatopoma Californica (Fewkes)," *Biochem.*, **31** [25] 5733–5738 (1992).

19. C. S. Wang, and R. J. Stewart, "Multipart Copolyelectrolyte Adhesive of the Sandcastle Worm, Phragmatopoma Californica (Fewkes): Catechol Oxidase Catalyzed Curing Through Peptidyl-DOPA," *Biomac.*, **14** [5] 1607–1617 (2013).

20. R. J. Stewart, J. C. Weaver, D. E. Morse, and J. H. Waite, "The Tube Cement of Phragmatopoma Californica: A Solid Foam," *J. Exp. Bio.*, **207**, 4727–4734 (2004).

21. K. Simkiss, "The Process of Biomineralization in Lower Plants and Animals – An Overview," In *Biomineralization in Lower Plants and Animals*, **30**, 19–37 (1986).

22. B. J. Endrizzi, and R. J. Stewart, "Glueomics: An Expression Survey of the Adhesive Gland of the Sandcastle Worm," *J. Adhes.*, **85**, 546–559 (2009).

23. M. J. Steven, R. E. Steren, V. Hlady, and R. J. Stewart "Multiscale Structure of the Underwater Adhesive of Phragmatopoma Californica: A Nanostructured Latex With a Steep Microporosity Gradient," *Langmuir*, **23** [9] 5045–5049 (2007).

24. J. Vovelle, "The Tube of Salbellaria Alveolata," *Arch. Zool. Exp. Gen.*, **106**, 1–187 (1965).

25. L. J. Gibson, and M. F. Ashby, *Cellualr Solids: Structure and Properties*. Cambridge University Press, Cambridge, UK, 1997.

26. C. S. Wang, K. K. Svendsen, and R. J. Stewart, "Morphology of the Adhesive System in the Sandcastle Worm, Phragmatopoma Californica," *Biological Adhesive Systems*. Editors J. V. Byern, I. Grunwalds. Springer, New York, 2010.

27. R. A. Jensen, and D. E. Morse, "The Bioadhesive of *Phragmatopoma Californica*

Tubes: a Silk-line Cement Containing L-DOPA," *J. Comp. Physiol. B*, **158**, 317–324 (1988).

28. J. H. Waite, and A. C. Rice-Ficht, "Presclerotized Eggshell Protein From Liver Fluke *Fasciola Hepatica*," *Biochem.*, **26** [24] 7819–7825 (1987).

29. J. H. Waite, "Adhesion a La Moule," *Integ. Comp. Biol.*, **42** [6] 1172–1180 (2002).

30. R. J. Stewart, C. S. Wang, and H. Shao, "Complex Coacervates as a Foundation for Synthetic Underwater Adhesives," *Adv. Colloid. Interface Sci.*, **167** [1–2] 85–93 (2011).

31. M. Yu, J. Hwang, and T. J. Deming, "Role of L-3,4-Dihydroxyphenylalaine in Mussel Adhesive Protein," *J. Am. Chem. Soc.*, **121**, 5825–5826 (1999).

32. L. A. Burzio, and J. H. Waite, "Cross-linking in Adhesive Quinoprotein: Studies With Model Decapeptides," *Biochem.*, **39** [36] 11147–11153 (2000).

33. S. Haemers, G. J. M. Koper, and G. Frens, "Effect of Oxidation Rate on Cross-linking Mussel Adhesive Protein," *Biomac.*, **4** [3] 632–640 (2003).

34. J. Monahan, and J. J. Wilker, "Cross-linking the Protein Precursor of Marine Mussel Adhesives: Bulk Measurements and Reagents Curing," *Langmuir*, **20** [9] 3724–3729 (2004).

35. IUPAC compendium of Chemical Technology 1997.

36. C. G. De Kruif, F. Weinbreck, and R. De Vries, "Complex Coacervation of Proteins and Anionic Polysaccharides," *Curr. Opin. in Coll. & Interfa. Sci.*, **9** [5] 340–349 (2004).

37. J. V. D. Gucht, E. Spruijt, M. Lemmers, and M. A. C. Stuart, "Polyelectrolyte Complexes: Bulk Phases and Colloidal Systems," *J. of Coll. and Inter. Sci.*, **361** [2] 407–422 (2011).

38. C. L. Cooper, P. L. Dubin, A. B. Kayitmazer, and S. Turksen, "Polyelectrolyte-protein Complexes," *Curr. Opin. Coll. Inter. Sci.*, **10** [1–2] 52–78 (2005).

39. F. W. Tiebackx, "Gleichzeitige Ausflockung Zweier Kolloide," *Chem. Ind. Kolloide.,* **8**, 198–201 (1911).

40. H. G. Bungenberg de Jong, "Crystallization-coacervation-flocculation," *Coll. Sci.*, Elsevier Publishing Company, Amsterdam, **2,** 232–255 (1949).

41. H. J. Bungenberg de Jong, and H. R. Kruyt, "Coacervation (Partial Miscibility in

Colloid Systems)," *Proc. K. Ned. Akad. Wet.*, **32**, 849–856 (1929).

42. M. J. Voorn, "Complex Coacervation. V Experiments on the Distribution of Salts. Comparison of Theory and Experiments," *Rec. Trav. Chim.*, **75**, 317–925 (1956).

43. J. T. Overbeek, and M. J. Voorn, "Phase Separation in Polyelectrolyte Solution; Theory of Complex Coacervation," *J. Cell. Comp. Physiol.*, **49**, 7–22 (1957).

44. M. J. Voorn, "Phase Separation in Polymer Solutions," *Fortsch Der Hochpoly-Forsch*, Springer, Berlin, 192–233, 1959.

45. A. Veis, and C. Aryani, "Phase Separation in Polyelectrolyte Systems. I. Complex Coacervates of Gelatin," *J. Phys. Chem.*, **64**, 1203–1210 (1960).

46. A. Nakajima, and H. Sato, "Phase Relationships of an Equivalent Mixture of Sulfated Polyvinyl Alcohol and Aminoacetalyzed Polyvinyl Alcohol in Microsalt Aqueous Solution," *Biopolymers*, **10**, 1345–1355 (1972).

47. K. Tainaka, "Study of Complex Coacervation in Low Concentration by Viral Expansion Method," *J. Phys. Soc. Japan*, **46**, 1899–1906 (1979).

48. K. Tainaka, "Effect of Counterions on Complex Coacervation," *Biopoly.*, **19**, 1289–1298 (1980).

49. D. J. Burgess, "Practical Analysis of Complex Coacervate Systems," *J. Coll. Inter. Sci.*, **140**, 227–238 (1990).

50. D. J. Burgess, and J. E. Carless, "Microelectrophoretic Studies of Gelatin and Acacia for the Prediction of Complex Coacervation," *J. Coll. Inter. Sci.*, **98**, 1–8 (1984).

51. C. Schmitt, C. Sanchez, F. Thomas, and J. Hardy, "Complex Coacervation Between β-lactoglobulin and Acacia Gum in Aqueous Media," *Food Hydrocoll*, **13**, 483–496 (1999).

52. E. Spruijt, M. A. C. Stuart, and J. van der Gucht, "Dynamic Force Spectroscopy of Oppositely Charged Polyectrolyte Brushes," *Macromolecules*, **43**, 1543–1550 (2010).

53. E. Spruijt, J. Sprakel, M. A. C. Stuart, and J. Van der Gucht, "Interfacial Tension Between a Complex Coacervate Phase and its Coexisting Aqueous Phase," *Soft Matter*, **6**, 172–178 (2010).

54. H. Sato, and A. Nakajima, "Complex Coacervation in Sulfated Polyvinyl Alcohol-aminoacetalyzed Polyvinyl Alcohol System 0.2, Formation of

Coacervate Droplets," *Colloid Polym. Sci.*, **252**, 944–948 (1974).

55. D. J. Clark, and T. J. Kimura, "Electrostatic Mechanism of Chromatin Folding," *J. Mol. Biol.*, **211** [4] 883–896 (1990).

56. Y. Wang, K. Kimura, and P. L. Dubin, "Polyelectrolyte-Micelle Coacervation: Effects of Micelle Surface Charge Density, Polymer Molecular Weight, and Polymer/Surfactant Ratio," *Macromolecules*, **33**, 3324–3331 (2000).

57. K. Kaibara, T. Okazaki, H. B. Bohidar, and P. L. Dubin, "pH-induced Coacervation in Complexes of Bovine Serum Albumin and Cationic Polyelectrolytes," *Biomacromolecules*, **1**, 100–107 (2000).

58. D. Leisner, and T. Imae, "Interpolyelectrolyte Complex and Coacervate Formation of Poly (Glutamic Acid) With a Dendrimer Studied By Light Scattering and SAXS," *J. Phys. Chem. B*, **107**, 8078–8087 (2003).

59. W. L. Hinze, and D. W. Armstrong, editors, *Ordered Media in Chemical Separation*, American Chemical Society, Washington DC, 1987.

60. J. Xia, K. Mattison, V. Romano, P. L. Dubin, and B. B. Muhoberac, "Complexation of Trypsin and Alcohol Dehydrogenase With Poly(Diallyldimethylammonium Chloride)," *Biopolymers*, **41** [4] 359–365 (1997).

61. E. D. Goddard, "Polymer/Surfactant Interaction," *J. Soc. Cosmet. Chem.*, **41**, 23–49 (1990).

62. P. B. Deasy, *Microencapsulation and Related Drug Process*, Marcel Dekker, New York, 1984.

63. Y. Wang, J. Banziger, P. L. Dubin, G. Filipelli, and N. Nuraje, "Adsorptive Partitioning of an Organic Compound Onto Polyelectrolyte-immobilized Micelles on Porous Glass and Sand," *Environ. Sci. Technol.*, **35** [12] 2608–2611 (2001).

64. S. S. Singh, V. K. Aswal, and H. B. Bohidar, "Structural Studies of Agar-gelatin Complex Coacervates by Small Angle Neutron Scattering, Rheology and Differential Scanning Calorimetry," Intern. J. Bio. Macrom., **41** [3] 301–307 (2007).

65. H. G. Bungenberg De Jong, "Morphology of Coacervates," *Colloid Science*, Elsevier Publishing C, Amsterdam, **2**, 433–482 (1949).

66. R. A. Jensen, and D. E. Morse, "Intraspecific Facilitation of Larval Recruitment: Gregarious Settlement of the Polychaete Phragmatopoma Californica (Fewkes)," *J. Exp. Mar. Bio. Ecol.*, **83** [2] 107–126 (1984).

67. Y. Gruet, J. Vovelle, and M. Grasset, "Composante Biominerale Du Ciment Du Tube Chez Sabellaria Alveolata (L.), Annelid Polychete," Can. J. Zool., **65**, 837–842 (1987).

68. H. Shao, G. M. Weerasekare, and R. J. Stewart, "Controlled Curing of Adhesive Complex Coacervates With Reversible Periodate Carbohydrate Complexes," *J. of Biomed. Mat. Res. A*, **97** [1] 46–51 (2011).

69. E. Danzer, R. M. Sydorak, M. R. Harrison MR, and C. T. Albanese, "Minimal Access Fetal Surgery," *European Journal of Obstetrics & Gynecology and Reproductive Biology*, **108** [1] 3–13 (2003).

70. J. Farrell, and L. J. Howell, "An Overview of Surgical Techniques, Research Trials, and Future Directions of Fetal Therapy," *Journal of Obstetric, Gynecologic, & Neonatal Nursing*, **41** [3] 419–425 (2012).

71. C. T. Albanese, and M. R. Harrison, "Surgical Treatment for Fetal Disease. The State of the Art," *Annals of the New York Academy of Sciences*, **847** [1] 74–85 (1998).

72. R. A. Quintero, W. J. Morales, M. Allen, P. W. Bornick, J. Arroyo, and G. LeParc, "Treatment of Iatrogenic Previable Premature Rupture of Membranes With Intra-amniotic Injection of Platelets and Cryoprecipitate (Amnio-patch): Preliminary Experience," *Am. J. Obstet. Gynecol.*, **181**, 744–749 (1999).

73. G. Bilic, C. Brubaker, P. B. Messersmith, A. S. Mallik, T. M. Quinn, C.Haller, E. Done, L. Gucciardo, et al., "Injectable Candidate Sealants for Fetal Membrane Repair: Bonding and Toxicity in Vitro," *Am. J. Obstet. Gynecol.*, **202** [1] 85.e1–9 (2010).

74. E. Gratacos, J. Sanin-Blair, L. Lewi, N. Toran, G. Verbist, L. Cabero, and J. Deprest, "A Histological Study of Fetoscopic Membrane Defects to Document Membrane Healing," *Placenta*, **27** [4] 452–456 (2006).

75. R. Devlieger, L. K. Millar, G. Bryant-Greenwood, L. Lewi, and J. A. Deprest, "Fetal Membrane Healing After Spontaneous and Iatrogenic Membrane Rupture: A Review of Current Evidence," *Am. J. Obstet. Gynecol.*, **195** [6] 1512–1520 (2006).

76. A. H. Zisch, and R. Zimmermann, "Bioengineering of Foetal Membrane Repair," *Swiss Med Wkly*, **138** [41–42] 596–601 (2008).

77. R. A. Quintero, "Treatment of Previable Premature Ruptured Membranes," *Clinnics in Perinatology*, **30** [3] 573–589 (2003).

78. J. Chang, T. F. Tracy Jr, S. R. Carr, D. L. Sorrells Jr, and F. I. Luks, "Port

Insertion and Removal Techniques to Minimize Premature Rupture of the Membranes in Endoscopic Fetal Surgery," *J. Pediatr. Surg.*, **41** [5] 905–909 (2006).

79. B. K. Young, A. S. Roman, A. P. MacKenzie, C. D. Stephenson, V. Minior, A. Rebarber, and I. Timor-Tritsch, "The Closure of Iatrogenic Membrane Defects After Amniocentesis and Endoscopic Intrauterine Procedures," *Fetal Diagn. Ther.*, **19** [3] 296–300 (2004).

80. P. A. Leggat, D. R. Smith, and U. Kedjarune, "Surgical Applications of Cyanoacrylate Adhesives: A Review of Toxicity," *ANZ J. Surg.*, **77** [4] 209–213 (2007).

81. M. L. Oyen, S. E. Calvin, and D. V. Landers, "Premature Rupture of the Fetal Membranes: Is the Amnion the Major Determinant?" *Am. J. Obstet. Gynecol.*, **195** [2] 510–515 (2006).

82. B. W. Paek, D. L. Farmer, C. C. Wilkinson, C. T. Albanese, W. Peacock, M. R. Harrison, and R. W. Jennings, "Hindbrain Herniation Develops in Surgically Created Myelomeningocele but is Absent After Repair in Fetal Lambs," *Am. J. Obstet. Gynecol.*, 183 [5] 1119–11123 (2000).

83. S. Bouchard, M. G. Davey, N. E. Rintoul, D. S. Walsh, L. B. Rorke, and N. S. Adzick, "Correction of Hindbrain Herniation and Anatomy of the Vermis after in Utero Repair of Myelomeingocele in Sheep," *J. Pediatr. Surg.*, **38** [3] 451–458 (2003).

84. L. L. Simpson, "Twin-Twin Transfusion Syndrome," *Am. J. Obstet. Gyneco.*, **208** [1] 3–18 (2013).

85. L. Lewi, J. Jani, I. Blickstein, A. Huber, L. Gucciardo, T. V. Mieghem, E. Done, et al., "The Outcome of Monochorionic Diamniotic Twin Gestations in the Era of Invasive Fetal Therapy: A Prospective Cohort Study," *Am. J. Obstet. Gynecol.*, **199** [5] 514–e1 (2008).

86. G. A. Machin, and L. G. Keith, "Can Twin-to-twin Transfusion Syndrome be Explained, and How is it Treated?" *Clin. Obstet. Gynecol.*, **41** [1] 104–113 (1998).

87. R. Acosta-Rojas, J. Becker, B. Munoz-Abellana, C. Ruiz, E. Carreras, and E. Gratacos, "Twin Chorionicity and the Risk of Adverse Perinatal Outcome," *Int. J. Gynecol. Obstet.*, **96** [2] 98–102 (2007).

88. I. Blickstein, "Monochorionicity in Perspective," *Ultrasound Obstet. Gynecol.*, **27** [3] 235–238 (2006).

89. F. Haverkamp, C. Lex, C. Hanisch, H. Fahnenstich, and K. Zerres, "Neurodevelopmental Risks in Twin-to-twin Transfusion Syndrome: Preliminary Findings," *Europ. J. Paediatr. Neurol.*, **5** [1] 21–27 (2001).

90. I. Blickstein, "The Twin-twin Transfusion Syndrome," *Obstet. Gynecol.*, **76** [4] 714–722 (1990).

91. http://www.sogi.net.au/mintdigital.net/SOGI.aspx?XmlNode=/Services/Fetal+Treatment/Laser+surgery

92. D. Roberts, S. Gates, M. Kilby, and J. P. Neilson, "Interventions for Twin-twin Transfusion Syndrome: a Cochrane Review," *Ultrasound Obstet. Gynecol.*, **31** [6] 701-711 (2008).

93. R. A. Quintero, C. Comas, P. W. Bornick, M. H. Allen, and M. Kruger, "Selective Versus Non-selective Laser Photocoagulation of Placental Vessels in Twin-to-twin Transfusion Syndrome," *Ultrasound Obstet. Gynecol.*, **16** [3] 230–236 (2000).

94. Center of Disease Control and Prevention: http://www.cdc.gov/ncbddd/spinabifida/data.html

95. S. Hirose, C. Meuli –Simmen, and M. Meuli, "Fetal Surgery for Myelomeningocele: Panacea or Peril?" *World J. Surg.*, **27** [1] 87–94 (2003).

96. D. S. Heffez, J. Aryanpur, N. A. Rotellini, G. M. Hutchins, and J. M. Freeman, "Intrauterine Repair of Experimental Surgically Created Dysraphism," *Neurosurgery*, **32** [6] 1105-1110 (1993).

97. D. G. McLone, and P. A. Knepper, "The Cause of Chiari II Malformation: A Unified Theory," *Pediatr. Neurosur.*, **15** [1] 1–12 (1989).

98. R. M. Bowman, D. G. McLone, J. A. Gran, T. Tomita, and J. A. Ito, "Spina Bifida Outcome: a 25 year Prospective," *Pediatr. Neurosur.*, **34** [3] 114–120 (2001).

99. http://www.glogster.com/stevko/spina-bifida-genetics/g-6l6ma4jtukd42g0jfaa89a0

100. J. P. Bruner, W. O. Richards, N. B. Tulipan, and T. L. Arney, "Endoscopic Coverage of Fetal Myelomeningocele in Utero," *Am. J. Obstet. Gynecol.*, **180** [1] 153–158 (1999).

101. J. P. Bruner, "Intrauterine Surgery in Myelomeningocele," *In Seminars in Fetal & Neonatal Medicine*, **12** [6] 471–476 (2007).

102. D. I. Farmer, C. S. Von Koch, W. J. Peacock, M. Danielpour, N. Gupta, and H. Lee, "In Utero Repair of Myelomeningocele: Experimental Pathophysiology, Initial Clinical Experience, and Outcomes," *Arch. Surg.*, **138** [8] 872–878 (2003).

103. R. Barini, M. W. G. Barreto, K. Cursino, H. Zambelli, A. Prando, and L. Sbragia, "Abruptio Placentae During Fetal Myelomeningocele Repair," *Fetal Diagnosis and Therapy*, **21** [1] 115–117 (2006).

104. M. Meuli, C. Meuli-Simmen, C. D. Yingling, G. M. Hutchins, K. M. Hoffman, M. R. Harrison, and N. S. Adzick, "Creation of Myelomeningocele in Utero: A Model of Functional Damage From Spinal Cord Exposure in Fetal Sheep," *J. Pediatr. Surg.*, **30** [7] 1028–1033 (1995).

CHAPTER 2

MULTIPHASE ADHESIVE COACERVATES INSPIRED BY THE SANDCASTLE WORM

2.1 Abstract

Water-borne, underwater adhesives were created by complex coacervation of synthetic copolyelectrolytes that mimic the proteins of the natural underwater adhesive of the sandcastle worm. To increase bond strengths, we created a second polymer network within cross-linked coacervate network by entrapping polyethylene glycol diacrylate (PEG-dA) monomers in the coacervate phase. Simultaneous polymerization of PEG-dA and crosslinking of the coacervate network resulted in maximum shear bond strengths of ~ 1.2 MPa. Approximately 40% of the entrapped PEG-dA polymerized based on attenuated total reflectance-Fourier transform infrared spectroscopy. The monomer-filled coacervate had complex flow behavior, thickening at low shear rates and then thinning suddenly with a 16-fold drop in viscosity at shear rates near 6 s^{-1}. The microscale structure of the complex coacervates resembled a three-dimensional porous network of interconnected tubules. The sharp shear thinning behavior is conceptualized as a structural reorganization between the interspersed phases of the complex coacervate. The

---

Adapted from a pre-peer-reviewed version with permission from S. Kaur, G. M. Weerasekare, R. J. Stewart, "Multiphase adhesive coacervates inspired by the Sandcastle worm," *ACS Appl. Mater. Inter.*, **3** [4] 941-4 (2011).

bond strength and complex fluid behavior of the monomer-filled coacervates have important implications for medical applications of the adhesives.

2.2 Introduction

Adhesive bonding in watery environments with common synthetic adhesives is confounded, in general, by poor interfacial adhesion leading to eventual failure by infiltration of water into the joint. Aquatic environments are populated with diverse organisms that have evolved a multitude of workable solutions to the underwater adhesion problem. Natural underwater adhesives have therefore been studied as potential sources of materials or concepts with the goal of creating or improving synthetic adhesives for wet applications, including repair of living tissues. One such model is the underwater adhesive of the Sandcastle worm (*Phragmatopoma californica*), a marine polychaete [1-3]. The Sandcastle worm employs an ingenious strategy to construct composite mineralized shells; the mineral phase is gathered from its environment preformed as sand grains and shell fragments that are then glued together with small dabs of an underwater adhesive [1].

The sandcastle worm glue is comprised of oppositely charged proteins and divalent cations [2, 3]. Copolyelectrolytes with the same chemical side chains (phosphates and amines) and in the same proportions as the natural proteins were synthesized. When mixed under the right conditions, the synthetic copolyelectrolytes condensed into fluid complex coacervates [4, 5]. As the basis for underwater adhesives, complex coacervates have several ideal properties: the dense, phase-separated fluids sink in water, are sufficiently cohesive that they do not mix with water on a time scale of several minutes, and readily adhere to wet surfaces, all of which allows the adhesive to

stay in place where it is applied underwater. The adhesive becomes load-bearing by triggered solidification of the complex coacervate after application. The sandcastle worm glue sets within 30 s through pH-triggered solidification of a polyphosphorylated protein and Ca^{2+} and Mg^{2+} [2, 6]. The initial set is followed up over several hours by covalent crosslinking through 3,4-dihydroxy-L-phenylalanine (dopa) residues. Both the pH-triggered set and dopa-mediated crosslinking were replicated in biomimetic adhesive coacervates [4, 5].

Though the natural sandcastle glue is suitable for the dimensions and lifecycle of sandcastle worms, it is not particularly strong, around 300 kPa [7]. Biomimetic adhesives will have to be much stronger than the natural adhesive to find broad utility. Incorporation of micro- or nanophases into the bulk adhesive phase is a well-known strategy for increasing adhesive bond strengths [8]. Our strategy for incorporation of an additional phase into our biomimetic adhesive was to form the coacervate in the presence of a water-soluble neutral monomer, as a first example, polyethylene glycol-diacrylate (PEG-dA). Polymerizable monomers dissolved in the aqueous copolyelectrolyte solutions become incorporated into the dense coacervate phase, which is mostly water by weight. Polymerization created a second polymer network within the coacervated copolyelectrolyte network. The coacervate functioned, in effect, as a container for the polymerizable monomers that could be accurately delivered underwater before polymerization of the second internal polymer network was initiated.

2.3 Materials and Methods

2.3.1 Materials

All reagents were used without further purification unless noted otherwise. Phosphorous oxychloride ($POCl_3$, 98%), 2-hydroxyethylmethacrylate (HEMA, 97%), and triethylamine (99%) were purchased from VWR. The 2,2'-azobisisobutyronitrile (AIBN) was purchased from Polysciences. Ultra filters Pellicon Ultracel Membranes by Millipore were used. N-(3-Aminopropyl) Methacrylamide, Hydrochloride, and Acrylamide (Chemzymes, ultra pure) were purchased from Polysciences. PEG-dA (Polyethylene glycol diacrylate, 760 Da) was purchased from sigma-aldrich.

2.3.2 Monomer Synthesis

2-(methacryloyloxy)ethyl phosphate (MOEP) was synthesized by adding phosphorus oxychloride (16.8g, 110 mmol) under argon to a stirred solution of 2-hydroxyethyl methacrylate (12g, 92 mmol) in toluene (340 mL). The reaction mixture was cooled to 0°C, and triethylamine (39 mL, 276 mmol) was added. The reaction proceeded at 0°C for 30 mins, then at room temperature for 6 hrs. The white solid precipitate was recovered by filtration. Water (240 mL) was added to the filtrate and stirred overnight. The two layers were separated, and the aqueous phase was acidified and then extracted with THF: Ether (1:2, 6×225 mL). The organic phases were combined, dried over Na_2SO_4, and solvent evaporated to obtain the product as a pale yellow oil (67%, 12.2g). ^{1}H NMR spectroscopy (300 MHz, D_2O) d 1.7 (3H, s), 4.0 (2H, m, POCH_2), 4.2 (2H, m, $POCH_2CH_2$), 5.5 (1H,s) 6.0 (1H, s); ^{13}C NMR (75 MHz, D_2O) d 17.4, 64.2 (d, $^2J_{POC}$ = 8.3 Hz), 64.4 (d, $^3J_{POCC}$ = 5.5Hz), 127.2, 135.6, 169.4; ^{31}P NMR (120 MHz, D_2O) d 0.97 (s). Dopamine methacrylamide (DMA) was synthesized as

previously described [4].

2.3.3 Copolyelectrolyte Synthesis

Poly(MOEP-co-DMA) was synthesized as previously described [4] by free radical polymerization of MOEP and DMA initiated with AIBN in methanol. The polymerization proceeded at 55°C for 16 hours (Figure 2.1). The copolymer was precipitated with acetone and then washed twice with acetone to remove residual monomers. The polymer was then dissolved in water and ultrafiltered on pellicon ultracel membranes with MWCO 1000 kDa followed by filtration with MWCO of 5 kDa. The concentrations of phosphate and *o*-DHP side chains were determined by NMR and UV/vis spectroscopy and were 76 and 19 mol%, respectively. The MW (64 kDa) and PDI (2.8) of the copolymer were determined by size exclusion chromatography (SEC) on an AKTA FPLC system with a Superose 6 HR 10/300 column (GE Healthcare) in 0.05 M phosphate and 0.15 M NaCl (pH 7.4).

Poly(acrylamide-co-aminopropyl methacrylamide) was synthesized by free radical polymerization of 90 mol% acrylamide and 10 mol% N-(3-amino-propyl) methacrylamide hydrochloride (Figure 2.2), as previously described [4]. The copolymer was purified by dialysis for 3 days and lyophilized. The amine concentration (mol/mg) was determined with ninhydrin using glycine as the standard. The MW and PDI, determined by SEC in 0.5 M NaCl and 0.1 M $NH_4CH_3CO_2$ on Superdex 200 column (GE Healthcare), were 288 kDa and PDI 1.36.

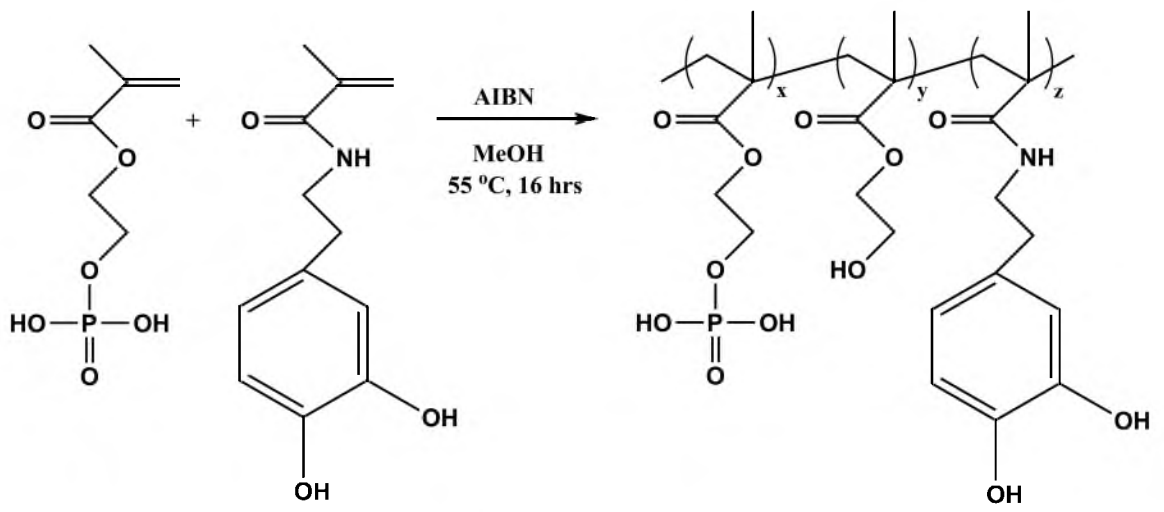

Figure 2.1 Synthesis schematic of Poly(MOEP-co-DMA) polymer, polymerized by free radical polymerization.

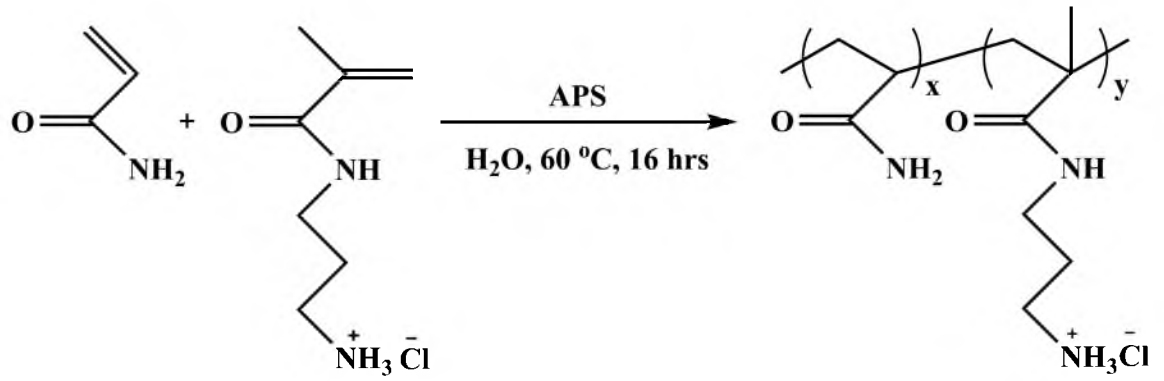

Figure 2.2 Synthesis schematic of Poly(acrylamide-co-aminopropyl methacrylamide) polymer, polymerized by free radical polymerization.

2.3.4 Coacervate Formation

PEG-dA was dissolved in degassed DI water at the desired concentration (0–25 wt%). Poly(acrylamide-co-aminopropyl methacrylamide) and poly(MOEP-co-DMA) were dissolved in separate PEG-dA solutions at a final concentration of 5 wt%. The poly(MOEP-co-DMA) PEG-dA solution also contained a 0.2 molar ratio of Ca^{2+} to phosphate side chains. The copolymer solutions were adjusted to pH 7.4±0.2 with NaOH. The poly(acrylamide-co-aminopropyl methacrylamide) PEG-dA solution was added dropwise while stirring to the poly(MOEP-co-DMA) PEG-dA solution to a molar ratio of 0.6 amine side chains to phosphate side chains. Within a few minutes a turbid coacervate settled out of solution.

2.3.5 Mechanical Testing

The adhesive PEG-dA filled coacervates were cross-linked through the *o*-DHP side chains of the polyphosphate and/or by polymerizing PEG-dA. *o*-DHP was oxidatively cross-linked by adding 1 equivalent of $NaIO_4$. To slow the oxidation of *o*-DHP side chains, in order to allow better control of the setting reaction, a sugar (1,2-O-Isopropylidene-D-glucofuranose, 98%) molecule was used to prepare an aqueous $NaIO_4$/sugar complex solution (100 mg/mL) with a $NaIO_4$:Sugar of 1:1.2 dissolved in water. PEG-dA was polymerized with 3.5 mol% ammonium persulfate (APS) and 5.2 mol% N,N,N',N'-tetramethylethylenediamine (TEMED). Immediately after adding $NaIO_4$, APS, and TEMED, 20 μl of coacervate was added to a wet 0.5 x 5 cm cleaned and polished Al adherend. A second wet Al was placed on the first with a 14–20 mm overlap, secured with a stainless steel clip, and submerged in water for 20–24 hours at 22–24°C. For each test condition 4–6 specimens were prepared. The shear strength of

the bonds were determined on a material testing system (Instron) with a 500 N load cell, crosshead speed 0.2 mm min^{-1}, while fully submerged in a temperature-controlled water bath.

2.3.6 Dynamic Rheology

Flow experiments were done on a stress-controlled rheometer (TA Instrument, AR 2000ex) using a 20 mm, 4° cone and plate, gap of 114 μm, and at 25°C with 150 μL coacervate samples. All rheology experiments were repeated with three independently prepared coacervate samples.

2.3.7 ATR-FTIR

Attenuated Total Reflectance-Fourier Transform Infrared Microscopy (ATR-FTIR, FTS 6000 Spectrometer BioRAD) was used to measure the amount of PEG-dA in coacervates as well as the conversion of polymerization. The scans were made on ZnSe reflective crystal by placing 50 μl of coacervate and running 30 scans per spectrum. Standard PEG-dA solutions of known concentration in water were scanned to get a standard curve (Figure 2.3A). Peak 1415 cm^{-1}, corresponding to the acrylate group in PEG-dA, was used to fit a linear model of normalized peak area versus known concentration (Figure 2.3B). This standard curve fit was used to analyze the amount of PEG-DA in coacervates. Each sample was measured three times to get an average value.

2.4 Results and Discussion

Coacervates were formed with 2-(methacryloyloxy) ethyl phosphate dopamine methacrylamide (poly(MOEP-co-DMA)), poly(acrylamide-co-aminopropyl methacrylamide) and Ca^{2+}, as described in detail previously [4], in solutions containing

A)

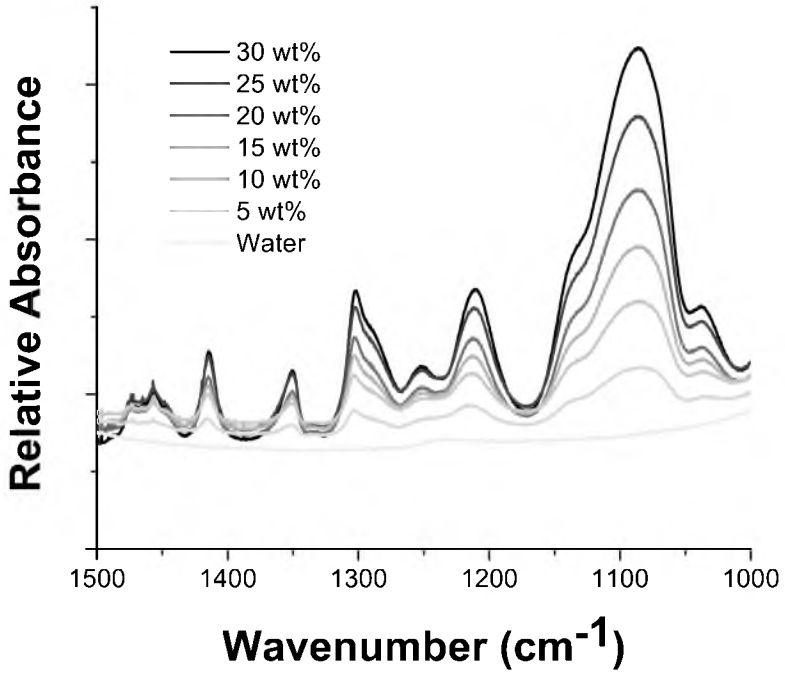

B)

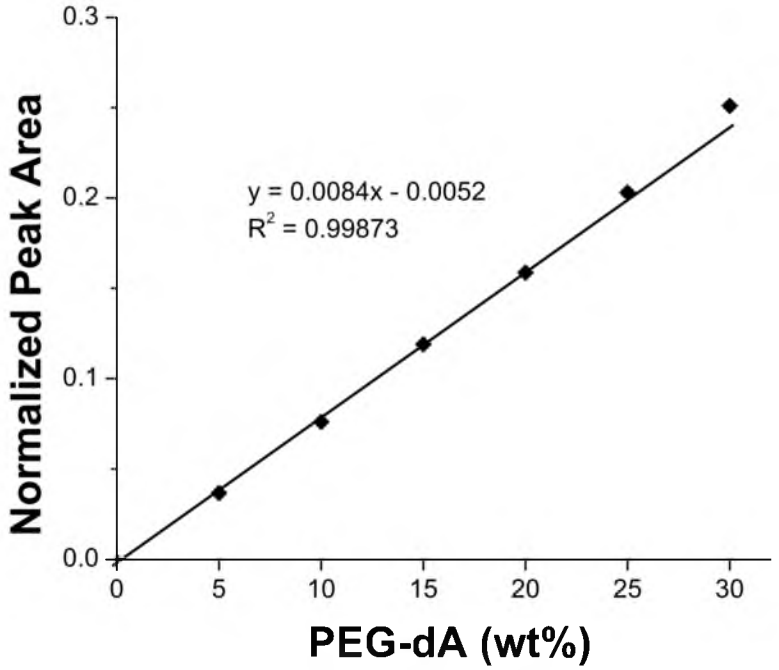

Figure 2.3 ATR-FTIR (A) ATR-FTIR of PEG-dA in water solutions of set concentrations were scanned to generate a standard curve. (B) Peak 1415 cm^{-1} was used to fit a linear model of normalized peak area vs. known concentration.

nominal wt% concentrations of 0, 5, 10, 15, 20, and 25 PEG-dA (MW 700 g/mol). Dense complex coacervates phase separated from the solutions. The concentration of PEG-dA entrapped in the coacervate phase was determined by Attenuated Total Reflectance-Fourier Transform Infrared Microscopy (ATR-FTIR). The absorbance peak at 1415 cm^{-1} was compared to the 1415 cm^{-1} acrylate groups of standard solutions of PEG-dA in water (Figure 2.4A) [9, 10]. On average the PEG-dA concentration in the coacervate was 73% of the initial concentration in solution. Above 25 wt% PEG-dA the coacervates were too viscous to work with conveniently. Free radical polymerization of entrapped PEG-dA was initiated by adding ammonium persulfate (APS) and tetramethylethylenediamine (TEMED) to the complex coacervate. The extent of PEG-dA polymerization within the coacervate was determined from the 1415 cm^{-1} ATR-FTIR peak corresponding to the acrylate functional group (Figure 2.4B). The complex coacervate containing 11.4 wt% PEG-dA reached ~40% conversion after 24 hr.

The shear bond strengths of the PEG-dA filled adhesive coacervates were determined in lap shear tests with polished aluminum adherends. Cross-linking of the coacervate network through the *o*-dihydroxyphenyl sidechains of poly(MOEP-co-DMA) and the amine side chains of poly(acrylamide-co-aminopropyl methacrylamide) was initiated by addition of $NaIO_4$. Free radical polymerization of PEG-dA was initiated simultaneously by addition of APS and TEMED. Immediately after initiation the coacervates were applied to wet Al adherends. The bonds were cured for 24 hours and fully submerged in water (22°C) before loading to failure on a material testing system. The maximum bond strengths increased with increasing PEG-dA (Figure 2.5), nearly doubling from a mean of 512 +/- 208 kPa without PEG-dA to a mean of 973 +/- 263 kPa

A)

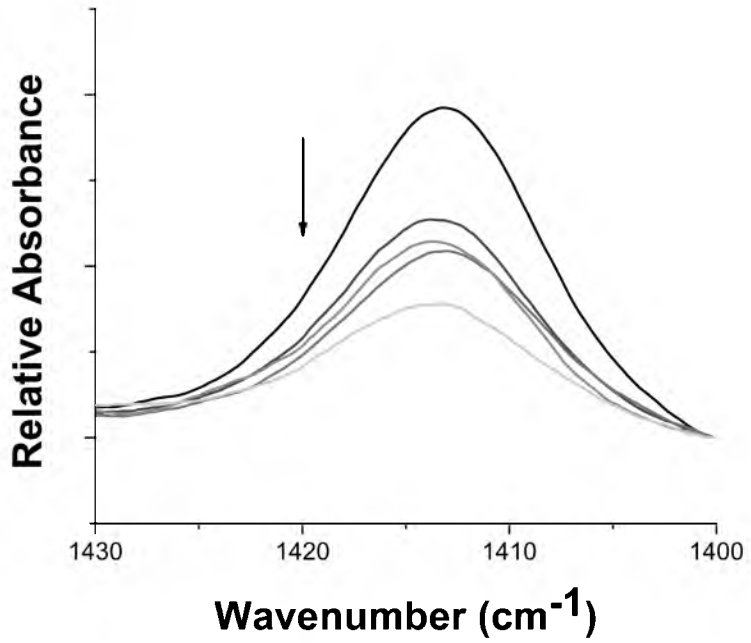

B)

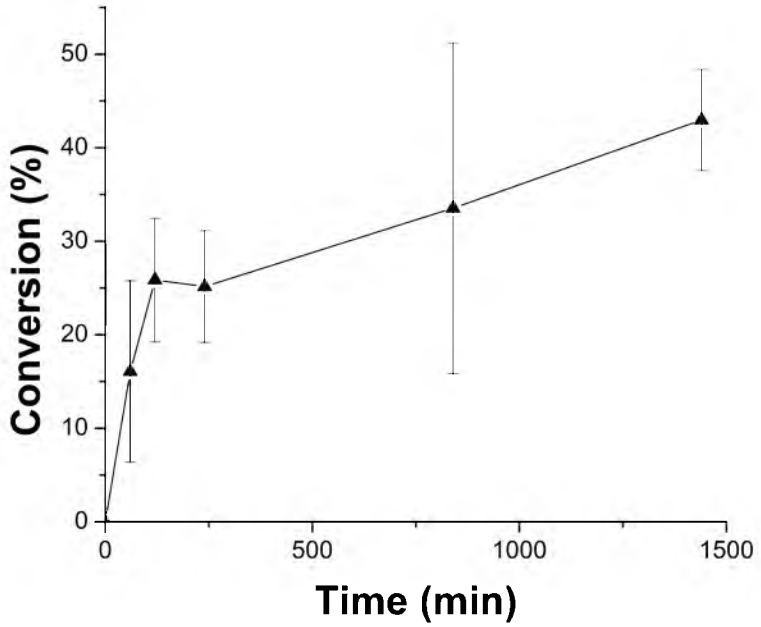

Figure 2.4 ATR-FTIR Study of 11.4 wt% PEG-dA complex coacervate. (A) Spectrum of acrylate group at 1415 cm^{-1} (↓ indicating peak of decreasing over time after polymerization. (B) Time course of PEG-dA conversion over 24 h. Error bars: ± s.d. (*n* = 3).

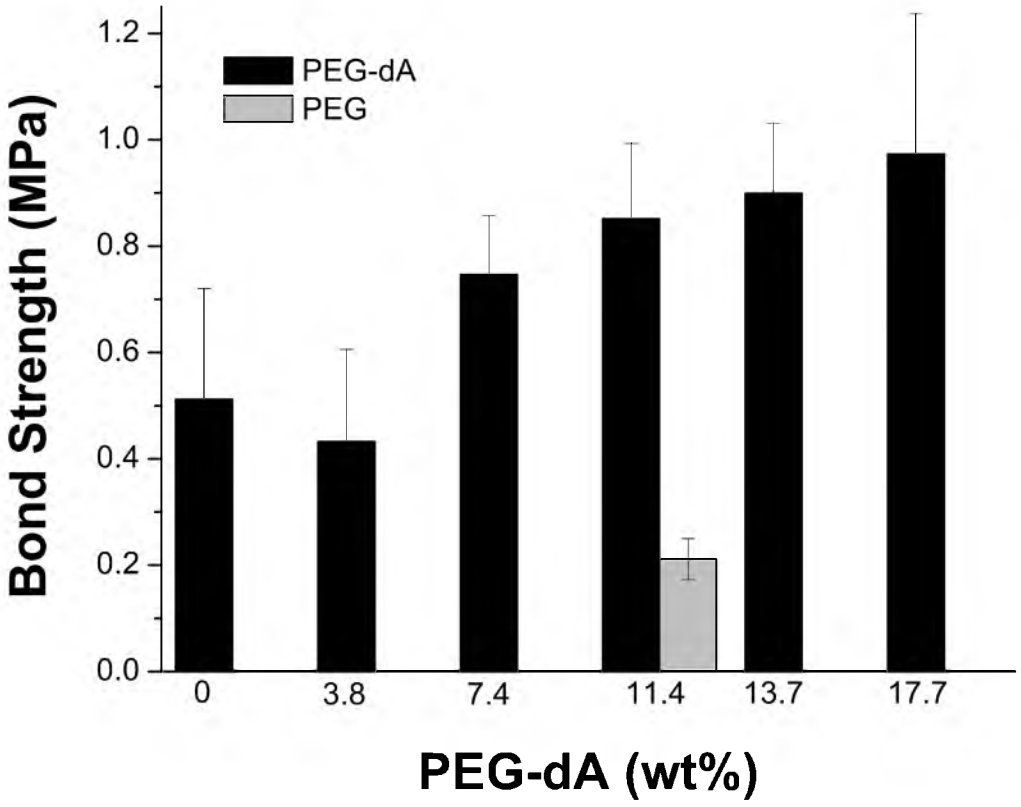

Figure 2.5 Shear bond strength of PEG-dA filled complex coacervates. The coacervate network was oxidatively cross-linked and PEG-dA polymerized by the simultaneous addition of $NaIO_4$ and APS/TEMED, respectively. Bonds were cured under water for 24 h at 25°C. Gray column: coacervate filled with 15 wt% nonacrylated PEG and cured with $NaIO_4$ and APS/TEMED. Error bars: ± s.d. (n = 5).

with 17.7 wt% PEG-dA. Maximum loads were ~1.2 MPa, more than four times higher than estimated bond strengths of the natural sandcastle glue [7] and mussel adhesive plaque byssal thread assemblies [11]. The shear modulus, approximately 25 MPa, was not statistically different between any of the PEG-dA concentrations. To confirm the increased bond strength was due to polymerization of PEG-dA, we formed coacervates with 15 wt% nonacrylated PEG (MW 400 g/mol) and treated with $NaIO_4$ and APS/TEMED. The underwater bond strengths were 211 +/- 39 kPa, less than 25% of the PEG/coacervate bond strengths.

The flow behavior is of critical importance for adhesives based on complex fluids such as coacervates. For medical applications, the viscosity should be sufficiently high at low shear rates that the adhesive does not flow away from the application site, yet low enough at high shear rates that it can be conveniently applied through a narrow gauge cannula, or catheter, without high pressure. At the same time, it is imperative to recognize shear-induced, irreversible structural transitions at high shear rates that may compromise cohesive bond formation. The viscosities of the adhesive complex coacervates containing 0 and 11.4 wt% PEG-dA were investigated as a function of shear rate using a cone and plate geometry (Figure 2.6). At low shear rates (0.01 s^{-1}) the viscosity of the 11.4 wt% PEG-dA filled coacervate (13.8 +/- 6.2 Pa s) was substantially higher than the complex coacervate with 0 wt% PEG-dA (0.9+/-0.1 Pa s). With increasing shear rate the PEG-dA-filled coacervates first thickened, then steadily thinned until a sudden 16-fold drop in viscosity occurred at a shear rate of 6 s^{-1} (Figure 2.6A). The shear thinning behavior was reversible; viscosity recovered with little hysteresis as the shear rate was decreased. The complex coacervate without PEG-dA shear thinned as

A)

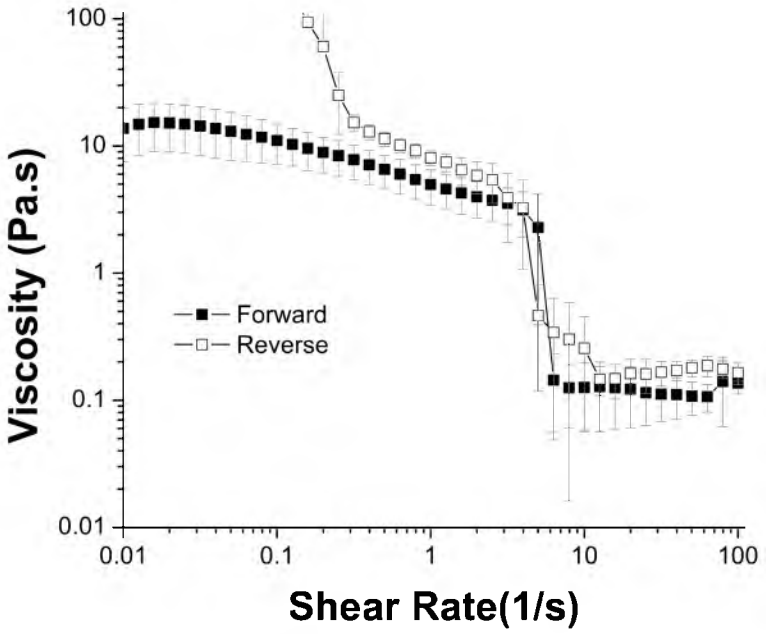

B)

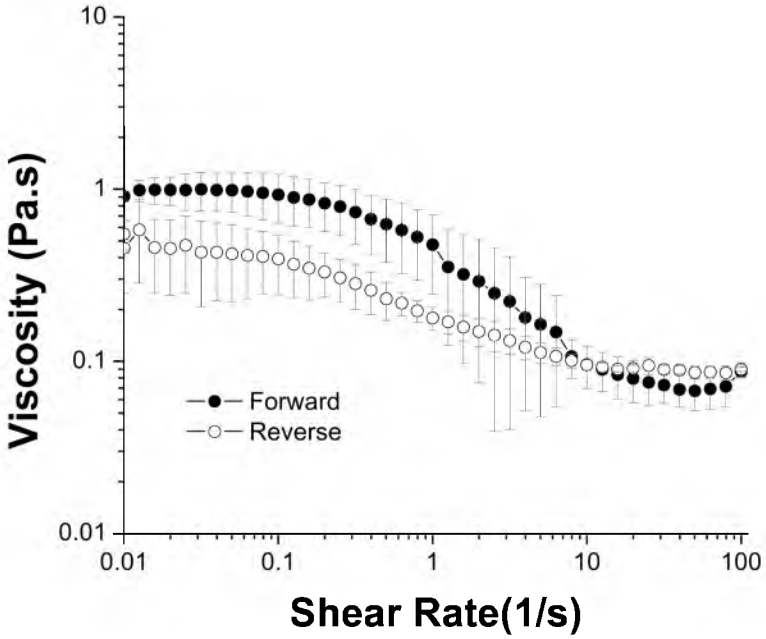

Figure 2.6 Flow curves of complex coacervates under steady shear. (A) Filled coacervates of 11.4 wt % PEG-dA: low to high shear rate (closed square) and high to low shear rate (open square). (B) Unfilled coacervate: low to high shear rate (closed circle), and reverse (open circle). Symbols and error bars are the average viscosity and s.d. at each shear rate of three independent coacervate samples.

well but did not display a similar sudden sharp drop in viscosity (Figure 2.6B).

The flow curves of the complex coacervate containing PEG-dA monomers are similar to other coacervate systems that have been investigated rheologically. Whey protein and gum arabic coacervates displayed a similarly abrupt shear-thinning transition that was accompanied by an increase in turbidity [12]. The transition was reversible. Polycation/mixed micelle coacervates, above a certain temperature, underwent a dramatic shear rate-dependent drop in viscosity before visibly phase separating [13]. In both cases, the visible changes suggest the abrupt shear-thinning events were due to microscale structural reorganizations of the interspersed phases of the complex coacervates. The quiescent nanoscale molecular structure of the complex coacervates were conceptualized as beads on compacted strings: globular whey proteins on gum arabic molecules in the first case, polyanionic mixed micelle beads on polyamine strings in the second case [14]. Abrupt shear thinning was attributed to shear-induced elongation of the beaded string structures, resulting in increased lateral intercomplex associations and coalescence of nanocomplexes into dense microphases.

The rich and complex flow behavior of the PEG-dA-filled coacervates suggests that similar shear-induced, reversible structural reorganization may occur within the PEG-dA filled coacervates. Unsheared complex coacervates with and without PEG-dA were frozen, lyophilized, and examined by scanning electron microscopy (SEM). The coacervates had a porous three-dimensional network of tubular structures (Figure 2.7) reminiscent of the sponge-like network of tubules observed in other complex coacervates by cryo-TEM [15]. There were no structural differences apparent between coacervates with and without PEG-dA monomers. Based on the flow behavior and SEM

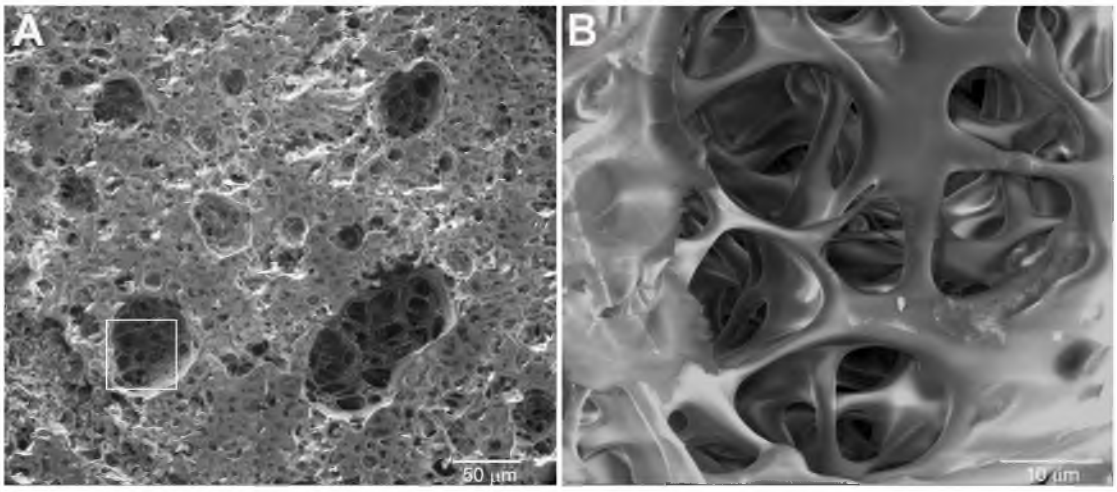

Figure 2.7 SEM Images of fractured surfaces of lyophilized complex coacervates. (A) 700x, (B) 5000x.

micrographs, a conceptual diagram of the PEG-dA-filled complex coacervate before and after the shear-induced structural transition is shown in Figure 2.8. The quiescent coacervate is pictured as a dense, interconnected, colloid-rich network interspersed within a watery, colloid-depleted network containing PEG-dA (Figure 2.8A). Above a critical shear rate, the interspersed networks may undergo shear-banding (Figure 2.8B), a phenomenon in which the components of a complex fluid phase separate into distinct bands under shear [16–18].

The practical significance of the shear thinning of the PEG-dA-filled coacervates is demonstrated in Figure 2.9, a still image from a supplemental video. A 11.4 wt% PEG-dA-filled coacervate was loaded into a 1 mL syringe fitted with a 27 gauge cannula. Despite the relatively high initial viscosity, it took little manual effort to eject a fine cohesive thread of the PEG-dA-filled coacervate under water. The shear rate during ejection was estimated to be 750 s^{-1}. The water-borne threads were denser than water, maintained their shape, and adhered where they contacted the glass surface. The coacervate also adhered when applied underwater to vertical glass surfaces. In principle, the coacervated threads, or any pattern of threads, can be cross-linked in place by coinjection of polymerization initiators. The ability to accurately deliver adhesive through a fine cannula or catheter will allow precise and less invasive repair of bone fractures [19] and other tissues.

2.5 Conclusion

In summary, the bond strength of the biomimetic adhesive coacervates was substantially improved to well above the estimated bond strength of natural bioadhesives by incorporating a second polymer network into the coacervate network. The viscous

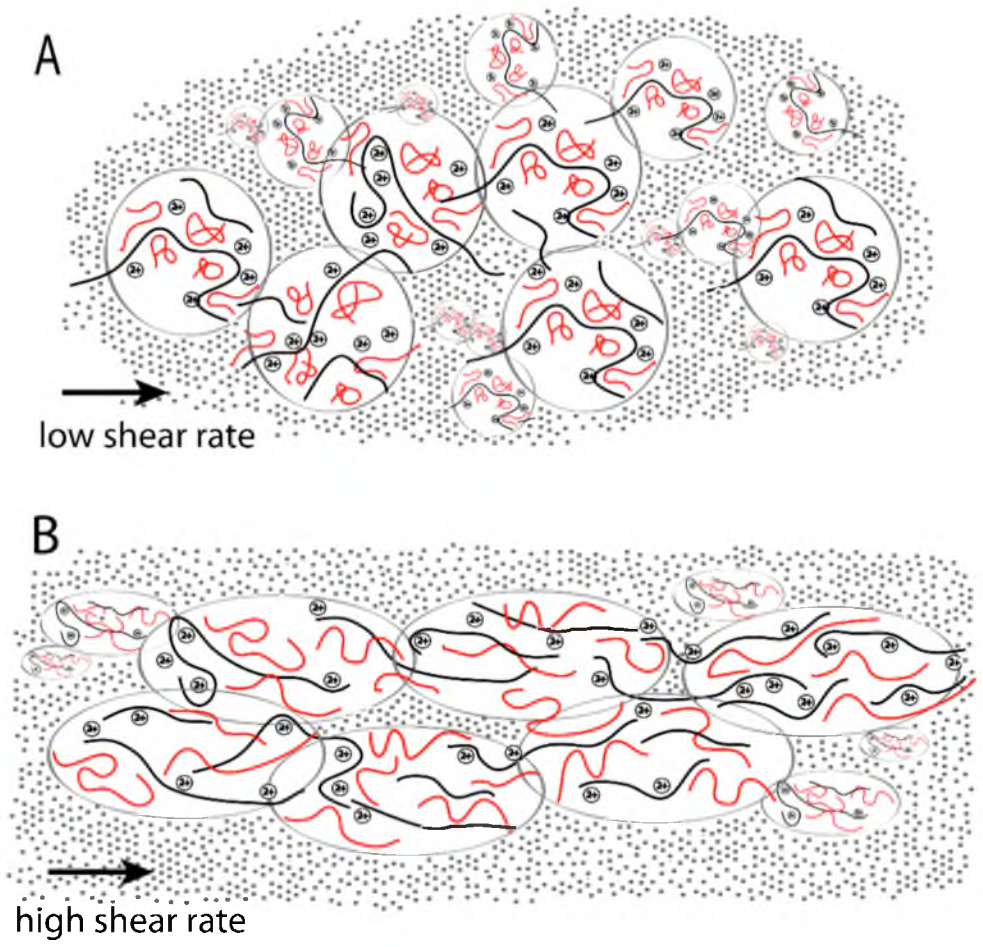

Figure 2.8 Conceptual diagram of the structure of the PEG-dA filled complex coacervate. (A) In the quiescent state, the electrostatically associated nanocomplexes form a fluid, interconnected, three-dimensional network. An aqueous phase containing PEG-dA is interspersed within the pores of the connected network of nanocomplexes. (B) At a critical shear rate, the nanocomplexes may be elongated leading to additional lateral interactions and a second, reversible macrophase separation.

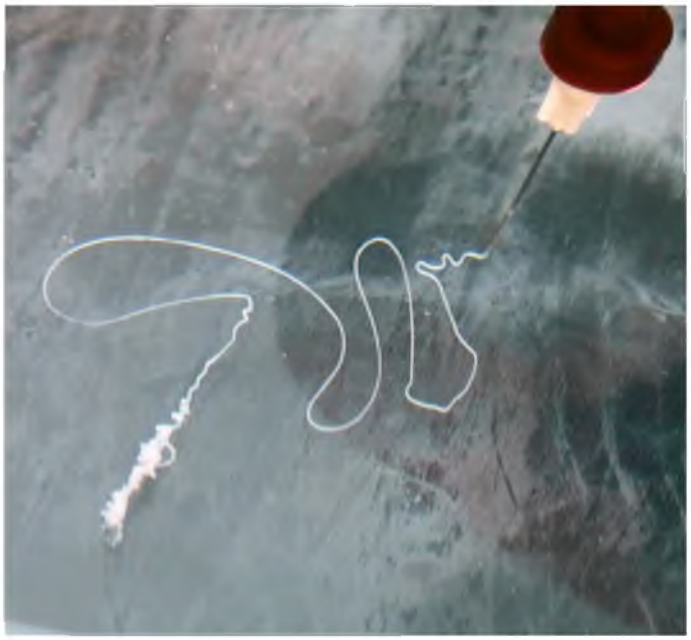

Figure 2.9 Image of a 11.4 wt % PEG-dA filled coacervate loaded into a 1 mL syringe with a 27 gauge cannula, being ejected under water.

PEG-dA filled coacervate could be easily ejected through a fine gauge cannula as a result of reversible shear thinning. The threads maintained their form underwater and adhered to wet glass surfaces. The successful incorporation of high concentrations of water-soluble monomers demonstrated that, in principle, almost any water-soluble molecule can be contained in a complex coacervate and precisely delivered in a wet environment, including noninvasive delivery into the body. Such properties merit further evaluation of the filled adhesive coacervates as injectable drug delivery depots in addition to their potential as wet field medical adhesives. Work in progress is focused on incorporating more and different types of nano- and microphases into complex coacervates to further improve underwater bond strengths.

2.6 References

1. R. A. Jensen and D. E. Morse, "The Bioadhesive of *Phragmatopoma Californica* Tubes: A Silk-like Cement Containing L-DOPA," *J. Comp. Physiol. B*, **158** [3] 317–324 (1988).

2. R. J. Stewart, J. C. Weaver, D. E. Morse, and J. H. Waite, "The Tube Cement of Phragmatopoma Californica: a Solid Foam," *J. Exp. Biol.*, **207** [26] 4727–4734 (2004).

3. H. Zhao, C. Sun, R. J. Stewart, and J. H. Waite, "Cement Proteins of the Tube-building Polychaete Phragmatopoma Californica," *J. Biol. Chem.*, **280** [52] 42938–42944 (2005).

4. H. Shao, K.N Bachus, and R. J. Stewart, "A Water-borne Adhesive Modeled After the Sandcastle Glue of P. californica," *Macromol. Biosci.*, **9** [5] 464–471 (2009).

5. H. Shao, and R. J. Stewart, "Biomimetic Underwater Adhesives With Environmentally Triggered Setting Mechanisms," *Adv. Mater.*, **22** [6] 729–733 (2010).

6. M. J. Stevens, R. E. Steren, V. Hlady, and R. J. Stewart, "Multiscale Structure of the Underwater Adhesive of Phragmatopoma Californica: A Nanostructured Latex With a Steep Microporosity Gradient," *Langmuir*, **23** [9] 5045–5049

(2007).

7. C. Sun, G. E. Fantner, J. Adams, P. K. Hansma, and J. H. Waite, "The Role of Calcium and Magnesium in the Concrete Tubes of the Sandcastle Worm," *J. Exp. Biol.*, **210** [8]1481–488 (2007).

8. A. J. Kinloch, J. H. Lee, and A. C. Taylor, "Toughening Structural Adhesives via Nano- and Micro-phase Inclusions," *J. of Adhesion,* **79** [8–9] 867–873 (2003).

9. R. P. Witte, A. J. Blake, C. Palmer, and W. J. Kao, "Analysis of Poly(ethylene glycol)-diacrylate Macromer Polymerization Within a Multicomponent Semi-interpenetrating Polymer Network System," *J. Biomed. Mater. Res.*, **71** [3] 508–518 (2004).

10. G. Kang, Y. Cao, H. Zhao, and Q. Yuan, "Preparation and Characterization of Crosslinked Poly(ethylene glycol) Diacrylate Membranes With Excellent Antifouling and Solvent-resistant Properties," *J. Membr. Sci.*, **318** [1–2] 227–232 (2008).

11. J. R. Burkett, J. L. Woitas, J. L. Cloud, and J. J. Wilker, "A Method for Measuring the Adhesion Strength of Marine Mussels," *J. Adhes.*, **85** [9] 601–615 (2009).

12. F. Weinbreck, R. H. Wientjes, H. Nieuwenhuijse, G. W. Robinjn, and C. G. de Kruif, "Rheological Properties of Whey Protein/Gum Arabic Coacervates," *J. Rheol.*, **48**, 1215 (2004).

13. P. L. Dubin, Y. Li, and W. Jaeger, " Mesophase Separation in Polyelectrolyte-mixed Micelle Coacervates," *Langmuir,* **24** [9] 4544–4549 [2008].

14. M. W. Liberatore, N. B. Wyatt, M. Henry, P. L. Dubin, and E. Foun, "Shear-induced Phase Separation in Polyelectrolyte/Mixed Micelle Coacervates," *Langmuir,* **25** [23] 13376–13383 (2009).

15. D. S. Hwang, H. Zeng, A. Srivastava, D. V. Krogstad, M. Tirrell , J. N. Israelachvili JN, and J. H. Waite, "Viscosity and Interfacial Properties in a Mussel-inspired Adhesive Coacervate," *Soft Matter,* **6**, 3232–3236 (2010).

16. R. Makhloufi, J. P. Decruppe, A. Ait-Ali, and R. Creesley, "Rheo-optical Study of Worm-like Micelles Undergoing a Shear Banding Flow," *Europhys Lett.*, **32** [3] 253–258 (1995).

17. P. Butler, "Shear Induced Structures and Transformations in Complex Fluids," *Current Opinion in Colloid and Interface Sci.*, **4** [3] 214–221 (1999).

18. H. A. Barnes, J. F. Hutton, and K. Walters, *An Introduction to Rheology*. Elsevier, Amsterdam, 1989.

19. B. D. Winslow, H. Shao, R. J. Stewart, and P. A. Tresco, "Biocompatibility of Adhesive Complex Coacervates Modeled After the Sandcastle Glue of Phragmatopoma Californica for Craniofacial Reconstruction," *Biomat.,* **31** [36] 9373–9381 (2010).

CHAPTER 3

FETAL MEMBRANE PATCH AND BIOMIMETIC ADHESIVE COACERVATES AS A SEALANT FOR FETOSCOPIC DEFECTS

3.1 Abstract

Iatrogenic preterm premature rupture of membranes after fetoscopic procedures affects 10–47% of patients, secondary to the nonhealing nature of membranes and the separation of layers during the entry. In this study we developed an in vitro model to mimic the uterine wall-fetal membrane interface using a water column with one end and sealed with human fetal membranes and poultry breast, and a defect was created with an 11 French trocar. In addition, a fetal membrane patch in conjunction with multiphase adhesive coacervates modeled after the sandcastle worm bioadhesive was tested for sealing of an iatrogenic defect. The sealant withstood an additional traction of 12 g for 30–60 minutes and turbulence of the water column without leakage of fluid or slippage. The adhesive is nontoxic when in direct contact with human fetal membranes in an organ culture setting. A fetal membrane patch with multiphase adhesive complex

---

This chapter is reorganized from a pre-peer-reviewed version of the following article: Reprinted from Acta Biomateria., 8(6), L. K. Mann, R. Papanna, K. J. Moise, R. H. Byrd, E. J. Popek, S. Kaur, S. C. G. Tseng, and R. J. Stewart, Fetal Membrane Patch and Biomimetic Adhesive Coacervates as a Sealant for Fetoscopic Defects, 2160–2165,

coacervates may help to seal the defect and prevent iatrogenic preterm premature rupture of the membranes.

3.2 Introduction

Iatrogenic preterm premature rupture of the membranes (iPPROM) after a fetal intervention procedure is a major complication that affects 10–47% of procedures [1–5]. iPPROM leads to an increased risk of preterm labor and worsens the perinatal mortality, undermining the true benefit of such interventions [6]. There are two possible explanations for the increased risk for iPPROM after invasive fetal procedures. One is the innate nonhealing nature of the fetal membranes, as demonstrated in both in vivo and in vitro studies [7,8]. The other is that separation of the amnion from the chorio-decidual layers that occurs during the introduction of instrumentation into the uterine cavity can cause a persistent parting of membranes with subsequent leakage of amniotic fluid [9]. There have been several attempts to study sealants at the site of the fetal membrane defect, both in vitro and in vivo [10–12]. However, there is no ideal in vitro model to simulate the relationship of the uterine wall, the fetal membranes, and the amniotic fluid environment. There is evidence to suggest that a decelluarized fetal membrane scaffold can promote cellular proliferation at the defect site [13]; however, no method to introduce a fetal membrane patch through a narrow operative cannula and deliver it to the site of the defect has ever been described. Additionally, after the patch has been deployed, the challenge of fixation to the membranes and the uterine wall remains due to the dynamic nature of the amniotic fluid and uterine musculature. An underwater adhesive that would fix a tissue scaffold to the edges of the defect in place for the remainder of the pregnancy would be an ideal solution to the problem iPPROM; however, no adhesive suitable for

this task is available.

Development of medical adhesives for the wet interior of the body is both chemically and biologically challenging. The adhesive must be delivered, bonded, and cured in the presence of moisture, must be nontoxic, and must not provoke a severe foreign body response. One approach to achieve underwater bonding is to study natural biological underwater adhesives, identify their key chemical features and copy that chemistry using nontoxic, biocompatible, and cost-effective synthetic polymers. Numerous aquatic organisms produce working underwater adhesives as part of their aquatic lifestyle to either position themselves in a suitable environment or to create a protective structure. The sandcastle worm, an intertidal marine polychaete (*Phragmatopoma californica*), produces a proteinaceous glue with which it joins together sand grains into a protective shell while fully submerged in seawater [14]. The proteins of the natural sandcastle glue are highly charged with opposite charges segregated into different proteins [15]. The polyacidic and polybasic nature of the glue proteins suggested complex coacervates—concentrated, phase-separated, associative polymer fluids—may be intermediates in natural bonding. Copying the side chain chemistry and molar ratios with synthetic poly(meth)acrylate copolymers resulted in adhesive complex coacervates that qualitatively replicated many of the features of the natural underwater adhesive [16]. Biodegradable versions [17] of the synthetic adhesive did not interfere with wound healing in a rat calvarial defect model [18]. Bond strength and other material properties were improved by introducing additional polymer networks into the adhesive coacervates [19].

In this study, we aimed to create an in vitro model to simulate the anatomical

relationship of the fetal membranes, uterine wall, and surrounding amniotic fluid. Using such a model, we introduced an iatrogenic defect in a similar fashion to that used in clinical fetal interventions. Furthermore, we tested a technique to introduce a fetal membrane patch through a cannula to the site of a defect and test its sealing capacity and evaluated the use of multiphase adhesive coacervates to adhere the fetal membrane patch to the defect. In addition, we examined the potential tissue cytotoxicity of the adhesive coacervates in an in vitro culture system.

3.3 Materials and Methods

3.3.1 Creating an In Vitro Uterine Model

The Institutional Review Board of Baylor College of Medicine, Houston, TX (#H-26110), approved the collection of human fetal membranes for the study. We created an in vitro uterine model using a filleted poultry breast and human fetal membranes. A 100 ml polypro cylinder (VWR International, West Chester PA) was cut at the base and the cut end was lipped using heat. The cylinder was then mounted on a stand. Fresh human fetal membranes were obtained from term vaginal deliveries and were transferred to the laboratory in a balanced salt solution (BSS). The fetal membranes were cut into 6-cm diameter patches and secured to the lipped end of the cylinder with the amnion facing towards the inside of the cylinder. A poultry breast was filleted to 1-cm thickness and pounded gently using a hammer to simulate the uterine wall musculature. A 6-cm diameter patch of poultry breast fillet was then wrapped over the fetal membranes on the cylinder and secured in place with a suture material. The column was filled using BSS.

3.3.2 Creating an Iatrogenic Defect

A defect in the fetal membrane through the poultry breast and the fetal membranes was created using an 18-gauge needle, followed by a guide wire (Cook® Urological Inc; Bloomington, IN, USA). Subsequently, an 11 French Teflon cannula (Cook® Medical Inc, Bloomington, IN, USA) was introduced over the guide wire using Seldinger's technique [20]. Then, the trocar was removed to leave the cannula in place. This entry method is identical to that used in most fetal intervention centers for fetal surgical procedures.

3.3.3 Technique to Introduce the Fetal Membrane Patch

Fetal membrane patches were supplied by Bio-Tissue, Inc. (Miami, FL) and processed in the same manner as described for human amniotic membrane currently used for ocular surface reconstruction [21]. Briefly, fetal membrane patches were placed on a nitrocellulose paper with the amniotic membrane facing up (for ease of handling). After being cut in a circular fashion to the desired size, they were lyophilized to reduce their thickness to facilitate their insertion into the cannula. Upon insertion, one edge of the membrane was removed from the paper and folded in half (Figure 3.1A). The center of the patch was lifted from the paper, and a 4-O Monocryl suture with a tapering needle (Ethicon Inc, San Angelo, TX) was passed through the center of the patch and a noose was tied (Figure 3.1B). The remainder of the patch was removed from the paper (Figure 3.1C). The needle was removed from the suture and the distal end was passed through a 9-French Teflon cannula while the self-check valve on the proximal end was removed using a knife. With gentle traction on the suture, the patch was retracted into the distal tip of the cannula (Figure 3.1D). The original trocar that was an integral part of the 9F

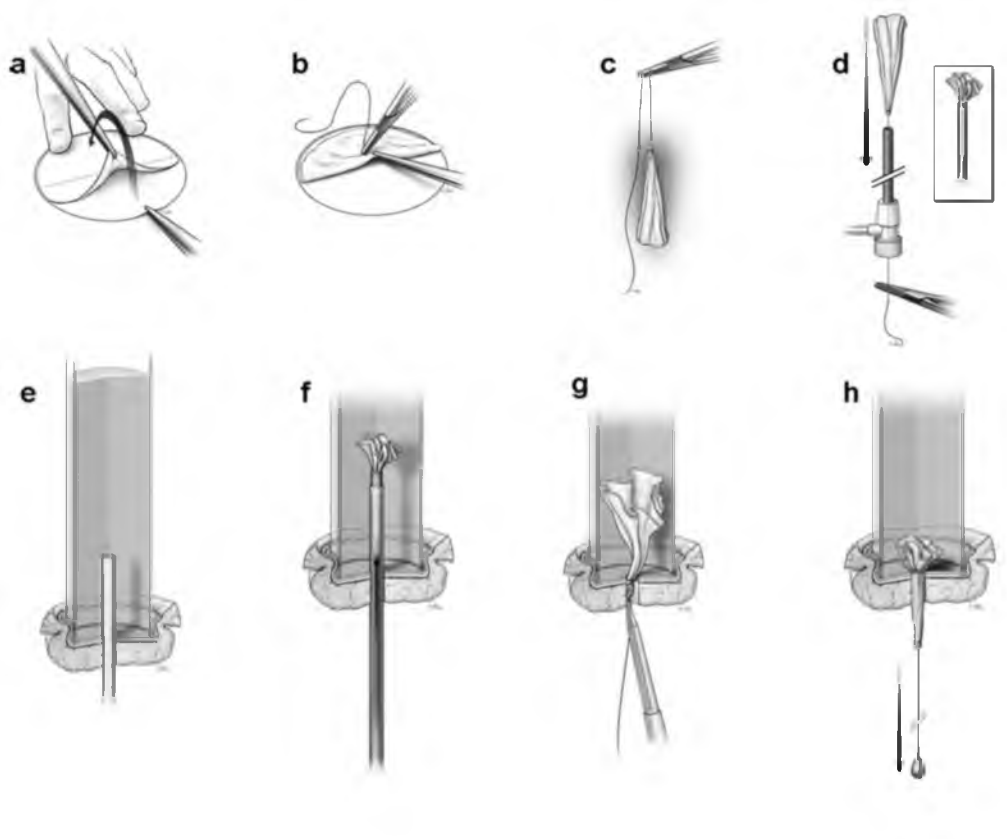

Figure 3.1 In vitro model for uterine wall and a fetal membrane patch for the defect. (A) The lyophilized amnion-chorion is lifted off of the nitrocellulose paper; (B) a 4-O Monocryl suture is passed through the center of the patch; (C) a noose is tied to the fetal membrane patch to form a firm knot; (D) the free end of the suture is passed through a 9-French cannula, to align the knot inside the cannula (insert); (E) an in vivo uterine model with an 11-French cannula in place; (F) the 9-French cannula carrying the fetal membrane patch is inserted through the 11-French cannula, and the patch is introduced into the fluid using a blunt plunger; (G) both cannulas are withdrawn and the patch is aligned to the effect, followed by glue is applied around the patch; (H) the patch and the glue are in place.

cannula was modified to serve as a blunt introducer. This blunt introducer was advanced from the proximal end of the cannula to abut the patch. Once the 11-French cannula had been introduced through the base of the in vitro model, the 9-French cannula containing the membrane patch was introduced through it. The column was filled to a height of 10 cm with BSS (Figure 3.1E). The patch was introduced into the fluid column advancing the blunt introducer. Once free within the fluid medium, the patch was allowed to swell for 2 minutes – a timescale that had been established for maximum swelling based on prior experiments (Figure 3.1F). Both cannulas were then withdrawn while keeping the suture and the patch in place. The suture was then withdrawn gently to position the patch in the defect so that the amnion faced the fluid medium mimicking the amniotic fluid while the chorion faced the poultry breast mimicking the uterine wall (Figure 3.1G).

3.3.4 Optimization of the Membrane Patch Size for Sealing

Triplicates of lyophilized fetal membrane patches were created as mentioned above, with diameters ranging from 1 to 5 cm to determine the minimum size necessary to seal the iatrogenic defect in the above in vitro model. These were used to determine the sealing strength that could withstand the dislodgement of the plug. A 25 cm height of fluid in the column was chosen to mimic the average intrauterine amniotic fluid pressure of 18 mm Hg that we had observed in patients with excess amounts of amniotic fluid (data not shown). We additionally applied 12 g of traction to the plug and created turbulence in the fluid by shaking the column multiple times in all directions to mimic the in vivo fluid dynamics.

3.3.5 Adhesive Complex Coacervate Formation

Polyethylene glycol diacrylate (PEG-dA, 760 Da, Aldrich) solutions were prepared in degassed, deionized water at the desired final concentration of 15 wt %. Poly(acrylamide-co-aminopropyl methacrylamide) (MW 288kDa, PDI 1.36) and poly (2-(methacryloyloxy)ethyl phosphate dopamine methacrylamide (MOEP-co-DMA, MW 64kDa, PDI 2.8) were then dissolved in separate PEG-dA solutions at final concentrations of 5 wt %. The poly(MOEP-co-DMA)-PEG-dA solution also contained a 0.2 M ratio of Ca^{2+} to phosphate side chains and 1 wt % nanosilica fillers (10 nm, Aerosil R 7200). The copolymer solutions were separately adjusted to pH 7.4 ± 0.2 with 6 M NaOH. The poly(acrylamide-co-aminopropyl methacrylamide)-PEG-dA solution was added dropwise while stirring to the poly(MOEP-co-DMA)-PEG-dA solution to a molar ratio of 0.6 amine side chains to phosphate side chains. Within a few minutes the complex coacervate settled out. The clear supernatant was removed.

The adhesive PEG-dA and nanosilica-filled coacervates were cross-linked through the *o*-DHP side chains of the polyphosphate with the amine side chains of the polyamine and/or by polymerizing PEG-dA. *o*-DHP was oxidized to initiate cross-linking by the addition of 1.0 M equivalents of $NaIO_4$ relative to the *o*-DHP sidechains. The rate of oxidative cross-linking was slowed by forming a reversible 1:1 complex between $NaIO_4$ and 1,2-O-Isopropylidene-D-glucofuranose (IPGF), as described previoulsy [22]. PEG-dA was polymerized by adding 3.5 mol % ammonium persulfate (APS) and 5.2 mol % N,N,N',N'-tetramethylethylenediamine (TEMED) at the same time as $NaIO_4$-IPGF.

Bond strengths of nanosilica-filled adhesive coacervates were tested in vitro on

aluminum adherends, as described previously for multiphase conplex coacervates [19]. Briefly, $NaIO_4$, APS, and TEMED were added to 20 μl of coacervates, which was then applied to a wet 0.5 x 5 cm cleaned and polished Al adhered. A wet Al was placed on the first with a 14–20 mm overlap, secured with a stainless steel clip and cured by submergence in water for 20–24 h at 37 °C. Four to six specimens were prepared for each test condition. The load to failure of the bonds was determined on a material testing system (Instron) with a 500 N load cell at a crosshead speed of 0.2 mm min^{-1}, while fully submerged in a temperature-controlled water bath at 37°C. In two separate experiments the loads were 524 ± 182 kPa (n = 5) and 698 ± 42 kPa (n = 3).

Bonding of the nanosilica-filled coacervates to aminiotic membranes was evaluated in vitro with fresh tissue cut into 1 cm × 6 cm patches. PEG-filled coacervates were prepared with and without nanosilica fillers. The coacervates (20μl) were applied to a 1 cm^2 area, then adhered to a second overlapping patch. The overlapped areas were pressed together under a 20 g weight for 60 min, then manually peeled apart from one end with forceps. The relative bond strengths of the coacervates were graded on a scale of 1–5, with 1 being the lowest bond strength and 5 being the highest. The nanosilica-filled adhesive coacervates formed substantially stronger bonds (4–5) with the amniotic membranes then the unfilled coacervates (1–2).

3.3.6 Sealing of the Defect with Adhesive Coacervates

After we identified the size of the patch that could seal the defect but slipped out at a water column of ≤ 10 cm height, we used that size for the remaining tests in conjunction with the glue. Four sets experiments were conducted with a different source

of fetal membrane at each time. The application of the glue to the patch was timed. The sealing strength of the glue was examined by adding the BSS solution to the column to 25 cm height and was further challenged by traction added to the patch with increments of 3 g (maxiumum of 12 g). If the patch held a weight of 12 g, we observed the experiment for 60 minutes (Figure 3.1H). Subsequently, the weights were removed and fluid turbulence was created by tilting the column in multiple directions for 5 min to evaluate for slippage of the glued plug.

3.3.7 In Vitro Cytotoxicity Test

The glue was evaluated for direct contact cytotoxicity on fresh term human fetal membranes obtained in a sterile fashion from three elective cesarean deliveries. These membranes were immediately transported to the laboratory in BSS with Pen-Strep (Gemini Bio-Products, West Sacramento, CA) sterilely cut into patches (2 x 2 cm) and placed in a six-well plate. In each test well, 200 µl of freshly prepared glue was applied over the amnion surface followed by the addition of 3 ml of Amniomax C-100 culture medium (Invitrogen Corporations, Carlsbad, CA). Membranes from control (n = 3) and test wells (n = 3) were harvested at 0, 24, and 48 h, fixed in 10% formalin, dehydration with 70% ethanol, embedded in paraffin, and sectioned for histological examination.

Slides were dewaxed, rehydrated, and digested in 0.02% trypsin solution and subjected to hematoxylin-eosin staining (H&E). TUNEL (terminal deoxynucleotidyle transferase dUTP nick end labelling) staining was also performed using ApopTag Peroxidase In Situ Apoptosis Detection Kit (Millipore, Billerica, MA). On the H&E slides, the overall morphological condition of the membranes was examined. In the TUNEL staining slides, the amniotic epithelial cells were counted in 10 high power fields

or until reaching 500 cell count per slide. The cytotoxicity was calculated by determining the ratio of apoptotic cells to total number of amniotic epithelial cells.

3.3.8 Statistical Analyses

Statistical analysis was performed using Wilcoxon's sum rank test for continuous variables and Fisher's exact test for categorical variables. A p-value of <0.05 was considered to be significant.

3.4 Results and Discussion

3.4.1 In Vitro Uterine Model With a Fetal Membrane Patch and Its Sealing Capacity Without Adhesive Coacervates

The in-vitro uterine model and the iatrogenic defect were created successfully. We created four identical models, with a flow rate of 100 cc over 20 s. A patch size of $\leq$ 2 cm did not seal the defect from the beginning, and the patches slipped out with a column height of 10 cm or above. A patch size of 3 cm started to leak fluid with a column height of 5–10 cm and failed completely with a water column of 25 cm. A patch size of 4 cm occluded the 11-French defect and was able to withstand a 25 cm column of fluid and 12 g of traction; when creating turbulence, two of the four patches were dislodged into the fluid column. A patch size of 5 cm did not fit into the 9-French cannula tip. Therefore, we chose a 3 cm lyophilized membrane for all subsequent adhesive coacervate experiments.

3.4.2 Sealing Test and Toxicity Testing With Adhesive Coacervates

As stated above, all four 3 cm patches began to exhibit leakage at a fluid column height between 5 and 10 cm without glue. The patches were dislodged spontaneously

once the height of the fluid column reached 20 cm in two cases and dislodged immediately after applying 3 g of traction in the other two cases. In contrast, with additional glue, none of the cases demonstrated any leakage at a fluid height of 25 cm. Furthermore, no leakage was observed upon challenge with 12 g of traction for 30 minutes in one experiment and 60 minutes in the other three (see Figure 3.2). The latter three cases also held the membrane patch in place even after turbulence created for 5 minutes. They were then harvested and sectioned through the center to examine the junction between the membrane patch and the poultry breast wall. The glue was present in most of the junction between the poultry breast and the fetal membrane defect. In situ examination of the patch showed that the glue was spread 360° between the patch and the defect, including the fetal membrane edges and the muscular wall.

Histological examination revealed that the glue-added experimental group did not show any signs of cytotoxicity at any of the three time points compared to controls. At time 0, the control exhibited 2.2% of TUNEL-positive apoptotic cells. At 24 hours, the experimental group demonstrated 2% apoptotic cells while the control showed 4.2% apoptotic cells ($p = 0.3$). At 48 hours, the experimental group had 0.2% apoptotic cells while the control had 1.6 % apoptotic cells ($p = 0.4$).

3.4.3 Discussion

To investigate the potential efficacy of sealants for an iatrogenic defect created during a fetoscopic procedure, we need a model that simulates the fetal membrane and the uterine wall as well as the fluid dynamics of a pregnant uterus. Additionally, the model should be able to test a sealant's capacity to occlude the defect and bind the fetal membrane to underlying layers to prevent leakage. In this regard, previously reported

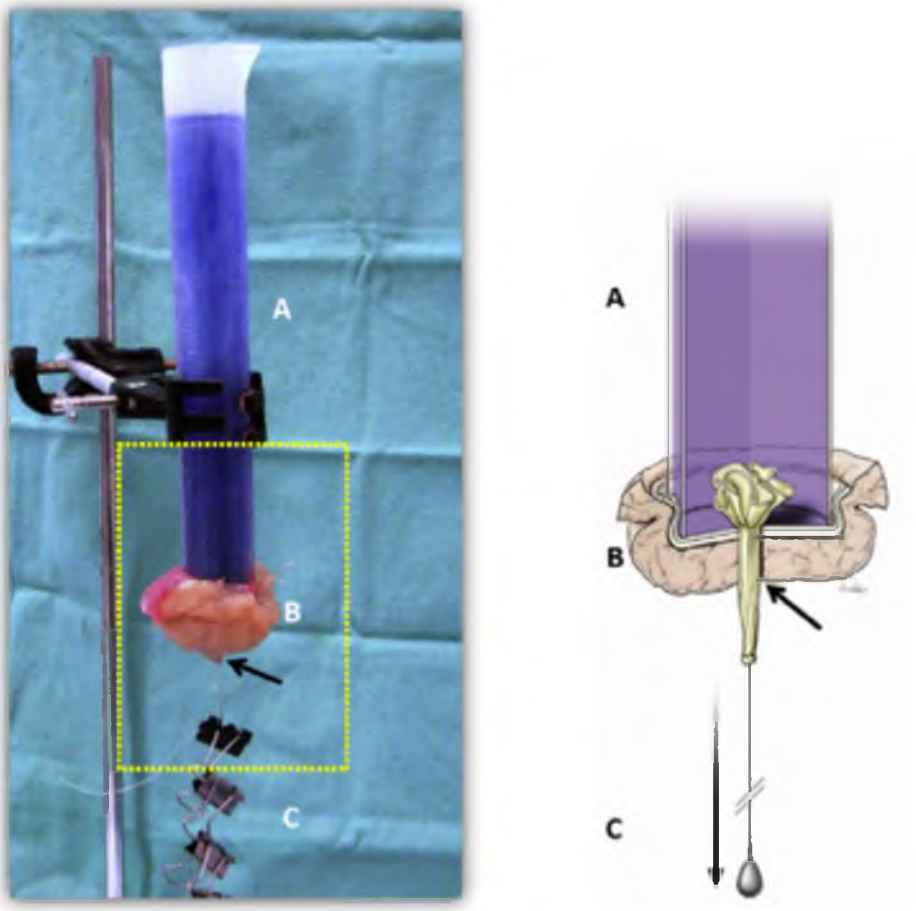

Figure 3.2 Fetal membrane patches sealing the defect with glue as an adhesive. The left image shows the experiment set-up for the in vitro uterine model. The illustration on the right shows the components of the model (dotted yellow line). (A) Fluid in a 100 cc column; (B) uterine wall simulation using fresh fetal membrane with the amnion facing the fluid column and the chicken breast on the outside; (C) traction of weight on the fetal membrane patch; → fetal membrane patch in the defect with glue between the patch and the defect wall.

models have not managed to reproduce these in vivo conditions. For example, Reddy et al. [23] used a 2.5 cm diameter 20 mL syringe with a human fetal membrane attached to the bottom lip. After creating a 20-gauge needle defect in the fetal membrane, various sealants were tested for their abilities to occlude the leakage without describing the height of the fluid column. Their model cannot address the issue of chorioamnion separation. Furthermore, their defect size was smaller than the 2–3 mm diameter that typically occurs after fetoscopic procedures. Suzuki et al. [11] also attached fetal membranes to the bottom of cylinder and applied a gradual pressure up to 100 mm H_2O using a water column. The defects created ranged from a pinhead hole to 5 and 10 mm slits. Because photocrosslinkable chitosan was applied as a sealant before adding fluid to the column, their model does not test the efficacy of the sealant in a fluid-filled environment. Bilic et al. [12] used a mechanical stretch device, the Cellerator, to study sealing of a 3.4 mm defect on a wet membrane with a "mussel inspired" PEG-based hydrogel. The efficacy of the glue to seal the defect was tested by stretching the membrane using the Cellerator. Their model also did not test the hydrogel in a fluid filled environment, and it remains unclear whether the mechanical stretching resembles the force caused by hydrostatic pressure. All three models did not consider binding of the fetal membrane to the underlying uterine wall, which is a likely solution to prevent iPPROM.

Our in vitro setting is a modified design of our previously published model [24], which was created to test the ability of a chicken ovomucin to seal a fetal membrane defect. The current model included a filleted chicken breast, simulating the uterine muscular layer, over the fetal membrane mimicking the natural anatomical relation. The aim of the model was to test the sealant's capacity to occlude and hold the membranes to

the muscular layer at the iatrogenic defect site. The model incorporates the biological and mechanical concerns leading to iPPROM. It is well known that the fetal membrane does not heal after an iatrogenic injury of greater than 2–3 mm in diameter, even up to 12 weeks after the injury [7]. The presence of a chorioamnion separation detected by ultrasound in nearly 25–30% of patients after a fetoscopic procedure increases the risk for iPPROM by 3- to 4-fold [9]. Because the absence of chorioamnion separation reduces the risk for iPPROM, we speculate that the binding of the two layers of the fetal membranes, the amnion to the chorion, is a critical step in preventing the leakage of fluid. This is why we included the filleted poultry breast and used its smoother surface facing the chorion layer of the fetal membrane to simulate the in vivo relationship between the uterine wall and the fetal membranes. An iatrogenic defect in the muscle and fetal membranes was created using Seldinger's technique, and the trocar was introduced in the same manner as it is introduced during clinical fetoscopic procedures. Our model therefore would be expected to produce similar stresses on tissue layers similar to those found in a clinical setting. Our method for introducing the patch through a narrower cannula is readily transferrable to a clinical application. The fetal membrane patch was designed in an "umbrella" shape, with an increasing thickness towards the amnioitc cavity. This helped to occlude the defect through a wedge effect by compressing the fetal membrane edges into the uterine wall to prevent chorioamnion separation. The pressure changes in a contractile uterus were simulated in our model by varying the height of the fluid column, while the traction challenge with fluid turbulence was added to simulate the complexity of uterine environment.

The fetal membrane patch used as a scaffold in our study was introduced with the

chorion facing the defect site and the amnion facing the fluid environment. Previous studies have shown that an amniotic membrane scaffold fabricated into a plug promoted cellular proliferation at the site of a fetal membrane defect in vivo over a 7-day period [10–13]. Mallik et al. [13] used a surgical plug from a term decellularized fetal membrane for closure of fetal membrane defect in midgestation rabbits, resulting in integration of the scaffold into the fetal membrane and uterine wall in 71% of cases, as evidenced by cellular proliferation. A 4-mm diameter fetal membrane patch was found to seal the defect site without glue, but 50% of the patches were dislodged from the defect site with fluid turbulence. The lyophilization of the fresh human fetal membranes in our study reduced the bulkiness of the scaffold, which helped in the delivery through a 9-French cannula. After being introduced into the fluid environment, the lyophilized fetal membrane took approximately 2–3 minutes to regain its thickness and was secured in place with the suture, giving rise to an "umbrella" shape that enhanced its sealing capability. It remains to be determined whether the use of such a fetal membrane patch as described herein will promote better healing because the chorion facing the defect site might promote local scarring and the amnion facing the amniotic cavity might help reepithelialization.

We also noted that the adhesive coacervates helped seal the defect when the fetal membrane was 3 mm in diameter even under weight traction and fluid turbulence. The glue was injected between the membrane patch and the defect in the poultry breast muscle layers directly with a short applicator. In future testing, the glue could be applied with an introducer placed through the main cannula via a percutaneous approach. The glue spread 360° around the patch and the muscular wall—a desirable effect for

preventing chorioamnion separation. A volume of 200–300 μL of glue was sufficient to seal the defect even in a water-filled environment. Future studies are needed to determine if the glue itself, or its degradative product, might be released into the amniotic cavity to generate any ill effect – although it did not cause apoptosis in the amniotic epithelium. We chose to assess only the amniotic epithelial damage, as the amnion is considered the most important layer to maintain the integrity of the fetal membrane [10, 25].

3.5 Conclusion

Collectively, our in vitro model has demonstrated that a lyophilized fetal membrane patch effectively occluded a model of an iatrogenic fetal membrane defect in an aqueous environment. The patch was more effective when used in conjunction with a nanosilica-filled adhesive coacervate. Further studies in live animal models are needed to evaluate the efficacy and durability of this fetal membrane patch and the adhesive coacervates to assist in preventing iPPROM.

3.6 References

1. J. C. Jani, K. H. Nicolaides, E. Gratacós, C.M. Valencia, E. Doné, J. M. Martinez, L. Gucciardo, R. Cruz, and J. A. Deprest, "Severe Diaphragmatic Hernia Treated by Fetal Endoscopic Tracheal Occlusion," *Ultrasound Obstet. Gynecol.,* **34** [3] 304–310 (2009).

2. R. Papanna, S. Molina, K. Y. Moise, K. J. Moise, and A. Johnson, "Chorioamnion Plugging and the Risk of Preterm Premature Rupture of Membranes After Laser Surgery in Twin-twin Transfusion Syndrome," *Ultrasound Obstet. Gynecol.,* **35** [3] 337–343 (2010).

3. R. Papanna, A. Johnson, R. T. Ivey, O. O. Olutoye, D. Cass, and K. J. Moise, "Laparoscopy-assisted Fetoscopy for Laser Surgery in Twin-twin Transfusion Syndrome With Anterior Placentation," *Ultrasound Obstet. Gynecol.,* **35** [1] 65–70 (2010).

4. M. V. Senat, J. Deprest, M. Boulvain, A. Paupe, N. Winer, and Y. Ville,

"Endoscopic Laser Surgery Versus Serial Amnioreduction for Severe Twin-to-twin Transfusion Syndrome," *N. Engl. J. Med.* **351** [2] 136–144 (2004).

5. A. Roman, R. Papanna, A. Johnson, S. S. Hassan, J. Moldenhauer, S. Molina, and K. J. Jr. Moise, "Selective Reduction in Complicated Monochorionic Pregnancies: Radiofrequency Ablation vs. Bipolar Cord Coagulation," *Ultrasound Obstet. Gynecol.* **36** [1] 37–41 (2010).

6. R. Papanna, S. Molina, K. Y. Moise, K. J. Moise, and A. Johnson, "Chorioamnion Plugging and the Risk of Preterm Premature Rupture of Membranes after Laser Surgery in Twin-twin Transfusion Syndrome," *Ultrasound Obstet. Gynecol.,* **35** [3] 337–343 (2010).

7. E. Gratacós, J. Sanin-Blair, L. Lewi, N. Toran, G. Verbist, L. Cabero, and J. Deprest, "A Histological Study of Fetoscopic Membrane Defects to Document Membrane Healing," *Placenta.* **27** [4–5] 452–456 (2006)

8. R. Devlieger, E. Gratacós, J. Wu, L. Verbist, R. Pijnenborg, and J. A. Deprest, "An Organ-culture for in Vitro Evaluation of Fetal Membrane Healing Capacity," *Eur. J. Obstet. Gynecol. Reprod. Biol.,* **92** [1] 145–150 (2000).

9. R. Papanna, L. K. Mann, A. Johnson, H. Sangi-Haghpeykar, and K. J. Jr. Moise, "Chorioamnion Separation As a Risk for Preterm Premature Rupture of Membranes After Laser Therapy for Twin-twin Transfusion Syndrome," *Obstet. Gynecol.* **115** [4] 771–776 (2010).

10. Devlieger R., L. K. Milar, G. Bryant-Greenwood, L. Lewi, and J. A. Deprest, "Fetal Membrane Healing After Spontaneous and Iatrogenic Membrane Rupture: A Review of Current Evidence," *Am. J. Obstet. Gynecol.* **195** [6] 1512–1520 (2006).

11. K. Suzuki, M. Shinya, and M. Kitagawa, "Basic Study of Healing Injuries to the Myometrium and Amniotic Membrane Using Photocrosslinkable Chitosan," *J. Obstet. Gynaecol. Res.,* **32** [2] 140–147 (2006).

12. G. Bilic, C. Brubarker, P. B. Messersmith, A. S. Mallik, T. M. Quinn, C. Haller, E. Done, L. Gucciardo, S. M. Zeisberger, R. Zimmermann, J. Deprest, and A. H. Zisch, "Injectable Candidate Selants for Fetal Membrane Repair: Bonding and Toxicity in Vitro," *Am. J. Obstet. Gynecol.,* **202** [1] 85 (2010).

13. A. S. Mallik, M. A. Fichter, S. Rieder, G. Bilic, S. Stergioula, J. Henke, K. T. Schneider, J. Kurmanavicius, E. Biemer, R. Zimmermann, A. H. Zisch, and N. A. Papadopulos, " Fetoscopic Closure of Punctured Fetal Membranes With Acellular Human Amnion Plugs in a Rabbit Model," *Obstet. Gynecol.,* **110** [5] 1121–1129 (2007).

14. R. A. Jensen, and D. E. Morse, "The Bioadhesive of *Phragmatopoma Californica* Tubes: A Silk-like Cement Containing L-DOPA," *J. Comp. Physiol. B*, **158** [3] 317–324 (1988).

15. H. Zhao, C. Sun, R. J. Stewart, and J. H. Waite, "Cement Proteins of the Tube-building Polychaete Phragmatopoma Californica," *J. Biol. Chem.*, **280** [52] 42938–42944 (2005).

16. H. Shao, K.N Bachus, and R. J. Stewart, "A Water-borne Adhesive Modeled After the Sandcastle Glue of P. Californica," *Macromol. Biosci.*, **9** [5] 464–471 (2009).

17. H. Shao, and R. J. Stewart, "Biomimetic Underwater Adhesives With Environmentally Triggered Setting Mechanisms," *Adv. Mater.*, **22** [6] 729–733 (2010).

18. B. D. Winslow, H. Shao, R. J. Stewart, and P. A. Tresco, "Biocompatibility of Adhesive Complex Coacervates Modeled After the Sandcastle Glue of Phragmatopoma Californica for Craniofacial Reconstruction," *Biomat.*, **31** [36] 9373–9381 (2010).

19. S. Kaur, G. M. Weerasekare, and R. J. Stewart, "Mutliphase Adhesive Coacervates Inspired by the Sandcastle Worm," *ACS Appl. Mater. Interfaces.*, **3** [4] 941–944 (2011).

20. S. I. Seldinger, "Catheter Replacement of the Needle in Percutaneous Arteriography; A New Technique," *Acta. Radiol.* **39** [5] 368–376 (1953).

21. J. Liu, H. Sheha, Y. Fu, L. Liang, and S. C. Tseng, "Update on Amniotic Membrane Transplantation," *Expert Rev. Ophthalmol.*, **5** [5] 645–661 (2010).

22. H. Shao, G. M. Weerasekare, and R. J. Stewart, "Controlled Curing of Adhesive Complex Coacervates With Reversible Periodate Carbohydrate Complexes," *J. Biomed. Mater. Res.* (2011).

23. U. M. Reddy, S. S. Shah, R. L. Nemiroff, S. K. Ballas, T. Hyslop, J. Chen, R. J. Wapner, and A. C. Sciscione, "In Vitro Sealing of Punctured Fetal Membranes: Potential Treatment for Midtrimester Premature Rupture of Membranes," *Am. J. Obstet. Gynecol.* **185** [5] 1090–1093 (2001).

24. H. Mendez-Figueroa, R. Papanna, D. L. Berry, and K. J. Jr. Moise, "Precipitated Egg White as a Selant for Iatrogenic Preterm Premature Rupture of the Membranes," *Am. J. Obstet. Gynecol.* **202** [2] 191 (2010).

25. H. Niknejad, H. Peirovi, M. Jorjani, A. Ahmadiani, J. Ghanavi, and A. M.

Seifalian, "Properties of the Amniotic Membrane for Potential Use in Tissue Engineering," *Eur. Cell. Mater.* **15**, 88–99 (2008).

CHAPTER 4

SYNTHESIS OF METHACRYLATED POLYPHOSPHATE AND POLYAMINE POLYMERS AND ADHESIVE COMPLEX COACERVATE FORMATION

4.1 Abstract

A stable complex coacervate adhesive was developed for long-term use in practical applications by modifying the chemistries of copolyelectrolytes. Two oppositely charged polymers, polyphosphate and polyamine, were synthesized with methacrylated group side chains as a new cross-linking system. Aqueous polymerization and grafting methods were carried out to improve biocompatibility of the final polymer. The polyamine polymer was synthesized by reversible addition-fragmentation chain transfer (RAFT) reaction to obtain a controlled molecular weight. Cross-linking kinetics were tailored by targeting specific methacrylation groups on each polymer. Complex coacervate range was explored by varying the polyamine to polyphosphate ratio for two different polyphosphate polymers. Coacervate concentration, flow behavior, and net charge varied depending on the polyamine to polyphosphate ratio. Nuclear magnetic resonance (NMR) was conducted on the varied polymer ratio coacervates to determine the actual charge on the adhesives. Viscosity measurements were made on the rheometer for flow behavior of the coacervates as well as a stability study of the adhesive for a month.

4.2 Introduction

The concept of complex coacervates was first introduced by Bungenberg de Jong in 1929 [1]. Complex coacervation occurs when two oppositely charged polyion solutions separate spontaneously upon mixing into two immiscible liquid phases. Both coacervate (dense) and a supernatant (dilute) liquid phase result, and both contain the two polyions [2]. Bungenberg explained that these phases were in thermodynamic equilibrium, and the formation was dependent on many factors like pH, temperature, concentrations, ionic strength, and molecular weight of the polyions. The term "complex coacervates" is defined as a system where two macropolyanions exist in a single solvent with formation of two phases. Following their work on gelatin/acacia coacervation, theoretical concepts on coacervation were being developed by Voorn-Overbeek [3–5] and Veis-Aranyi [6]. Voorn-Overbeek theory believed that a distributed electrostatic interaction allows coacervation to spontaneously exist, whereas Veis-Aranyi argued that entropy gain and rearrangement of oppositely charged polyions upon aggregation drives coacervation; these interactions can take hours to days to form coacervates. The contradiction in these theories and many more that followed occur because of the different type of coacervate systems that each studied. Over the years a lot of research has been underway to understand the coacervation phenomena especially due to it occurring naturally in biological environments [6]. The theories and its understanding were limited until the last decade, where improved techniques and characterization tools have aided in a better understanding [7–8].

Today ranges of examples of complex coacervates exist in nature in conjugation to synthetically derived coacervates used in applications [9–14]. Coacervates are found in

applications of adhesives, coatings, biotechnology, and water purification systems [9]. These applications have played a key role behind the motivation to study the mechanism of coacervation and factors that impact it. Characterization techniques like dynamic light scattering (DLS), turbidity, rheology, and AFM have helped understand the mechanism behind these systems better [10–13]. Phase diagrams and viscoelastic behavior of coacervates to interfacial tension have all led to a better understanding of how coacervates are formed and aid in tailoring these properties to unlimited applications in the future.

There is a lot that can be learned from nature about the coacervate phenomena. Relative to our studies is the sandcastle worm underwater adhesive (*Phragmatopoma californica, a marine polychaete*) [15–17]. The sandcastle worm has a unique way of constructing composite mineralized shells that it lives in by binding sand grains and shells from aquatic environments. It does this by small amounts of underwater adhesive that it naturally secretes. This natural adhesive formed by the complex coacervation method is able to withstand strong forces in the ocean and tackle the adhesion of sand grains under aqueous conditions. These natural underwater adhesives are being studied in order to come up with solutions for synthetic adhesives [18–21]. The worm glue contains oppositely charged proteins, phosphates and amines, and divalent cations that form into a complex coacervate adhesive [16–17]. Research of the sandcastle worm led us to a biomimetic adhesive complex coacervate that mimicked the chemistries of the worm glue [18–21]. Copolyelectrolytes of oppositely charged phosphates and amines were synthesized, and when mixed under the set conditions a complex coacervate formed. The beauty of this adhesive lies in that it forms in water where the dense coacervate

(adhesive) phase sinks to the bottom, it is immiscible in water, and adheres to wet surfaces where it stays in place underwater. The natural worm glue is chemically cross-linked by 3,4-dihydroxy-L-phenylalanine (DOPA). The pH-triggered solidification occurs within seconds of its secretion from the worm. The synthetic version of this biomimetic was also cross-linked using DOPA residues on the synthetic polymeric chains [19–22].

Our current research is focused on developing a synthetic underwater adhesive targeted for medical applications, in particular soft tissue adhesion [22]. These biomimetic adhesives are advantageous because they can build on the natural phenomena and yet have highly tunable physical and mechanical properties [23]. With an application in mind, the biomimetic can be tailored to the needs of a commercial products. In the past we targeted high strength injectable multiphase adhesive coacervates for biomedical applications and attained our goals of a high strength deliverable adhesive through a fine cannula [21]. From the prospect of a commercial product, these adhesives need to be stored and be stable for extended periods of time in order to sustain its key properties until delivery to the site. The DOPA is well known to play a key role of cross-linking precursor [24–25], but its drawback lies in the oxidation of DOPA over time, leading to unstable and uncontrolled cross-linking of the adhesive taking place. Although many studies are underway to control the curing of DOPA mediated adhesives [26], tackling the problem of a stable adhesive for time periods of days is tricky. From an industrial standpoint, packaging and delivery of these adhesives play as much of a role as the product itself. These synthetic complex coacervates are unique, such that the polymeric backbones can be modified to meet the needs of the applications without losing the base

concept of coacervation. This chapter is focused on modifying the synthetic polymeric backbones to incorporate a new cross-linking system that is more stable, controlled, and yet still meets the standards of a practical adhesive.

Putting vinyl groups on macromolecules is a well-known strategy for cross-linking polymers. Both polymers in the synthetic complex coacervates were modified to incorporate reactive vinyl bonds. For the phosphate polymer, a carbon-carbon π-bond was incorporated into the structure via glycidyl methacrylate (GMA) [27–30]. Grafting with GMA in aqueous environments [30] is advantageous to our water-soluble polymers. The polymer gains more flexibility and longer chains from the GMA grafting. The amine polymer synthesized by aqueous RAFT (reversible addition-fragmentation chain transfer) polymerization [31–33] and incorporated the vinyl bond by reacting MAA (Methacrylic acid) and EDC (1-Ethyl-(3-dimethylaminopropyl) carbodiimide hydrocholoride).

In this chapter, we describe the method of synthesizing and methacrylating the two copolyelectrolytes used in complex coacervate systems. The coacervation system for a range of polymeric ratios and pHs were studied. The storage stability and coacervate adhesive properties are evaluated.

4.3 Materials and Methods

4.3.1 Materials

All reagents were used without further purification unless noted otherwise. Phosphorous oxychloride ($POCl_3$, 98%), 2-hydroxyethylmethacrylate (HEMA, 97%), and triethylamine (99%) were purchased from VWR. The 4-Methoxy phenol was purchased from TCI. Methacrylic acid (MAA) was purchased from VWR and 2,2'-azobisisobutyronitrile (AIBN) from Polysciences. Inhibitor removing resin was

purchased from Alfa Aesar. Glycidyl methacrylate(GMA) was purchased from Sigma Aldrich. Ultra filters Pellicon Ultracel Membranes (10 KDa) by Millipore were used. N-(3-Aminopropyl) Methacrylamide Hydrochloride and Acrylamide (Chemzymes, ultra pure) was purchased from Polysciences. 2,2'-Azobis(2-(2-imidazolin-2-yl) propane) dihydrochloride (VA-044) was purchased from Wako. EDC (1-Ethyl-(3-dimethylaminopropyl) carbodiimide hydrocholoride, anhydrous, 99.9%) was purchased from Chem-Impex Int. PEG-dA (Polyethylene glycol diacrylate, 540 Da was purchased from Sigma-Aldrich.

4.3.2 Polyphosphate Monomer Synthesis

The monomer 2-(methacryloyloxy)ethyl phosphate (MOEP) was synthesized by adding $POCl_3$ (16.8g, 110 mmol) under flowing argon to a stirred solution of HEMA (12g, 92 mmol) in dry toluene (340 ml). The reaction mixture was cooled to 0°C, and triethylamine (39 ml, 276 mmol) was added slowly. The reaction proceeded at 0°C for 10 minutes, then at room temperature for 2 hours. The white solid precipitate was recovered by filtration. Water (240 ml) was added to the cooled filtrate at 0°C and stirred at room temperature for 2 hours. The two layers were separated and the aqueous phase acidified, then extracted with THF: Ether (1:2, 8×110 ml). The organic phases were combined, dried over anyhydrous Na_2SO_4, and solvent evaporated to obtain the product as a pale yellow oil (67%, 12.2g). Inhibitor 4-methoxy phenol (1000 ppm) was added to the MOEP monomer and stored at -20°C. ^{1}H NMR spectroscopy (400 MHz, D_2O) d 1.7 (3H, s), 4.0 (2H, m, POCH_2), 4.2 (2H, m, $POCH_2CH_2$), 5.5 (1H,s) 6.0 (1H, s); ^{13}C NMR (75 MHz, D_2O) d 17.4, 64.2 (d, $^2J_{POC}$ = 8.3 Hz), 64.4 (d, $^3J_{POCC}$ = 5.5Hz), 127.2, 135.6, 169.4; ^{31}P NMR (120 MHz, D_2O) d 0.97 (s).

4.3.3 Polyphosphate Copolyelectrolyte Synthesis

Poly(MOEP-co-MAA) was synthesized by free radical polymerization of MOEP and MAA. Inhibitor removing resin was used to remove the inhibitor from the MOEP and MAA before starting the polymerization. The comonomers were dissolved in methanol and purged with argon for 30 minutes. Recrystallized AIBN dissolved in methanol was purged separately. Reaction mixture was then brought to a temperature of 55°C on oil bath before AIBN was added to initiate the polymerization. The reaction took place overnight for 16 hours and cooled to room temperature. The Poly(MOEP-co-MAA) was precipitated from methanol using acetone, and a gummy white polymer remained. The polymer was washed two more times with acetone to remove residual monomers. Two types of polyphosphate polymer were formed: 70 MOEP polymer starting out with 85 mol% MOEP, and 40 MOEP polymer starting out with 55 mol% MOEP.

The Poly(MOEP-co-MAA) was chemically modified by GMA, modifying the MAA side chain. Varied amounts of methacrylated polymers were made depending on the degree of MAA in the copolymer. The precipitated polymer was dissolved (15 g) in 100 mL of DI water. GMA (MAA mol%, 10X excess) was added to vigorously stirring polymer solution at room temperature overnight. The Poly(MOEP-GMA) was purified on ultrafilters with MWCO of 10 kDa. Purified polymer was stored as salt at pH 7.2, freeze-dried, and stored at -80 °C.

4.3.4 Polyamine Copolyelectrolyte Synthesis

Poly(acrylamide-co-aminopropyl methacrylamide) was synthesized by aqueous RAFT polymerization of acrylamide and N-(3-amino-propyl) methacrylamide

hydrochloride. A water-soluble RAFT chain transfer agent (CTA, Figure 4.1)[1] [34] was synthesized and used in this polymerization along with VA-044 as the initiator. The degree of polymerization (DP) was calculated to be the set $MW/([M1]_0 + [M2]_0)$. The [CTA] was the total moles of monomer/DP. The CTA to initiator ratio was set to [CTA] to $[I_0]$ of 5:1. All reagents were dissolved in water (5 mL for every gram of reagent) and purged for 30 minutes in Argon. The polymerization took place at 60 °C overnight. The copolymers were purified by dialysis (MWCO 12 kDa) for 3 days and freeze dried. Two different polyamine polymers were polymerized: 75 mol % acrylamide with 25 mol % N-(3-amino-propyl) methacrylamide hydrochloride and 60 mol % acrylamide with 40 mol % N-(3-amino-propyl) methacrylamide hydrochloride with molecular weight of 30 KDa.

The Poly(acrylamide-co-aminopropyl methacrylamide) was chemically modified by MAA and EDC. The polymer was dissolved in DI H_2O at a concentration of 30 mg/ml. In the 25% amine content 5% amines were targeted to be methacrylated, which led to the ratio of 5% amines to MAA of 1:1, and MAA to EDC of 1 to 1.2. To get the targeted methacrylation, 5X excess MAA and EDC was added. To the dissolved polymer, MAA was added and pH rose to 5 using 6 M NaOH. EDC was then added to the reaction flask stirring at room temperature. The final pH was adjusted to pH 5.5 and stirred the reaction overnight at room temperature. The methacrylated amine polymer was then dialyzed for 3 days and freeze-dried and stored at -80 °C until use.

4.3.5 Copolymer Characterization

The molecular weight of the copolymers was determined by size exclusion chromatography (SEC, AKTA FPLC) in 20 mM phosphate and 500 mM NaCl (pH 7.4)

[1] Achille Mayelle Bivigou-Koumba synthesized the water soluble CTA.

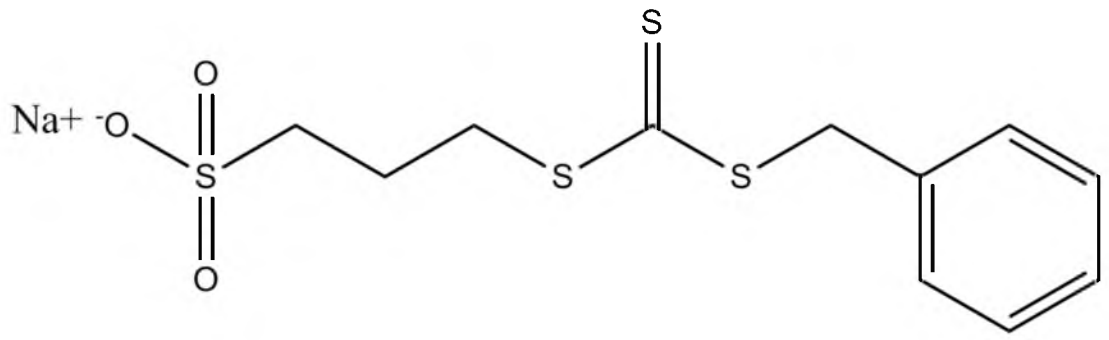

CTA Water Soluble MW = 374.54

Figure 4.1 Water-soluble RAFT chain transfer agent.

on column Superdex 210/300 GL (GE Healthcare). The columns were calibrated with polymethacrylate standards. The RAFT amine molecular weight was also measured using UV-vis (Perkin Elmer, Lambda Bio 20) absorption [35].

A Mercury Varian 400 MHz NMR spectrometer was used to characterize the polymers. ^{1}H NMR (collection of 32 scans with a relaxation delay of 1.0 second) was able to quantify the amount of side chains on the polymers. Phosphorous-31 NMR was helpful in measuring the purity of the MOEP monomer. All the polymers were dissolved in Deuterium oxide (D_2O) and run on NMR at a concentration of 10 mg/mL. Ninhydrin assay [26] was also used to compare the content of amine to NMR.

A Dynamic Titrator (Metrohm 808 Titrando) was used to carry out titrations of the monomer and polymers to determine the pKa's.[2] To titrate the phosphate, 0.005 M NaOH solution was used and for the amine, 0.15 M NaOH. Raw titration data were processed using a Gaussian moving average smoothing function in Matlab. PKa's of the molecules were taken to be the pHs at the graphical inflection points as determined by a second derivative function in Matlab.

4.3.6 Complex Coacervate Formation

Methacrylated Poly(MOEP-co-MAA) and methacrylated Poly(acrylamide-co-aminopropyl methacrylamide) were dissolved separately in 150 mM aqueous NaCl solution at a concentration of 50 mg/mL polymeric solution. The copolymer solutions were adjusted to correct pH with NaOH, to pH 7.2 or pH 8.2. The poly(acrylamide-co-aminopropyl methacrylamide) solution was added dropwise while stirring to the poly(MOEP-co-MAA) solution to a set molar ratio of amine side chains to phosphate

[2] Oscar V. Jasklowski carried out the titration of the monomer and polymers.

side chains (A/P). In less than a minute a turbid coacervate settled out of solution. The coacervate was allowed to phase separate from the supernatant over a set time interval before being used for further analysis.

4.3.7 Complex Coacervate Characterization

Concentration of coacervates was measured on coacervates ripened for 24 hours at pH 7.2 for 70 MOEP and 40 MOEP polymers, and pH 8.2 for 70 MOEP polymers. Varied A/P ratios ranging from 0.1 to 1.3 and 0.1 to 2.5 were made to see the coacervation range. The coacervates formed within the range were separated into coacervate and supernatant phases. The coacervates and the supernatant were freeze-dried to measure the dry mass. The volume was measured from the images of the coacervate study. The concentration in mg per mL was measured at each ratio.

4.3.8 Complex Coacervate NMR Ratio Study

NMR study of the complex coacervates at various theoretical A/P ratios was conducted for 70 MOEP (pH 7.2 and pH 8.2) and 40 MOEP (pH 7.2) polymers. The coacervates were formed in 150 mM NaCl solution made in D_2O and ripened for 24 hours. The supernatant phase was removed and the coacervates were redissolved in 1M NaCl solution made in D_2O. The dissolved coacervates in D_2O salt were then run on ^1H NMR. Using the NMR scans, the A/P ratio of the coacervates was determined.

4.3.9 Dynamic Rheology

Flow experiments were conducted on stress-controlled Rheometer (TA instrument, AR 2000 ex) using a 20 mm 4° cone geometry, gap 114 μm, at 25°C with

150 μL coacervate samples. Coacervates were ripened for 24 hours. Viscosity of the uncross-linked coacervates at shear rate of $0.01(s^{-1})$ was measured (Peak hold, 24 data points per 2 minutes) at 25°C. For the Ripening study, coacervates were also formed and tested the same way after set time intervals. An average of three independently prepared coacervate samples were measured for each A/P ratio.

4.4 Results and Discussion

4.4.1 Polyphosphate Synthesis

The schematic of Poly(MOEP-co-MAA) polymerization and methacrylation is shown in Figure 4.2 A. Polyphosphate polymer was polymerized with MOEP and MAA (In 40 MOEP, polymer hydroxyethylmethacrylate (HEMA) was also polymerized). The HEMA results as a byproduct in the reaction by cleavage of the phosphate group from the MOEP side chain. The chemical modification of the Poly(MOEP-co-MAA) in the second step resulted in grafting of GMA onto the MAA side chain, where 10X excess GMA results in a high degree of conversion. This ring opening pathway isomer results due to the grafting taking place at very acidic conditions. Both isomers are possible but this one is more prevalent. Targeted methacrylation of this polymer resulted from controlling the amount of MAA in the polymerization step.

4.4.2 Polyamine Synthesis

Aqueous RAFT polymerization of Poly (acrylamide-co-aminopropyl methacrylamide) and methacrylation are shown in Figure 4.2 B. A set molecular weight polymer with a targeted amount of side chains was achieved. The synthesis was carried out in H_2O using water-soluble RAFT agents. To achieve a controlled polymerized

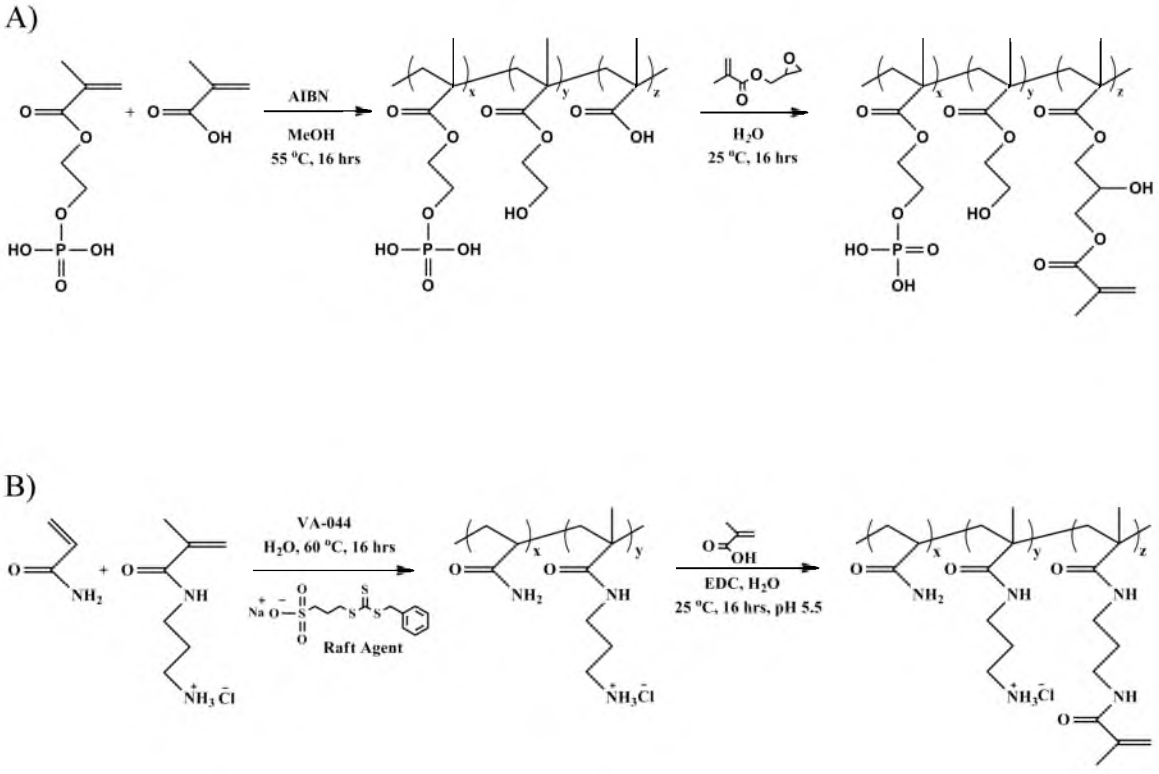

Figure 4.2 A) Schematic of Methacrylated Poly(MOEP-co-MAA) polymer, and B) schematic of Methacrylated RAFT Poly (acrylamide-co-aminopropyl methacrylamide).

polyamine polymer, a kinetics study of the reaction was carried out. At set time intervals, aliquots of the reaction were taken out and quenched and tested on the SEC FPLC. The data show the reaction goes to completion in 2 hours and plateaus. The FPLC curves generated from each data set showed that molecular weight peak getting narrower over time, which shows a very controlled synthesis. Within a few hours the targeted molecular weight with a sharp narrow peak with low PDI is achieved. Most of the monomer is consumed at that point, and the reaction is done.

4.4.3 Copolymer Characterization

SEC measured the molecular weights of both copolymers in this study. To control the molecular weight of Poly(MOEP-co-MAA) polymer, led by free radical polymerization method, a controlled initiator and temperature study was carried out. The AIBN initiator concentration ranged from 1.8–5 mol% of the total monomer, and temperature was varied from 50°C to 60°C. To get the targeted range of MW for the polyphosphate polymer, 4.5 mol% AIBN of the monomers and 55°C were used. The Poly(MOEP-co-MAA) polymer used in this study had the MW of 70.3 KDa and PDI of 1.37 for 70 MOEP polymer, and MW of 85.1 KDa and PDI 1.3 for 40 MOEP polymer. For the Poly (acrylamide-co-aminopropyl methacrylamide), targeted MW polymers by aqueous RAFT polymerization were synthesized, a 40 KDa and a 100 KDa. The polymers used in this study measured to have MW of 40.1 KDa and PDI of 1.1, and the second one of MW 96.1 and PDI of 1.0. The molecular weights of the RAFT polyamine were also confirmed by UV/Vis method and reported to be in agreement with the FPLC data.

The methacrylation and the amount of each group on the polymer side chains were verified by NMR spectroscopy. By NMR methacrylated Poly(MOEP-co-MAA) used in this study contained 73.9 mol% MOEP, 8.1 mol% HEMA, and 18.0 mol% grafted GMA side chains (Figure 4.3A). The Methacrylated Poly (acrylamide-co-aminopropyl methacrylamide) contained 77.2 mol% Acrylamide, 16.5 mol% Aminopropyl Methacrylamide, and 6.3 mol% Grafted Amine (Figure 4.3B). Targeted amount of methacrylation for each polymer was achieved with precise control on the synthesis. In the polyphosphate polymer all of the MAA had to be converted to the methacrylated group; therefore, 10 X excess GMA had to be added to get 100% conversion. For the polyamine polymer, however, only part of the aminopropyl side chain was being converted to the methacrylated side chain, so a very controlled grafting reaction had to take place. Figure 4.3C shows the controlled grafting reaction by addition of EDC and MAA to the aminopropyl in the RAFT amine polymer, starting from the bottom 0, 0.5, 1, 2.5, 5, and 10 X excess reagents. So to target 5% of the amines of the total 25% of the amine groups, 5X excess MAA and EDC were added. A set amount of grafting of each polymer is the key in getting the mechanical properties needed in the final cross-linked complex coacervates. The content of the amine in the Poly (acrylamide-co-aminopropyl methacrylamide) polymer was also verified by ninhydrin Assay, which confirmed similar content.

The titration data of methacrylated Poly (acrylamide-co-aminopropyl methacrylamide) and its monomer aminopropyl methacrylamide, and methacrylated Poly(MOEP-co-MAA) polymer and its MOEP monomer, are overlaid together on the same curve as shown in Figure 4.4 over a broad pH range. Moderate slope changes for

A)

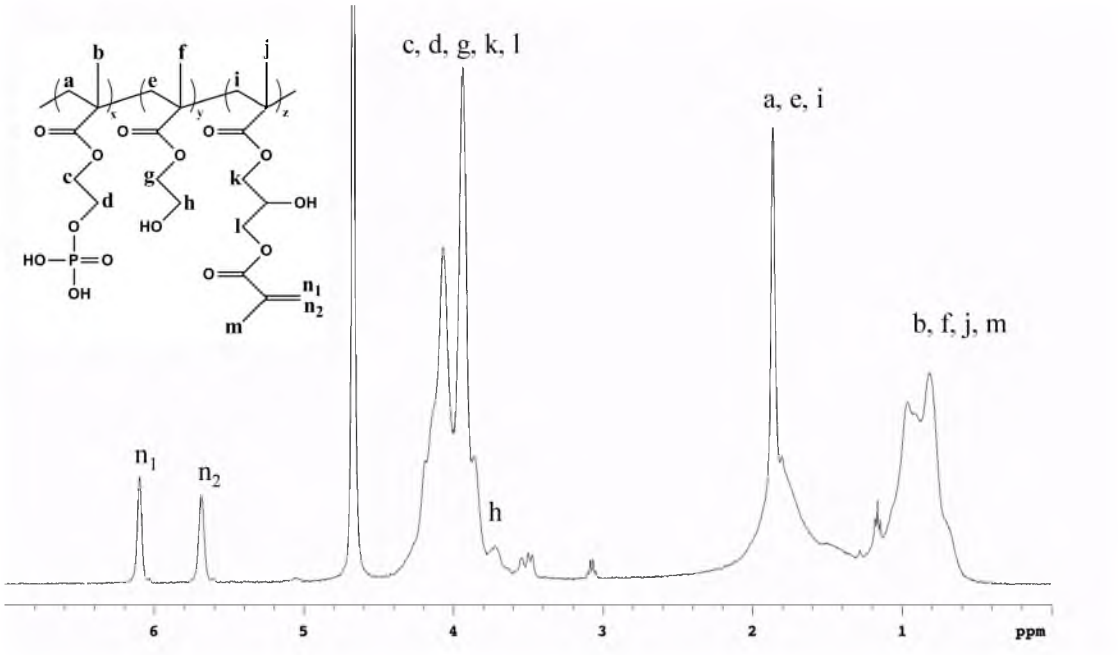

B)

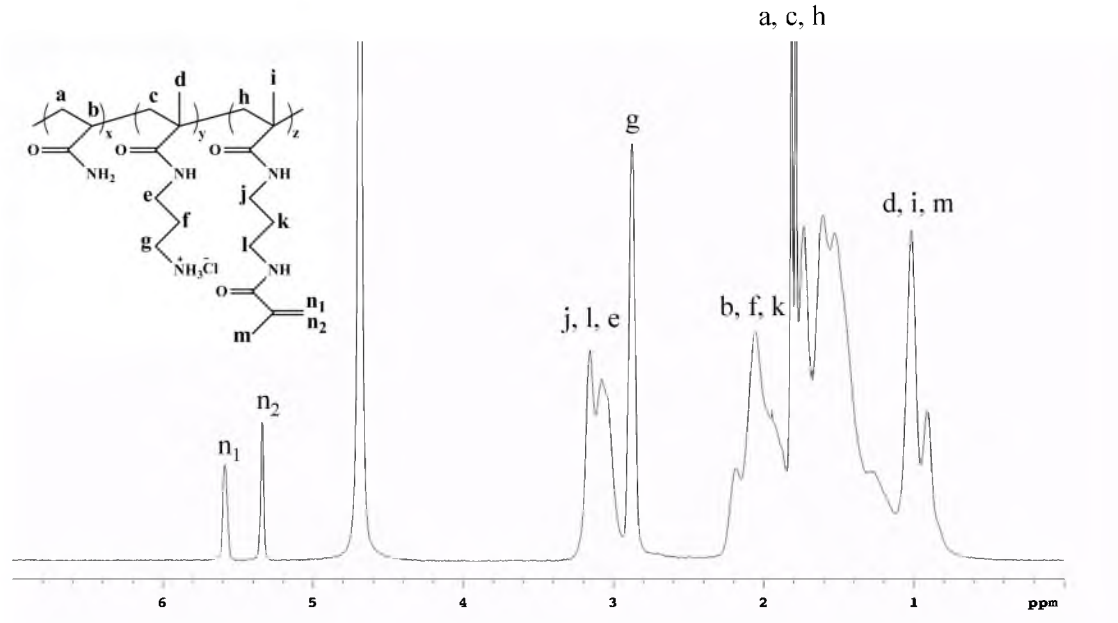

Figure 4.3 H^1 NMR Spectra: A) Methacrylated Poly(MOEP-co-MAA) polymer, B) Methacrylated Poly (acrylamide-co-aminopropyl methacrylamide), C) Controlled grafting of the polyamine polymer.

C)

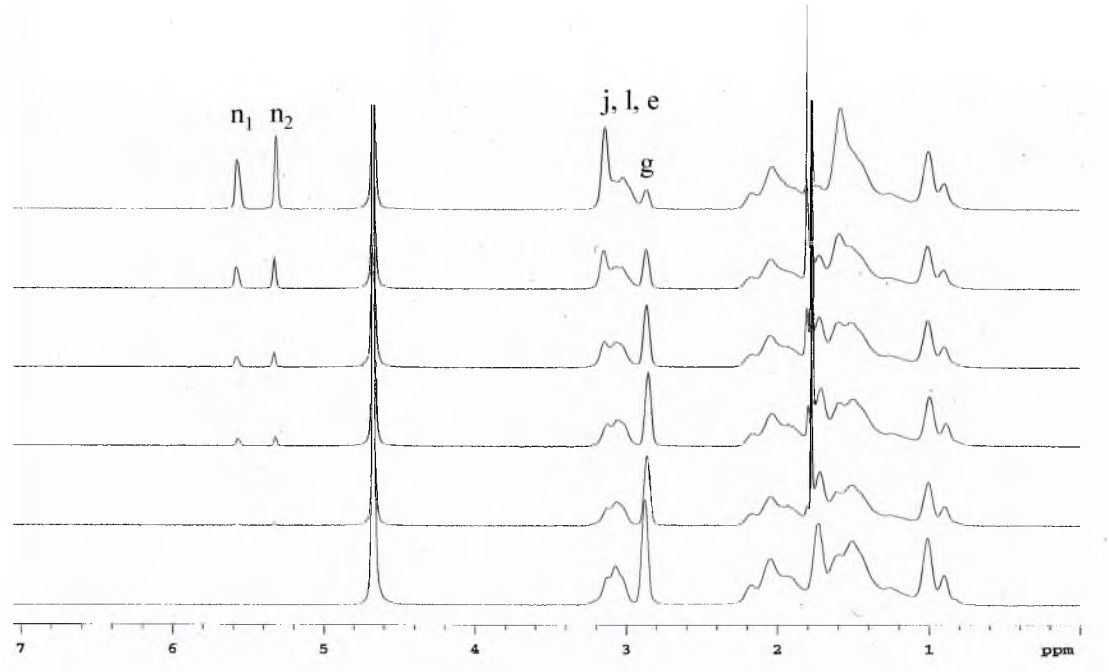

Figure 4.3 Continued.

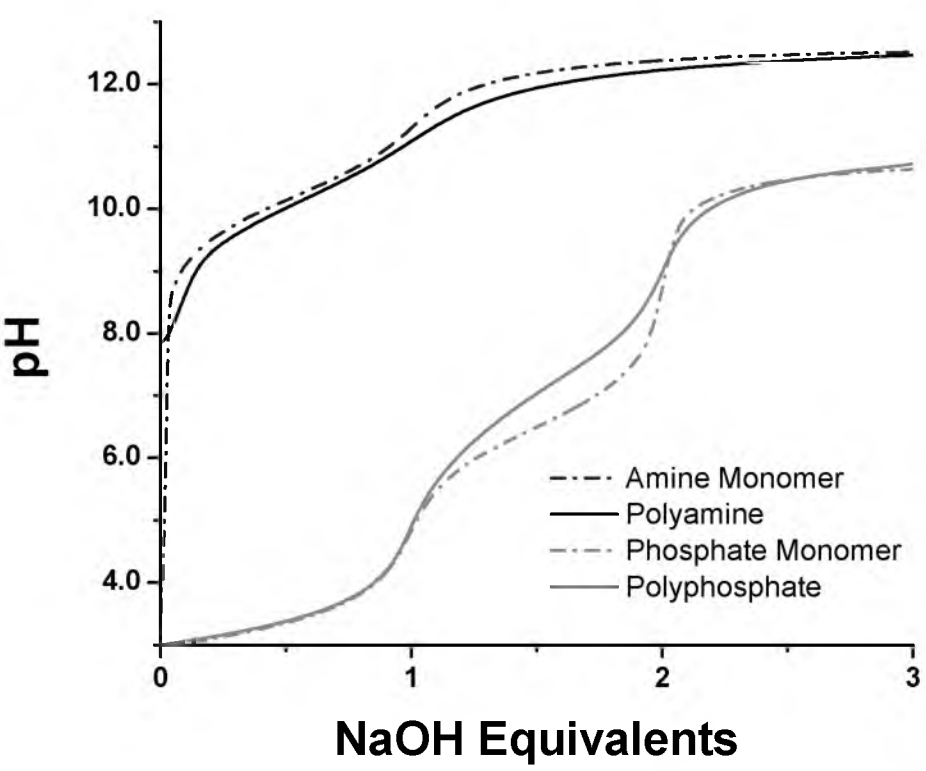

Figure 4.4 Titration curves of Methacrylated Poly (acrylamide-co-aminopropyl methacrylamide)[pKa 10.13] and its monomer Aminopropyl Methacrylamide [pKa 10.17], and Methacrylated Poly(MOEP-co-MAA) polymer [pKa 7.28], and its MOEP monomer [pKa 6.46].

polymers demonstrate improved buffering capacity as compared to monomers. The amine polymer demonstrates a lowered pKa as compared to the monomer, as elevated positive charge density facilitates deprotonation with increasing pH. The phosphate polymer features an elevated second pKa as a result of high negative charge density on the phosphate polymer inhibiting further deprotonation. The disparity between monomer/polymer pKa differences between amines and phosphates can be attributed to the high charge density on phosphate polymers as compared to low charge density on amine polymer. Between pH's of 8 and 9 there is minimal change in protonation state for either polymer, providing a functional pH range in which coacervate properties that depend on interactions between the polyelectrolytes are consistent.

4.4.4 Complex Coacervate Ratio Study

The complex coacervate adhesive formation with methacrylated polymers was extensively studied. The coacervates were formed for two different polymers, 70 MOEP and 40 MOEP, over a range of A/P ratios and two different pHs (Figure 4.5). With increasing A/P ratio, the solution went from clear to the coacervate phase to cloudy and then clear again. At pH 8.2, there was an extra ratio that the coacervate formed compared to pH 7.2 (Figure 4.5A and 4.5B). In 40 MOEP polymer coacervate a higher range of coacervation occurred than 70 MOEP, from A/P ratio 0.7 to 2.2 (Figure 4.5C). The coacervates formed had different appearance and flow behavior at the varied A/P ratios. With increasing ratio the coacervates became apparently more viscous as shown in Figure 4.5D.

To characterize these coacervates further NMR characterization study was conducted as listed in Table 4.1. The NMR A/P ratio comes from direct correlation of

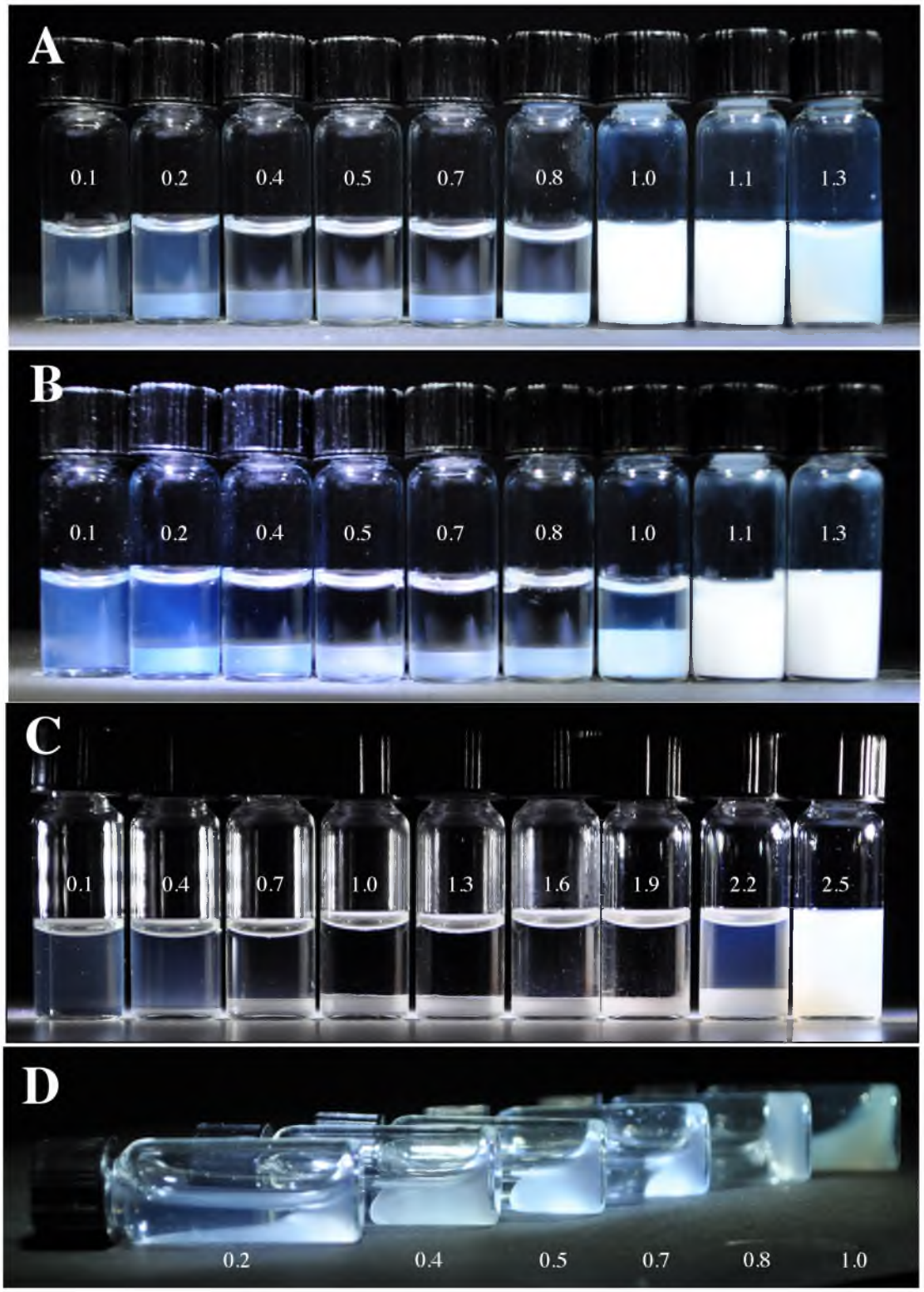

Figure 4.5 Complex coacervate range of methacrylated polymers with varying A/P ratios after 24 hour ripening for A) 70 MOEP polymer from 0.1 to 1.3 at pH 7.2, B) 70 MOEP polymer from 0.1 to 1.3 at pH 8.2, C) 40 MOEP polymer from 0.1 to 2.5 at pH 7.2, and D) flow behavior of 70 MOEP coacervate at pH 8.2.

Table 4.1 Coacervate ratio study with theoretical ratio, NMR ratio, net charge ratio, concentration, and viscosity [at shear rate of 0.01 (s^{-1})] at pH 7.2 for 70 and 40 MOEP polymers, and pH 8.2 for 70 MOEP polymers, after 24 hour of ripening

70 MOEP, pH 7.2

A/P Ratio Theoretical	A/P Ratio NMR	Net Charge Ratio	Concentration (mg/mL)	η (Pa·s)
0.25	0.51	-0.99	103.9	1.6±1.4
0.40	0.55	-0.95	140.0	1.9±0.9
0.55	0.66	-0.84	139.0	4.6±1.8
0.70	0.75	-0.75	158.7	10.5±1.2
0.85	0.95	-0.55	130.2	13.6±2.4

70 MOEP, pH 8.2

A/P Ratio Theoretical	A/P Ratio NMR	Net Charge Ratio	Concentration (mg/mL)	η (Pa·s)
0.25	0.50	-1.50	104.0	3.3±0.7
0.40	0.57	-1.43	126.9	4.7±1.5
0.55	0.70	-1.30	132.7	7.4±1.8
0.70	0.82	-1.18	165.3	12.4±2.0
0.85	0.96	-1.04	150.4	30.7±3.7
1.00	1.14	-0.86	98.0	51.1±7.3

40 MOEP, pH 7.2

A/P Ratio Theoretical	A/P Ratio NMR	Net Charge Ratio	Concentration (mg/mL)	η (Pa·s)
0.70	1.22	-0.28	171.8	2.6±0.4
1.00	1.48	-0.02	180.2	3.7±0.5
1.30	1.79	+0.29	203.7	8.4±1.5
1.60	2.04	+0.54	210.4	11.5±1.8
1.90	2.47	+0.97	209.1	8.2±1.9
2.20	2.62	+1.12	132.6	2.8±1.5

amines to phosphates on the NMR spectra of the coacervates. The H^1 NMR peak of the coacervate compared polyamine peak at 3ppm (Figure 4.3B) to polyphosphate peak at 4ppm (Figure 4.3A), and the NMR ratio was calculated. The coacervate forms with the addition of polyamine solution to the polyphosphate solution, under vortex, despite the theoretical A/P ratio being set. The coacervate has a natural way of forming into a polyelectrolyte charge ratio and taking that into the coacervate and leaving the excess polyelectrolyte into the supernatant. In both polymers and the two pHs, the NMR ratio is higher than the theoretical.

The net charge ratio was also calculated based on the NMR ratio data listed in Table 4.1. Each phosphate group has a negative 1.5 charge at pH 7.2 and negative 2 charge at pH 8.2. Taking the A/P NMR ratio into account gives us the net charge ratio of these coacervates. Coacervates made from 70 MOEP polymers at the two pHs are negatively charged. At pH 8.2 they are more negatively charged than pH 7.2. And after getting to the lower negative ratio, the coacervates do not form and instead a milky solution results. However, for 40 MOEP, polymer coacervates at pH 7.2 negative and positive charged coacervates result. The concentration (mg/mL) of these coacervates was measured using the dry mass from coacervates and volume from the images, after 24 hrs of ripening. The quantitative values show an increasing density with increasing A/P ratio, which then decreases at the end of the A/P range coacervates. Both the concentration and net charge of the coacervates show that these charged polyelectrolytes have their own way of formation and balance of charges for it to take place.

4.4.5 Rheology: Viscoelastic Properties of Complex Coacervates

The flow behavior of these coacervates was quantified on the Rheometer by measuring the viscosity at very low shear rates, an average of 20 data points for 2 minutes. The coacervates were allowed to settle naturally over a 24-hour period. The viscosity results shown in Table 4.1 show increasing viscosity over increasing amine to phosphate ratios for both pHs and polymers. These data correlate well with Figure 4.5 D, showing increasing viscosity coacervate with increasing A/P ratio.

Ripening over a longer period of time was also conducted at the two different pH's for the lower, middle, and upper range A/P ratio (Figure 4.6). Viscosity measurements were measured the same way at low shear rates. The results showed very stable coacervates over a period of a month. With a very minimal increase in viscosity over time, these coacervates can be stored over a month.

4.4.6 Discussion

We can learn and understand many things from the coacervation phenomena and apply its science to many current day solutions. Especially when they exist in nature, like in the case of sandcastle worm secreting its underwater adhesive to bind sand grains. Biomimetics are very unique because they build on nature's concepts. The synthetic can be designed with tunable properties to the desired application. Our synthetic complex coacervate adhesive inspired by nature was developed for adhesion and repair of the soft tissue. The adhesive must meet the following criteria: adhere to soft tissue with sufficient strength; be biocompatiable, nontoxic, and deliverable; and have adhesive stability, dimensional stability under biological conditions, and controlled curing kinetics. In the past, our work has shown adhesives that are biocompatible, nontoxic, and deliverable

A)

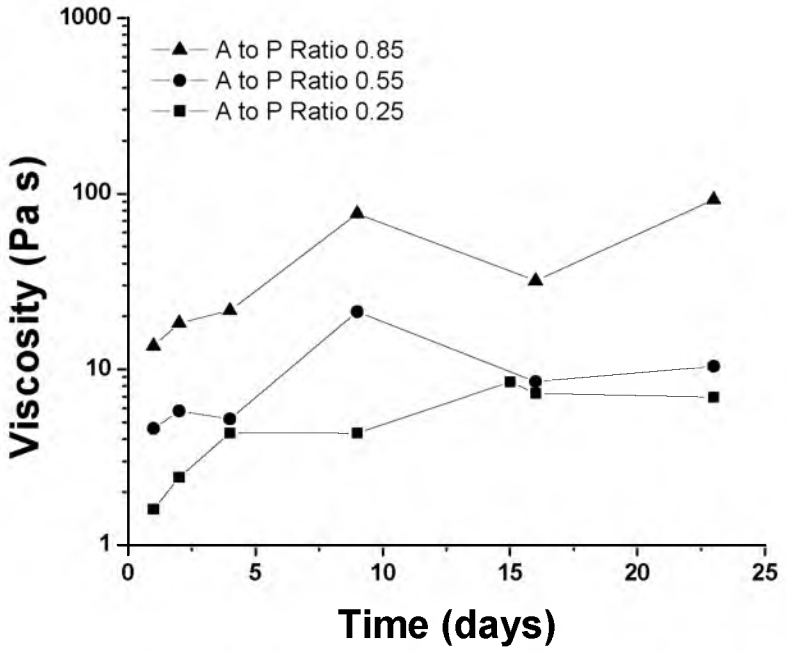

B)

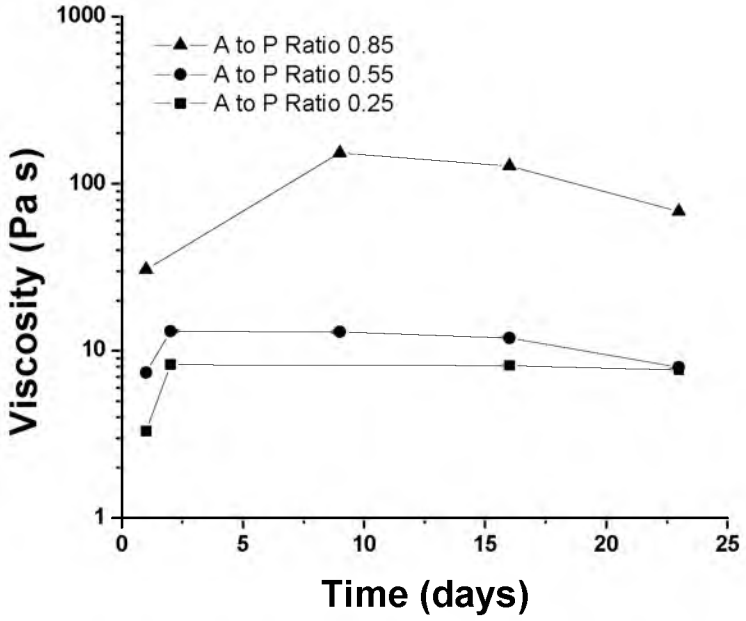

Figure 4.6 Viscosity at shear rate 0.01 (s^{-1}) over ripening time course at various Amine to Phosphate Ratio's at A) pH 7.2, B) pH 8.2.

with sufficient bond strengths [19–22, 26]. But adhesive stability with a DOPA-mediated precursor has always been challenging.

To overcome the challenges of a stable complex coacervate adhesive over extended periods of time, new crosslinking chemistries were introduced into the polymers. The concept of methacrylating polymers is not new, but the incorporation of the vinyl group into the phosphate and amine polymer backbone was tricky. Through trial and error, we developed the final method of having controlled, characterized, and stable polymers. The synthesis and grafting of poly(MOEP-co-MAA) was highly efficient in getting the right amount of side chains and vinyl groups on the polymeric backbone. The molecular weight of the polymer was controlled by the initiator concentration and temperature. Aqueous RAFT polymerization of poly(acrylamide-co-aminopropyl methacrylamide) improves the narrow window of targeted molecular weight and side chains. The narrow molecular weight distribution is confirmed by the SEC and UV/Vis data. NMR, titration data, and the Ninhydrin Assay confirm the content of the amine in this polymer. The methacrylated groups are well distinguished on both polymers in H^1 NMR.

The modified polymers formed stable complex coacervates at different pH's and polymers at varied amine to phosphate ratios. The coacervation ratio study was insightful in predicting the A/P to use for a set viscosity. The rheological flow behavior of these coacervates confirmed the value by quantifying the viscosity measurements (Table 4.1). The range of viscosities open up the complex coacervate adhesive to a wide variety of applications to be used by picking the set ratio of the polymer or pH range. In designing the adhesive for a set application, this is a unique property. The ripening/stability of these

coacervates show a very stable coacervate over a period of a month. This again confirms that storage stability of these polymers and coacervate adhesives.

4.5 Conclusion

Methacrylated polyphosphate and methacrylated polyamine polymers were synthesized for stable complex coacervate formation. An aqueous grafting of the poly(MOEP-co-MAA) polymer resulted in a clean methacrylated polymer. RAFT polymerization of poly(acrylamide-co-aminopropyl methacrylamide) resulted in a controlled molecular weight polyamine polymer. Targeted methacrylation on each polymer was achieved. The coacervation ratio study gave us a range of properties to choose from for its application. The coacervates formed with this new crosslinking system are more stable for long term use.

4.6 References

1. H. J. Bungenberg de Jong, and H. R. Kruyt, "Coacervation (Partial Miscibility in Colloid Systems)," *Proc. K. Ned. Akad. Wet.*, **32**, 849–856 (1929).

2. H. J. Bungenberg de Jong, "Complex Colloid Systems," *Coll. Sci.*, **2**, 335–432 (1949).

3. M. J. Voorn, "Complex Coacervation: IV. Thermodynamic Calculations on Four-component Systems," *Rec. Trav. Chim.*, **75**, 925–937 (1956).

4. J. T Overbeek, M. J. Voorn, "Phase Separation in Polyelectrolyte Solution; Theory of Complex Coacervation," *J. Cell. Comp. Physiol.*, **49**, 7–22 (1957).

5. M. J. Voorn, "Phase Separation in Polymer Solutions," *Fortsch Der Hochpoly-Forsch*, Springer, Berlin, 192–233, 1959.

6. A. Veis, and C. Aryani, "Phase Separation in Polyelectrolyte Systems. I. Complex Coacervates of Gelatin," *J. Phys. Chem.*, **64**, 1203–1210 (1960).

7. D. J. Burgess, "Practical Analysis of Complex Coacervate Systems," *J. Coll. Inter. Sci.*, **140**, 227–238 (1990).

8. A. Veis, "A Review of the Early Development of the Thermodynamics of the Complex Coacervation Phase Separation," *Adv. Coll. Inter. Sci.*, **167** [1] 2–11 (2011).

9. J. Lee, Y. O. Popov, and G. H. Fredrickson, "Complex Coacervation: A Field Theoretic Simulation Study of Polyelectrolyte Complexation," *J. Chem. Phys.*, **128** [22] 224908–224913 (2008).

10. P. L. Dubin, Y. Li, and W. Jaeger, "Mesophase Separation in Polyelectrolyte-mixed Micelle Coacervates," *Langmuir*, **24** [9] 4544–4549 (2008).

11. J. Sprakel, E. Spruijt, M. A. C. Stuart, M. A. Michels, and J. Van Der Gucht, "Intermittent Dynamics in Transient Polymer Networks Under Shear: Signs of Self-organized Criticality," *Physi. Rev. E*, **79** [5] 172–178 (2009).

12. E. Kizilay, A. B. Kayitmazer, and P. L. Dubin, "Complexation and Coacervation of Polyelectrolytes With Oppositely Charged Colloids," *Adv. Coll. Inter. Sci.*, **167** [1] 24–37 (2011).

13. E. Kizilay, S. Maccarrone, E. Foun, A. D. Dinsmore, and P. L. Dubin, "Cluster Formation in Polyelectrolyte-micelle Complex Coacervation," *J. Phys. Chem. B*, **115** [22] 7256–7263 (2011).

14. J. Van der Gucht, E. Spruijt, M. Lemmers, and M. A. C. Stuart, "Polyelectrolyte Complexes: Bulk Phases and Colloidal Systems," *J. Coll. Inter. Sci.*, **361** [2] 407–422 (2011).

15. R. A. Jensen, and D. E. Morse, "The Bioadhesive of *Phragmatopoma Californica* Tubes: A Silk-line Cement Containing L-DOPA," *J. Comp. Physiol. B*, **158**, 317–324 (1988).

16. J. H. Waite, R. A. Jensen, and D. E. Morse, "Cement Precursor Proteins of the Reef-building Polychaete Phragmatopoma Californica (Fewkes)," *Biochemistry*, **31** [25] 5733–5738 (1992).

17. R. J. Stewart, J. C. Weaver, D. E. Morse, and J. H. Waite, "The Tube Cement of Phragmatopoma Californica: A Solid Foam," *J. Exp. Bio.*, **207**, 4727–4734 (2004).

18. H. Zhao, C. Sun, R. J. Stewart, and J. H. Waite, "Cement Proteins of the Tube-building Polychaete Phragmatopoma Californica," *J. Biol. Chem.*, **280**, 42938–42944 (2005).

19. H. Shao, K. N. Bachus, and R. J. Stewart, "A Water-borne Adhesive Modeled After the Sandcastle Glue of P. Californica," *Macromol. Biosci.*, **9** [5] 464–471 (2009).

20. H. Shao, and R. J. Stewart, "Biomimetic Underwater Adhesives With Environmentally Triggered Setting Mechanisms," *Adv. Mater.*, **22** [6] 729–733 (2010).

21. S. Kaur, G. M. Weerasekare, and R. J. Stewart, "Multiphase Adhesive Coacervates Inspired by the Sandcastle Worm," *ACS Appl. Mater. Inter.*, **3** [4] 941–944 (2011).

22. L. K. Mann, R. Papanna, K. J. Moise, R. H. Byrd, E. J. Popek, S. Kaur, S. C. G. Tseng, and R. J. Stewart, "Fetal Membrane Patch and Biomimetic Adhesive Coacervates As a Sealant for Fetoscopic Defects," *Acta Biomater.*, **8** [6] 2160–2165 (2012).

23. J. N. Hunt, K. E. Feldman, N. A. Lynd, J. Deek, L. M. Campos, J. M. Spruell, B. M. Hernandez, E. J. Kramer, and C. J. Hawker, "Tunable, High Modulus Hydrogels Driven by Ionic Coacervation," *Adv. Mater.*, **23** [20] 2327–2331 (2011).

24. M. Yu, J. Hwang, and T. J. Deming, "Role of L-3, 4-dihydroxyphenylalanine in Mussel Adhesive Proteins," *J. Am. Chem. Soc.*, **121** [24] 5825–5826 (1999).

25. T. J. Deming, and M. Yu, "Mechanistic Studies of Adhesion and Crosslinking in Synthetic Analogs of Marine Adhesive Proteins," *J. Poly. Mater. Sci. Eng.*, **80**, 471–472 (1999).

26. H. Shao, G. M. Weerasekare, and R. J. Stewart, "Controlled Curing of Adhesive Complex Coacervates With Reversible Periodate Carbohydrate Complexes," *J. of Biomed. Mat. Res. A*, **97** [1] 46–51 (2011).

27. W. N. E. Van Dijk-Wolthuis, J. J. Kettenes-Van Den Bosch, A. Van der Kerk-Van Hoof, and W. E. Hennink, "Reaction of Dextran With Glycidyl Methacrylate: An Unexpected Transesterification," *Macromol*ecules, **30** [11] 3411–3413 (1997).

28. W. N. E. Van Dijk-Wolthuis, O. Franssen, H. Talsma, M. J. Van Steenbergen, J. J. Kettenes-Van Den Bosch, and W. E. Hennink, "Synthesis, Characterization, and Polymerization of Glycidyl Methacrylate Derivatized Dextran," *Macromol*ecules, **28** [18] 6317–6322 (1995).

29. A. V. Reis, O. A. Cavalcanti, A. F. Rubira, and E. C. Muniz, "Synthesis and Characterization of Hydrogels Formed From a Glycidyl Methacrylate Derivative of Galactomannan," *Int. J. Pharm.*, **267** [1] 13–25 (2003).

30. A. R. Fajardo, A. V. Reis, M. R. Guilherme, I. T. Schuquel, G. J. Vidotti, A. F. Rubira, and E. C. Muniz, "Clearing the Mechanism of Reaction of Glycidyl

Methacrylate at the Hydroxyl and Carboxylic Groups of Poly (Vinyl Alcohol) and Poly (Acrylic Acid)," *Polymer*, **47**, 2023–2029 (2006).

31. C. L. McCormick, and A. B. Lowe, "Aqueous RAFT Polymerization: Recent Developments in Synthesis of Functional Water-soluble (Co)polymers with Controlled Structures," *Acc. Chem. Res.*, **37** [5] 312–325 (2004).

32. J. Skey, and R. K. O'Reilly, "Facile One Pot Synthesis of a Range of Reversible Addition-fragmentation Chain Transfer (RAFT) Agents," *Chem. Commu.*, **35**, 4183–4185 (2008).

33. A. H. Alidedeoglu, A. W. York, D. A. Rosado, C. L. McCormick, and S. E. Morgan, "Bioconjugation of D-glucuronic Acid Sodium Salt to Well-defined Primary Amine-contatining Homopolymers and Block Copolymers," *J. Poly. Sci. Part A: Polym. Chem.*, **48** [14] 3052–3061 (2010).

34. S. Glatzel, N. Badi, M. Pach, A. Laschewsky, and J. F. Lutz, "Well-defined Synthetic Polymers With a Protein-like Gelation Behavior in Water," *Chem. Commu.*, **46** [25] 4517–4519 (2010).

35. K. Skrabania, A. Miasnikova, A. M. Bivigou-Koumba, D. Zehm, and A. Laschewsky, "Examining the UV-vis Absorption of RAFT Chain Transfer Agents and Their Use for Polymer Analysis," *Polym. Chem.*, **2** [9] 2074–2083 (2011).

CHAPTER 5

METHACRYLATED POLYMERS COMPLEX COACERVATE ADHESIVE FOR SEALING FETAL DEFECTS IN TWIN-TO-TWIN TRANSFUSION SYNDROME

5.1 Introduction

According to the USA National Center for Health Statistics, in 2005 there were 4,500 cases of twin-to-twin transfusion syndrome (TTTS) involving 9,000 babies [1]. TTTS is a birth defect in which two fetuses get an unequal or unbalanced blood supply from the mother, leading to asymmetrical fetal growth and fetal mortality. It is a progressive disease, which when left untreated can lead to fatal consequences for the mother and the babies. This condition occurs in monozygotic (MZ) twins where the twins share a common placenta with connecting blood vessels, giving excess blood supply to one baby and too little to the other. An effective treatment used in TTTS is fetoscopic laser photocoagulation, in which the laser is used to photocoagulate the vessels crossing the intertwin membrane. This method not only stops the blood supply between the twins, but also stops the transfer of any vasoactive mediators [2]. Despite the improved outcome of the laser photocoagulation treatment of TTTS, there are major postintervention challenges. Iatrogenic preterm premature rupture of the fetal membrane (iPPROM) is the major threat. In the TTTS treatment an 8 mm diameter fetoscope punctures the amniotic

fetal membrane, and the laser optic is inserted through the scope. The fetal membrane does not naturally heal [3], leading to amniotic fluid leakage. The iPPPROM is a common drawback of all fetoscopic procedures, limiting the use of these procedures in diagnosis and treatment. Adhesives that can plug up these fetal defects after fetoscopic procedures have shown promising results, but the adhesion in aqueous environments along with cytotoxicity poses major challenges [4].

Aquatic organisms like the sandcastle worm, *Phragmatopoma californica*, a marine polychaete, can teach us immensely about underwater adhesion [5–7]. This worm living along the coastlines secretes glue out of its building organ, which binds sandgrains and shells from the ocean, and builds a shell that it lives in. Despite all temperature, pressures, and salt changes in the ocean, this mineralized shell does not fall apart. The sandcastle worm has evolved its solutions over the years to tackle the underwater adhesion problem, where so many synthetic glues have fail. This animal is the inspiration behind our synthetic analog to make this bioadhesive [8–11]. The worm glue contains many components, but of interest to us are the oppositely charged proteins, mainly phosphates and amines. These proteins led us to our biomimetic adhesive formed by the method of complex coacervation.

Complex coacervation is a fluid-fluid phase separation of two oppositely charged copolyelectrolytes in aqueous solution. The dense phase, also known as coacervate, settles to the bottom and the dilute phase, known as supernatant, remains on top [12]. Both phases coexist in equilibrium and are dependent on many factors like pH, temperature, concentration, ionic strength, and molecular weight of the polyelectrolytes. For the biomimetic adhesive, oppositely charged phosphate and amine polymers were

synthesized, and when mixed under the set conditions, a complex coacervate resulted. Preliminary studies on sealing fetal defects have shown that our synthetic analog adheres well to fetal tissue and is able to hold the amniotic membrane plug in place [13]. This synthetic complex coacervate adhesive is chemically cross-linked through 3,4-dihydroxy-L-phenylalanine (DOPA), which makes it unstable and difficult to control the crosslinking. This limits the use of DOPA-based analog adhesives in practical applications.

This chapter is focused on developing a synthetic complex coacervate adhesive based on the methacrylated copolyelectrolytes (shown in Chapter 4), which are more stable to use, for TTTS repair. Vinyl groups are put on the polymers, consisting of the oppositely charged phosphates and amines, as a better crosslinking system. A chemically cross-linked adhesive system is created. This adhesive in conjunction with the fetal membrane patch will be used to plug the punctured fetal membranes in pig animal studies. Sodium (meta) periodate ($NaIO_4$) is the crosslinker used to crosslink the methacryalted complex coacervate adhesive. The crosslinking kinetics of the adhesive system is optimized to practical clinical timing. The adhesion properties of this chemically crosslinked glue are tested on the lap shear test. The cytotoxicity of the glue is tested to make sure it is not toxic. Sterile complex coacervate adhesive packets are prepared for the animal surgeries. In this chapter we have prepared the sterile adhesive packets that are successfully being used in current animal studies, where the initial results are showing promising results.

5.2 Materials and Methods

5.2.1 Materials

All reagents were used without further purification unless noted otherwise. Inhibitor removing resin was purchased from Alfa Aesar. PEG-dA (Polyethylene glycol diacrylate, 540 Da), PEG-dMA (Polyethylene glycol dimethacrylate, 750 KDa), Sodium (meta) periodate (≥99.0%), and basic aluminum oxide were purchased from Sigma-Aldrich.

5.2.2 Purification of PEG Monomers

The inhibitor in PEG-dA and PEG-dMA monomer had to be removed. The liquid monomers were passed through an activated basic aluminum oxide column, removing the inhibitor hydroquinone monomethyl ether (MEHQ).

5.2.3 Complex Coacervate Adhesive Formation

Methacrylated Poly(MOEP-co-MAA) (as described in Chapter 4) and methacrylated Poly(acrylamide-co-aminopropyl methacrylamide) (as described in Chapter 4), were dissolved separately in aqueous 150mM NaCl solution at a concentration of 50 mg/mL. The copolymer solutions were adjusted to the correct pH of 7.2±0.2, with NaOH. The poly(acrylamide-co-aminopropyl methacrylamide) solution was added dropwise to the poly(MOEP-co-MAA) solution under vortex. The molar ratio of amine sidechains to phosphate sidechains (A/P) was fixed. For 40 MOEP polymer, a coacervate A/P ratio of 1 was used and for 70 MOEP polymer, a coacervate A/P ratio of 0.65 was used. In less than a minute, turbid coacervate settled out of solution. The coacervates were allowed to phase separate from the supernatant for 24 hrs before being

used for further analysis. The multiphase complex coacervate incorporating PEG-dA was formed the same way with the additional step of dissolving the desired concentration (0–15 wt%) of PEG-dA into dissolved methacrylated Poly(MOEP-co-MAA) polymer, taking into account a fixed volume in the end.

5.2.4 Polymeric Solution for Crosslinking Kinetics on the Rheometer

Methacrylated Poly(MOEP-co-MAA) and methacrylated Poly(acrylamide-co-aminopropyl methacrylamide) were dissolved separately in aqueous 150mM NaCl solution at a concentration of 200 mg/mL. The pH of each solution was adjusted to a set pH.

5.2.5 Dynamic Rheology

The gelation kinetics of the adhesive complex coacervate was conducted on a stress-controlled Rheometer (TA instrument, AR 2000 ex) using a 20 mm, 4° cone geometry, gap 114 μm, at 37°C with 150 μL coacervate samples. Gelation kinetics of crosslinked coacervates were measured using the Oscillatory time sweep method on the Rheometer. The change in elastic (G') and viscous (G") moduli over time was measured at a constant frequency of 1 Hz and constant strain of 1%. The coacervates were crosslinked through vinyl groups on both polymers with $NaIO_4$ in varied mM concentrations (10–50 mM). The 10 μl of $NaIO_4$ stock solution was mixed into 200 μl coacervate. The mixed coacervate was loaded onto the rheometer, and the method initiated. The gelation kinetics of polymeric solutions was also measured the same way, by mixing 10 μl of $NaIO_4$ stock solution with 200 μl polymeric solutions.

5.2.6 Mechanical Testing

The adhesion properties of complex coacervates were tested using a lap shear test on a material testing system (Instron). Aluminum substrates of dimensions 0.5 x 5 cm were used in the lap shear method. The substrates were cleaned using a standard method: polished on 600 grit sand paper, washed twice in a ultrasonic methanol bath, washed 10 min in sulfuric acid bath, and finally washed in water. To bond the aluminum substrates, the complex coacervate were mixed in with 5% dilution of 20 mM $NaIO_4$. About 20 μl of coacervate/mixed with $NaIO_4$ were applied to wet Al adherend. The second wet Al were placed on the first with a 14–20 mm overlap. The two substrates at the overlap were secured with a stainless steel clip. The samples were than placed in a water bath, at 37°C, for 2 hours until testing. The shear strength of the bonds were determined on a material testing system (Instron) with a 100 N load cell, crosshead speed 10 mm min^{-1}. Once the substrates failed, the overlap area was taken into to account as well as the failed load to calculate the bond strength. For each condition four specimens/measurements were tested.

5.2.7 Cytotoxicity[1]

Mouse osteoblasts (MC3T3-E1 subclone 4, ATCC CRL-2593, Manassas, VA, USA) were used as the cell line. The cells were maintained in essential medium supplemented with 10% fetal bovine serum, 100 U/ml penicillin, and 100 μg/ml streptomycine in a humidified 5% CO_2 and 95% air balanced incubator at 37°C. The medium was changed every other day. The direct contact cell culture test was used to evaluate cytotoxicity of the complex coacervate. To 32 μl, adhesive uncrosslinked or

[1]Hui Shao carried out the cytotoxicity assay.

crosslinked, and 256 μl medium was added into a culture well plate and incubated 37°C for 24 hours. In another plate MC3T3-E1 osteoblast cells were plated, with density of 100, 000 cells/well in the growth medium, incubated at 37°C for 48 hours. After 48 hours the medium from the MC3T3-E1 cells was removed, and from the adhesive plate the medium was added into the cell plate. After 48 hours the cell number of MC3T3 on the adhesive was determined using the MTT assay. MTT was dissolved in sterile PBS (5 mg/ml). 100 μl of the MTT stock solution was added to each well and incubated at 37°C for 4 hours. After incubation, 1000 μl of the SDS-HCl solution (0.1 g/ml in 0.01 M HCl) were added to each well and mix thoroughly using pipette to extract the formazan crystals. The plate was then incubated at 37°C for another 4 hours in a humidified chamber. After incubation, the extract of each sample was transferred to the 96-well plate and the absorbance intensities were measured at 570 nm using a microplate reader.

5.2.8 Sterilization of Coacervates

Sterile coacervate adhesive packets were prepared for the animal studies. In a sterile hood, all aqueous polymeric solutions were filtered through a 0.22 μm sterile filter. The sterile poly(acrylamide-co-aminopropyl methacrylamide) solution was added dropwise to the sterile poly(MOEP-co-MAA) solution under vortex. The coacervates were ripened for 24 hours. The adhesives were packed in 1 mL syringes with a tight seal cap, (Qosina, Inc), sterilized by ethylene oxide sterilization (40°C). The loaded sterile syringe was then put into a sterile 50 mL centrifuge tube to be kept in a sterile packet till surgery. The chemical initiator, $NaIO_4$, was loaded into the second syringe the same way. The $NaIO_4$ stock solution was filtered through the 0.22 μm filter to make it sterile.

5.2.9 Complex Coacervate Adhesive Packets used in Animal Studies

The adhesive and the initiator were packaged separately in two different leur-lock sterile syringes. At the animal study surgery room, a sterile mixing nozzle is connected to the two syringes by pushing all of the material of one syringe into the other, and vice versa, mixing 5–10 times in the initiator with the adhesive. Once mixed, all of the adhesive/initiators were pushed into one syringe, the empty syringe was removed, and the mixing nozzle was removed, and by attaching a cannula to the leur-lock, syringe adhesive can be applied to the test site. The adhesive has to be applied within a minute of mixing.

5.3 Results and Discussion

5.3.1 Rheology

The crosslinking kinetics of complex coacervate adhesive was measured on the Rheometer. Varied polymer composition coacervates of polyphosphate and polyamine polymers (Figure 5.1) were compared. It is important for this newly crosslinked system to crosslink fast enough for the physician so that they do not have to wait hours for the glue to set and yet not set too fast that it turns into a solid gel before applying to the site. The crosslinking time can be optimized on the rheometer using dynamic oscillatory rheology by time sweep method. For this application we want the adhesive to fully set between 5 to 10 minutes. Sodium (meta) periodate was used as the crosslinker to crosslink the methacrylated complex coacervate adhesive. The coacervates were formed at the biological pH of 7.2±0.2 and temperature of 37°C. The elastic modulus of complex coacervate, made of 40 mol% MOEP and 1% methacylated polyphosphate with 5% methacrylated polyamine, was optimized for $NaIO_4$ concentration as shown in Figure 5.2. The coacervates initially crosslinked in less than a minute for all concentrations, not

Polyphosphate Polymer

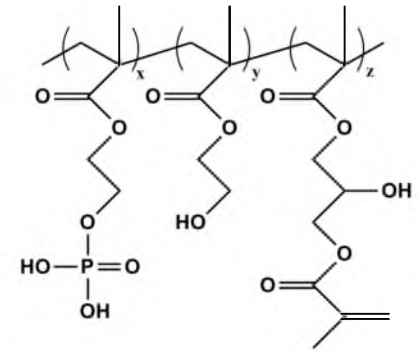

Varied Polymers

x	y	z
40	59	1
40	56	4
40	51	9
40	45	15
70	10	20

* x (% MOEP), y (%HEMA), z (% Methacrylation)

Polyamine Polymer

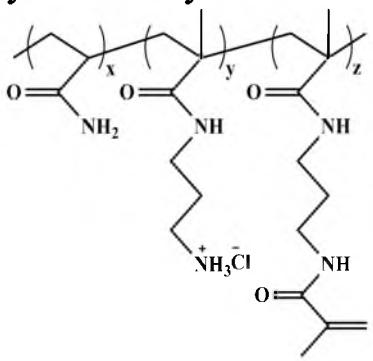

x	y	z
25	75	0
20	75	5

* x (% Amine), y (% Acrylamide), z (% Methacrylation)

Figure 5.1 The varied polymers used in this study: polyphosphates (Methacrylated Poly(MOEP-co-MAA)) and polyamines (Poly (acrylamide-co-aminopropyl methacrylamide)).

A)

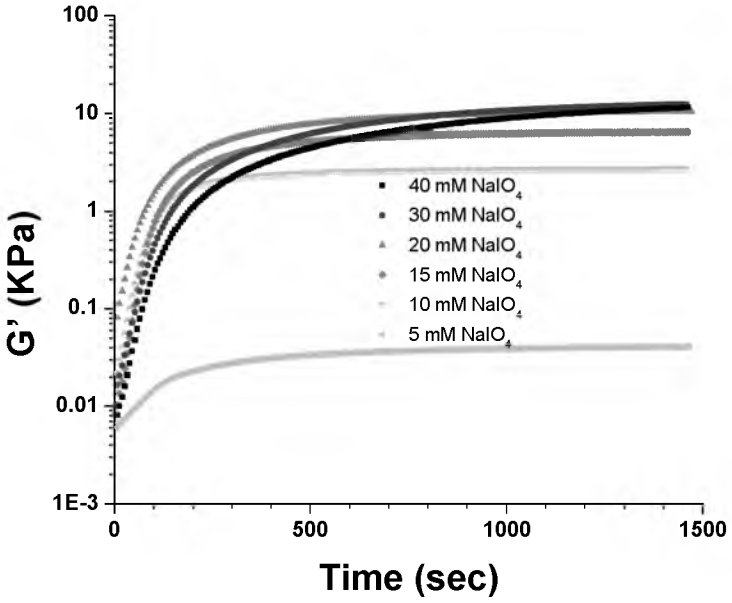

B)

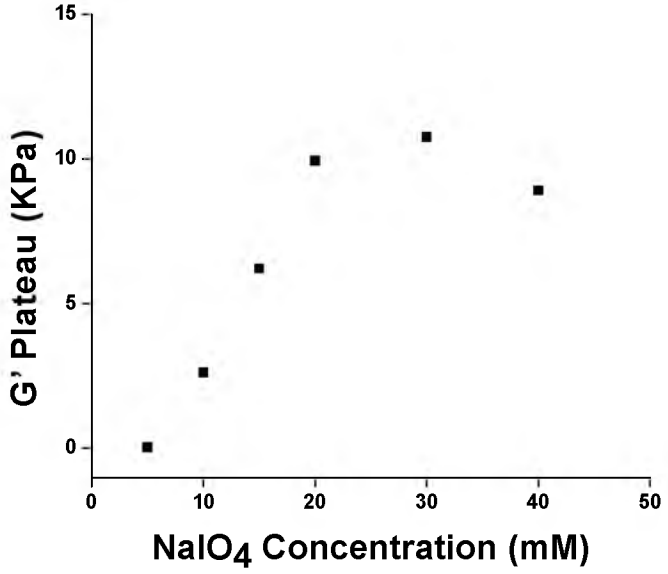

Figure 5.2 Elastic modulus of complex coacervates made of 40 MOEP-1% methacrylation on the polyphosphate polymer and 5% methacrylation on the polyamine polymer at pH 7.2, with varied $NaIO_4$ concentrations at 37°C: A) Time sweep curve, and B) showing elastic modulus vs. $NaIO_4$ concentration.

shown in the figure, where the G' crosses over the G", also known as the reference point where the adhesive starts to go from a viscous fluid to crosslinked elastic network [14]. The G' plateaus eventually over time for all the $NaIO_4$ concentrations as shown in the time sweep curve in Figure 5.2A. The elastic modulus for the 40 MOEP-1% methacrylated coacervate reached a maxiumum around 10 KPa, optimizing the $NaIO_4$ concentration between 20 and 30 mM (Figure 5.2B). The elastic modulus plateau was also evaluated for varied methacrylated polymers within the coacervate, as shown in Figure 5.3. As the methacrylation on the polyphosphate increased within the coacervate, the elastic modulus increased. The difference between the nonmethacrylated polyamine and the methacrylated polyamine was very large. This result is insightful because the methacrylation on both polymers is necessary to maximize the modulus. These data also show us the range of properties of elastic modulus that we can choose from for our application of TTTS. The correct modulus for this soft tissue adhesive application, however, is difficult to pinpoint. We know that the modulus should be somewhere comparable to that of the fetal tissue membrane. We do not want the modulus of the adhesive to be too stiff where it hardens into a stiff gel, nor do we want a mushy gel that is only partially crosslinked. We want something in between that adheres well to the fetal tissue without a modulus mismatch between the interfaces of the soft tissue. We observed the effect of modulus upon the geometry on the rheometer, as it is being lifted off as the complex coacervate adhesives have reached a plateau (Figure 5.4A). This sample shown in the image is the 70 MOEP-20% methacrylated polyphosphate and 5% methacrylated polyamine coacervate crosslinked with 10 mM $NaIO_4$ at 37° C. The adhesive here is stuck to both the top geometry and the bottom pelitier plate (Figure 5.4B). These data

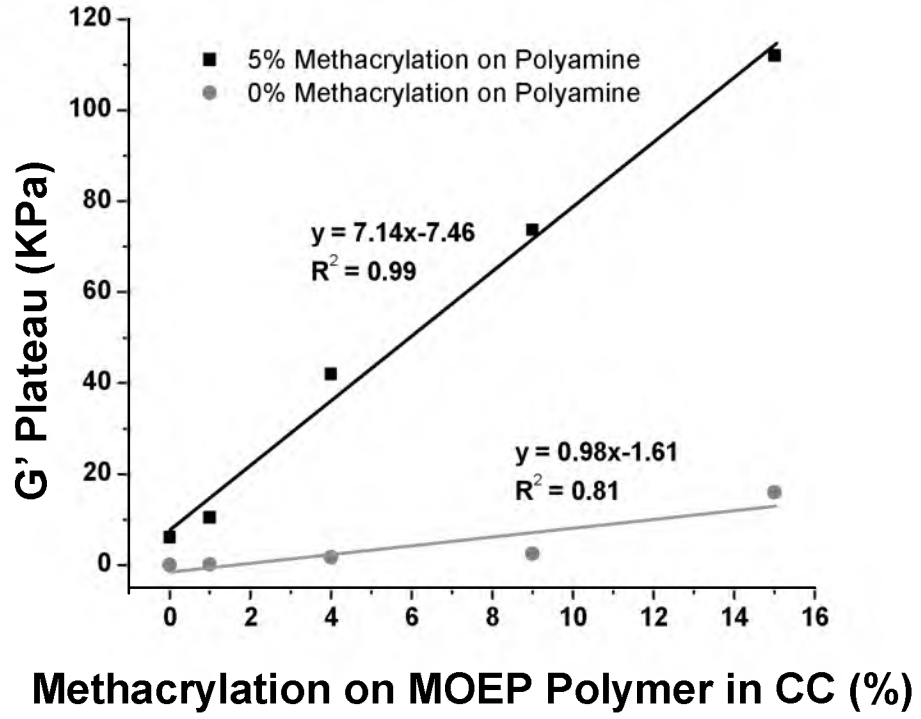

Figure 5.3 Elastic modulus of complex coacervates, made with varied methacrylations on 40 MOEP polymers and polyamine polymers, at pH 7.2, with 20mM $NaIO_4$ at 37°C.

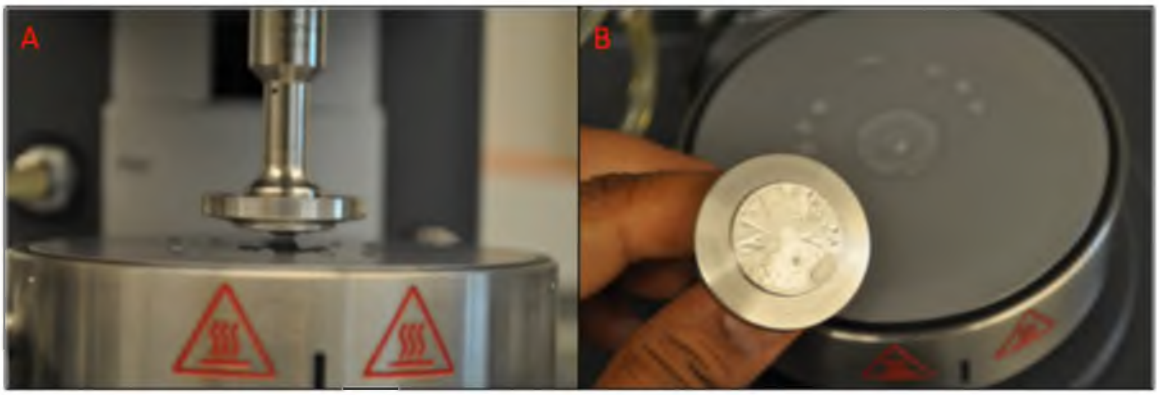

Figure 5.4 Images of the geometry being lifted off the pelitier plate on the rheometer with complex coacervate adhesive in between: A) as the geometry is being pulled off, B) the adhesive stuck on both the top geometry and bottom pelitier plate in the back.

suggest that the coacervates we are using are not too stiff and have a potential to be used in this application. Compositions that are too stiff are left stuck on only one side, top geometry or the bottom plate.

The complex coacervate adhesive is crosslinked by sodium periodate as the chemical initiator. But the exact mechanism behind the crosslinking is unknown. Looking at the individual components of the adhesive one at a time on the rheometer, we taped into the mechanism (Figure 5.5). As shown in Figure 5.5A, 20% methacrylated polyphosphate polymer solution at a high concentration of 200 mg/mL (compared to 50 mg/mL in the coacervate), with 20 mM $NaIO_4$, at 37°C, show no crosslinking taking place. The nonmethacrylated polyamine polymer solution, without any initiator added at 37°C, pH 9, also does not crosslink (Figure 5.5B). The nonmethacryalted polyamine at pH 9, with 20 mM $NaIO_4$, at 37°C, however, does crosslink at very low modulus (Figure 5.5C). When we monitor the effect of pH on plateau modulus on 5% methacrylated polyamine solution, we see the modulus increasing with increasing pH (Figure 5.5D). At pH 5 the 5% methacrylated polyamine solution does not crosslink, but with increasing pH after that the polyamine crosslinks. For periodate crosslinking to take place, all we need is the presence of sodium periodate and polyamine. Methacrylation on the polyamine gives a more profound effect. At pH 7.2 the nonmethacrylated polyamine does not show any crosslinking.

5.3.2 Mechanical Testing

The adhesion properties of the complex coacervate adhesive were tested via lap shear mechanical test on the Instron. The bonded aluminum adherends were cured and tested after 2 hours of submersion underwater, at 37°C. The lap shear measurements

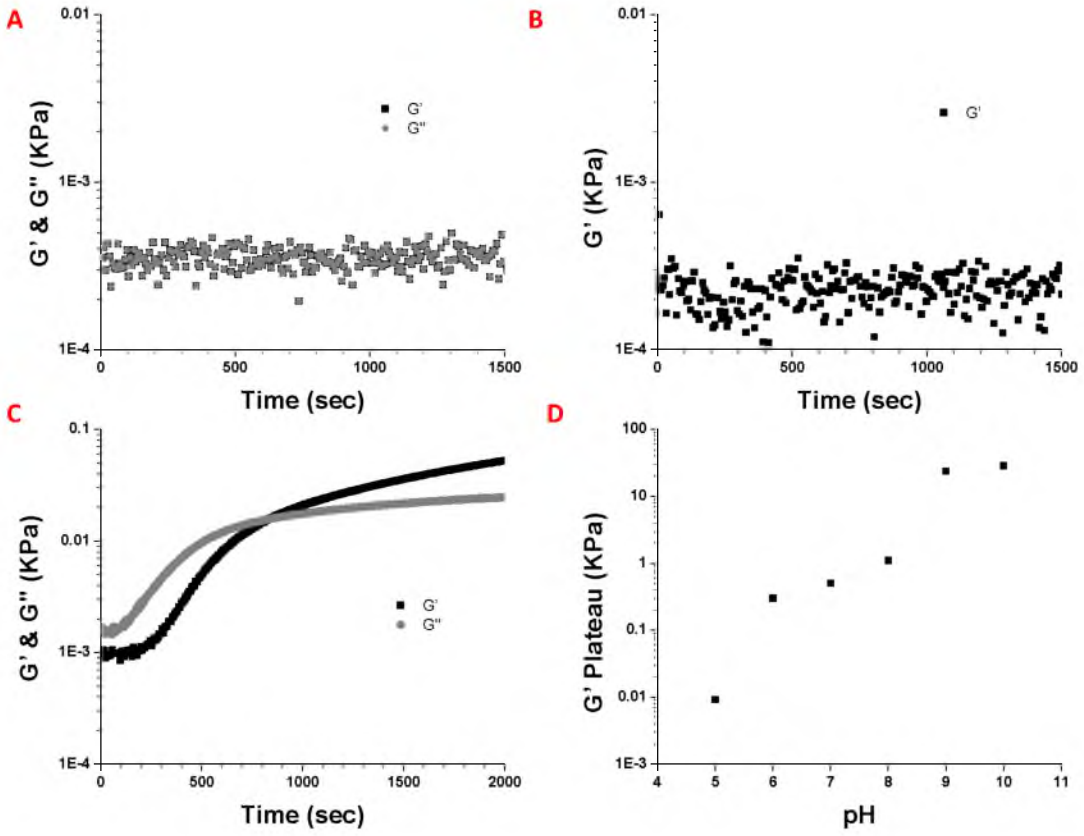

Figure 5.5 Sodium periodate mechanism: A) Elastic and viscous modulus of 70 MOEP-20% methacrylated polymer solution with 20 mM $NaIO_4$, at pH 9 37° C. B) Elastic modulus of nonmethacrylated polyamine at pH 9, 37° C. C) Elastic and viscous modulus of nonmethacrylated polyamine at pH 9, with 20 mM $NaIO_4$ 37° C. D) Elastic modulus plateau of 5% methacrylated polyamine at varied pH's, with 20 mM $NaIO_4$, at 37°C.

were made on the complex coacervates of 40 MOEP, varied methacrylation polymers with 5% methacrylation on the polyamine, with PEG-dA entrapped within the coacervate network (Figure 5.6). The bonding results showed increased bond strength over increasing PEG-dA concentration, and increasing methacrylation on the polyphosphate polymer. The maximum mean bond strength was measured for the 40 MOEP – 15% methacrylated polyphosphate polymer within a coacervate containing 15 wt% PEG-dA concentration, of 473 ± 82 KPa. Each value is a measure of four bonded substrates. Bond strength of 70 MOEP – 20% methacrylated polyphosphate coacervate with 5% methacrylation was also tested as shown in Figure 5.7. The bond strength also increased with increasing amounts of PEG-dA concentration, reaching a maximum of 437 ± 118 KPa.

5.3.3 Cytotoxicity

The direct contact cytotoxicity assay was used to measure the toxicity of the complex coacervate (Table 5.1). Mouse osteoblast cell line MC3T3-EI was used. The uncrosslinked coacervate made from 70 MOEP-20 % methacrylated polymer with 5% methacryalted polyamine was not toxic. All of the polymer syntheses were purified of toxins, and this result confirms it. The crosslinked coacervate was tested with 10mM $NaIO_4$ concentration and was also not toxic. At high concentration, above 50 mM, sodium periodate is toxic.

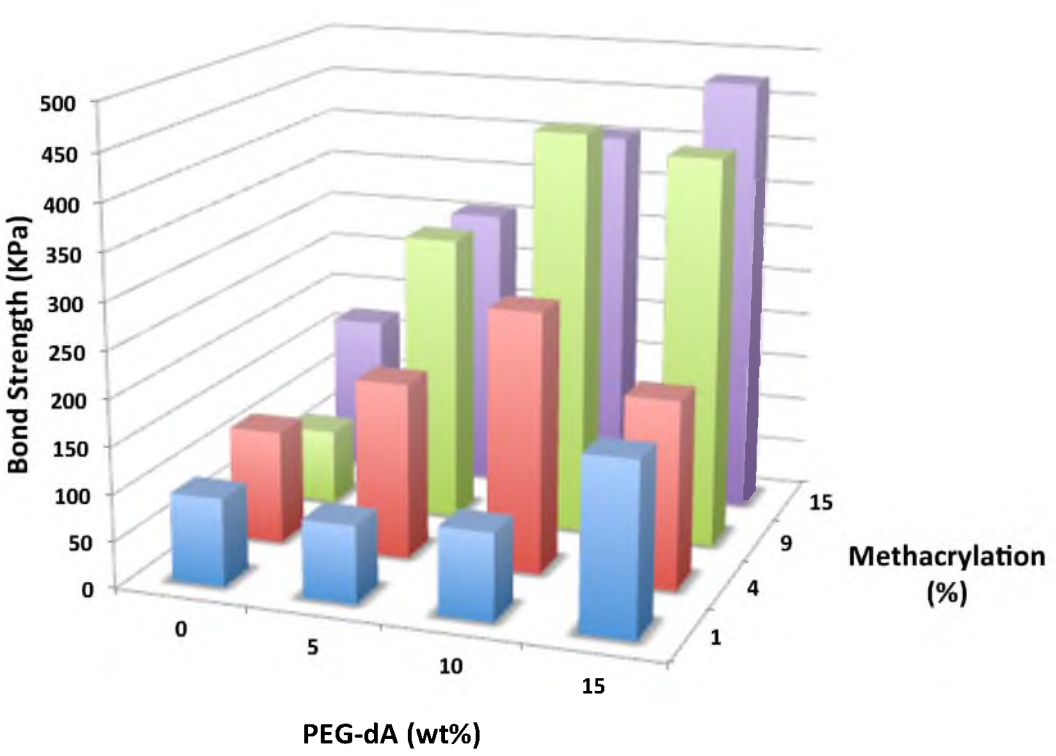

Figure 5.6 Lap shear on aluminum substrates testing 40 MOEP coacervates with varied PEG-dA (575) concentration and varied methacrylation on polyphosphate polymer, bonded for 2 hours underwater at 37°C using 20 mM $NaIO_4$.

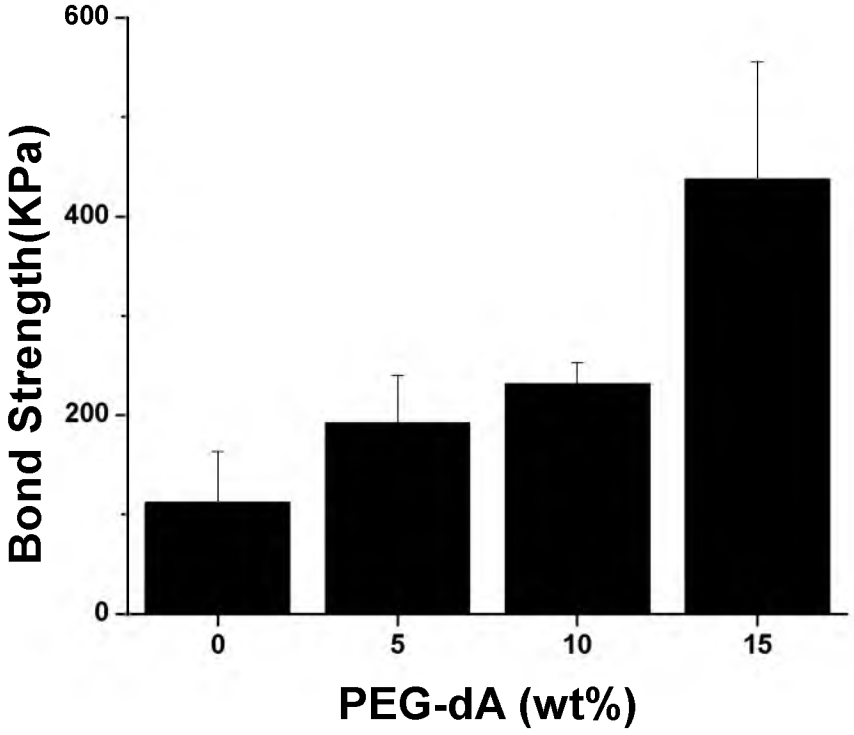

Figure 5.7 Lap shear on aluminum substrates testing 70 MOEP, 20% methacrylation polyhphosphate coacervate with varied PEG-dA (575) concentration, bonded for 2 hours underwater at 37°C using 20 mM $NaIO_4$.

Table 5.1 Cytotoxicity by direct contact cell assay, using mouse osteoblast cell line, was measured on 70 MOEP-20 % methacrylated polymer with 5% methacryalted polyamine coacervate.

Samples	% cell Survival	Toxicity
70 MOEP-20% Methacrylation CC, uncrosslinked	81.1%	Not Toxic
70 MOEP-20% Methacrylation CC, 10 mM $NaIO_4$	84.3%	Not Toxic

5.3.4 Sterile Adhesive Complex Coacervate Packets used in Pig Animal Surgeries

Sterile adhesive packets were sent for pig animal studies that took place in University of Texas Houston, Fetal Center (Figure 5.8). Pregnant Pigs were used as the animal model to test the twin-to-twin transfusion syndrome adhesive patch, as tested in vitro in Chapter 3. A normal pig is pregnant for 114 days, consisting of 5 to 8 fetal sacs. At day 70, (midterm), the fetal surgery is performed. Where in each animal some sacs were left alone as controls, some were tested with a Human Amniotic membrane (hAM plug only), and some were tested with underwater coacervate adhesive in conjunction with hAM (UAC + hAM).

Each sac, if tested for the hAM plug or hAM plug + UAC, was punctured and the patch was pulled through to plug the punctured fetal pig membrane as shown in Chapter 3, Figure 3.2. Pig is a good model for this study because the pregnant animal has many sacs. After the surgery, the animal is sent back to recovery. The animal is euthanized after 21 days, and with histology study the fetal membrane specimens are examined.

Preliminary results of animal studies are showing positive results. The adhesive adheres well to the human aminiotic membrane (hAM) as well the defect site without any adverse effect to the fetus. It is a promising result, as well as a novel method to promote healing of human fetal defects after invasive fetal surgeries.

The stability of complex coacervate adhesives packets made for the pig animal study is tested over time for crosslinking kinetics as shown in Figure 5.9. The samples are made of coacervates of 70 MOEP-20% methacrylation on the polyphosphate polymer and 5% methacrylation on the polyamine polymer, 10 wt% PEG-dMA (Polyethylene

Figure 5.8 Sterile complex coacervate adhesive packets used in the animal studies. One syringe contains the coacervate adhesive and the second the chemical initiator. Upon use, the two solutions are mixed by connecting the two syringes with a mixing nozzle. The adhesive/initiator are mixed by pushing out the matter from one syringe to the other, 5–10 times, or 30 sec. The adhesive is then pushed into one syringe; the empty syringe is removed, with a cannula secured on the leur-lock adhesive syringe, and the adhesive is applied at the site within a minute.

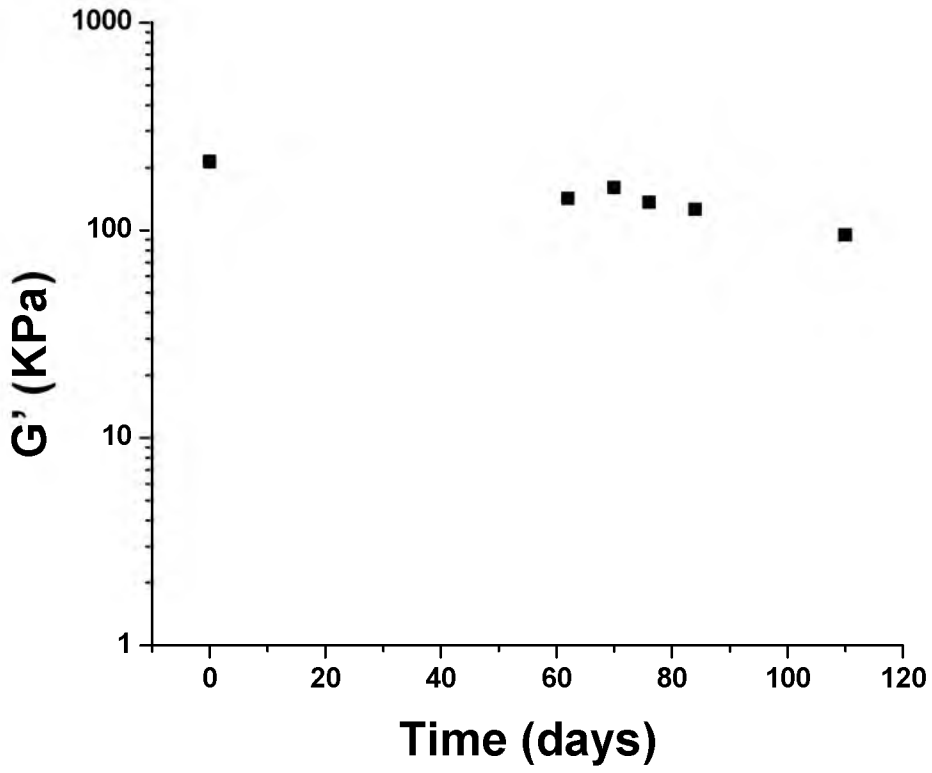

Figure 5.9 Stability study of complex coacervate adhesive sent for pig animal studies, made of 70 MOEP-20% methacrylation on the polyphosphate polymer and 5% methacrylation on the polyamine polymer, 10 wt% PEG-dMA within the coacervate, pH 7.2, with 35 mM $NaIO_4$ concentrations at 37°C. Showing plateau elastic modulus of samples that are chemically cured adhesive over a time period.

glycol dimethacrylate, MW 750) within the coacervate, pH 7.2, with 35 mM $NaIO_4$ concentrations at 37°C. PEG-dMA is a more stable monomer than the PEG-dA and was used for this animal study. The results show very stable coacervate packets. Even after 110 days there is not much change in the elastic modulus.

5.4 Conclusion

Complex coacervate adhesive, inspired by the sandcastle worm, is unique because of its use in aqueous environments. The adhesive's novelty lies in it being made in water, being applied under water, and adhering to wet surfaces. The synthetic adhesive properties were tuned to the design of the application. This adhesive was designed and developed for the TTTS, fetal membrane repair application. The adhesive adhered to pig fetal membrane tissue (with sufficient strength), cured in a controlled manner, is biocompatible, nontoxic, deliverable through an injectable system, and is stable for long term use. The methacrylated polymer complex coacervate was successfully chemically crosslinked, in curing time needed. The preliminary results of the animal studies show promising results.

5.5 References

1. http://www.tttsfoundation.org/help_during_pregnancy/how_often.php

2. M. Habli, F. Y. Lim, and T. Crombleholme, "Twin-to-twin Transfusion Syndrome: A Comprehensive Update," *Clin. Perinatol.*, **36** [2] 391–416 (2009).

3. E. Gratacos, J. Sanin-Blair, L. Lewi, N. Toran, G. Verbist, L. Cabero, and J. Deprest, "A Histological Study of Fetoscopic Membrane Defects to Document Membrane Healing," *Placenta*, **27** [4] 452–456 (2006).

4. G. Bilic, C. Brubaker, P. B. Messersmith, A. S. Mallik, T. M. Quinn, C.Haller, E. Done, L. Gucciardo, et al., "Injectable Candidate Sealants for Fetal Membrane Repair: Bonding and Toxicity in Vitro," *Am. J. Obstet. Gynecol.*, **202** [1] 85.e1–9

(2010).

5. R. A. Jensen, and D. E. Morse, "The Bioadhesive of *Phragmatopoma Californica* Tubes: A Silk-line Cement Containing L-DOPA," *J. Comp. Physiol. B*, **158**, 317–324 (1988).

6. J. H. Waite, R. A. Jensen, and D. E. Morse, "Cement Precursor Proteins of the Reef-building Polychaete Phragmatopoma Californica (Fewkes)," *Biochem.*, **31** [25] 5733–5738 (1992).

7. R. J. Stewart, J. C. Weaver, D. E. Morse, and J. H. Waite, "The Tube Cement of Phragmatopoma Californica: A Solid Foam," *J. Exp. Bio.*, **207**, 4727–4734 (2004).

8. H. Zhao, C. Sun, R. J. Stewart, and J. H. Waite, "Cement Proteins of the Tube-building Polychaete Phragmatopoma Californica," *J. Biol. Chem.*, **280**, 42938–42944 (2005).

9. H. Shao, K. N. Bachus, and R. J. Stewart, "A Water-borne Adhesive Modeled After the Sandcastle Glue of P. Californica," *Macromol. Biosci.*, **9** [5] 464–471 (2009).

10. H. Shao, and R. J. Stewart, "Biomimetic Underwater Adhesives With Environmentally Triggered Setting Mechanisms," *Adv. Mater.*, **22** [6] 729–733 (2010).

11. S. Kaur, G. M. Weerasekare, and R. J. Stewart, "Multiphase Adhesive Coacervates Inspired by the Sandcastle Worm," *ACS Appl. Mater. Inter.*, **3** [4] 941–944 (2011).

12. H. G. Bungenberg de Jong, "Crystallization-coacervation-flocculation," *Colloid Science*, **2**, 232–258 (1949).

13. L. K. Mann, R. Papanna, K. J. Moise, R. H. Byrd, E. J. Popek, S. Kaur, S. C. G. Tseng, and R. J. Stewart, "Fetal Membrane Patch and Biomimetic Adhesive Coacervates as a Sealant for Fetoscopic Defects," *Acta Biomater.*, **8** [6] 2160–2165 (2012).

14. S. A. Madbourly, and J. U. Otaighe, "Rheokinetics of Thermal-induced Gelation of Waterborne Polyurethane Dispersions," *Macromolecules*, **38** [24] 10178–10184 (2005).

CHAPTER 6

PHOTOPOLYMERIZED METHACRYLATED POLYMER COMPLEX COACERVATE ADHESIVE PATCH FOR SPINA BIFIDA

6.1 Introduction

There are 1,500 children born with Spina Bifida each year in the United States [1]. Spina Bifida is a congenital birth defect with the neural tissue of the posterior spinal column of the fetus being exposed to the amniotic fluid. This condition is detected by ultrasound between 16 to 20 weeks of pregnancy. The exposed neural tissue, in the amniotic cavity, leads to many neurological impairments at birth like paraplegia, sphincter incontinence, cranial nerve disturbances, hydrocephalus, respiratory problems, and death in some cases [2–3]. The severity of Spina Bifida varies from case to case, with myelomeningocele (MMC) being the most severe, where the spinal column protrudes through an opening and a sac is formed enclosing the spinal material. Current treatment includes MMC repair surgery closing the neural defect. Animal studies have shown promising results if the repair of neural tube closure takes place in the life of a fetus [4–5]. MMC repair by fetal surgery poses major challenges and trauma for the patient [6]. In fetal surgery the repair takes place by closure of the fetal neural tube defects in a multilayer fashion by closing the final skin layers with sutures. This multilayering closure is lengthy in time and technically difficult to do [7]. To get maximum closure at times it

is necessary to add a secondary sutured patch [7–8]. Adding to the difficulty of the procedure, fetal membrane sac rupturing is another big risk. Animal studies are showing that instead of a major invasive fetal surgery, a minimally invasive fetal surgery covering the MMC defect with an adhesive patch until birth, followed by a more complex open surgery at birth, could be just as effective in better outcome of the life of the baby [9-10]. But the difficulty lies in the delivery of an adhesive patch under aqueous conditions in the amniotic sac to seal the spina bifida defect. Out of the bioadhesives available commercially, eventually all will fail under aqueous conditions over time.

Marine organisms living in watery interfaces have solved the challenges that we face in developing bioadhesives in aqueous conditions [11]. The sandcastle worm, also known as P-*californica* living along the coastline of California has a unique way of constructing composite mineralized shells that it lives in by binding sandgrains and shells from aquatic environments by small amounts of underwater adhesive that it secretes. Despite all the turbulent forces in the ocean, the shell that it lives in does not fall apart. We have copied the chemistries and mechanism of this worm glue to make a synthetic analog bioadhesive [11–14]. Chemistries that we have mimicked in the synthetic version are the oppositely charged proteins, phosphates and amines, and divalent cations that form an adhesive by the method of complex coacervation. Coacervation is defined as phase separation of solution mixture into one rich and one poor phase of particular components. Bungenberg de Jong in 1929 [15] named complex coacervates as phase separation of two oppositely charged polyelectrolytes, separating into a dense coacervate and dilute supernatant [16]. The oppositely charged water-soluble polymers, polyphosphate and polyamine, form the synthetic adhesive, by coacervation.

Our current research is focused on developing a synthetic underwater adhesive targeted for medical applications, in particular soft tissue adhesion. These biomimetic adhesives are advantageous because they can build on the natural phenomena and yet have highly tunable physical and mechanical properties [17]. With an application in mind the biomimetic can be tailored to the needs of a commercial product. In the past we have targeted high strength injectable multiphase adhesive coacervate for biomedical applications and attained our goals of a high strength deliverable adhesive through a fine cannula [14]. In this chapter, our focus is to develop an adhesive for Spina Bifida. An ideal solution would be a fast and simple adhesive patch that can minimize the complication and time of this fetal procedure [18]. We want to make an adhesive patch that we can deliver and apply under amniotic fluid, by a minimally invasive fetal surgery. Photopolymerizing the complex coacervate adhesive patch with sufficient strength would solve the fast curing problem under water. The fetoscope already has a light source attached to it to view inside the dark amniotic sac, which can be used to insert the laser to photocure the adhesive. The advantage of photopolymerization is that it is fast, simple, controllable, and well established [19–21]. In the case of Spina Bifida, photopolymerization is a great technique for fast underwater curing, with minimally invasive procedure. In this study nontoxic water-soluble photoinitiators Eosin-Y with low concentrations of triethanolamine (TEA) were used [22]. The crosslinking kinetics and tailoring of the elastic modulus were monitored on the rheometer. The adhesion properties of the photocrosslinked adhesive were measured on a double lap shear test, on commercially available Strattice (Life Cell Corp.) and semitransparent skin graft material Dermafill (AMD-Ritmed), used as a patch. The cytotoxicity was evaluated. Sterile

adhesive packages were created for sheep animal surgeries. Current sheep studies are using the sterile adhesive packets designed for the Spina Bifida adhesive patch.

6.2 Materials and Methods

6.2.1 Materials

All reagents were used without further purification unless noted otherwise. PEG-dA (Polyethylene glycol diacrylate, 540 Da) and basic aluminum oxide were purchased from sigma-aldrich. Eosin-Y was purchased from Acros Organics. Triethanolamine (TEA, ≥98.0%) was purchased from Alfa Aesar.

6.2.2 Purification of PEG Monomers

The inhibitor in PEG-dA monomer had to be removed. The liquid monomer was passed through an activated basic aluminum oxide column to remove the inhibitor, hydroquinone monomethyl ether (MEHQ).

6.2.3 Complex Coacervate Adhesive Formation

Methacrylated Poly(MOEP-co-MAA) (as described in Chapter 4) and methacrylated Poly(acrylamide-co-aminopropyl methacrylamide) (as described in Chapter 4), were dissolved separately, in aqueous 150mM NaCl solution, at a concentration of 50 mg/mL. The copolymer solutions were adjusted to the correct pH of 7.2±0.2, with NaOH. The poly(acrylamide-co-aminopropyl methacrylamide) solution was added dropwise, to the poly(MOEP-co-MAA) solution, under vortex. The molar ratio of amine sidechains to phosphate sidechains (A/P) was fixed. For 40 MOEP polymer coacervate, an A/P ratio of 1 was used and for 70 MOEP polymer coacervate, an A/P ratio of 0.65 was used. In less than a minute, turbid coacervate settled out of solution.

The coacervate was allowed to phase separate from the supernatant for 24 hrs before being used for further analysis. The multiphase complex coacervate incorporating PEG-dA was formed the same way with an additional step of dissolving the desired concentration (0–15 wt%) of PEG-dA into dissolved methacrylated Poly(MOEP-co-MAA) polymer, taking into account a fixed volume in the end.

6.2.4 Dynamic Rheology

Gelation kinetics of the coacervates were conducted on a stress-controlled Rheometer (TA instrument, AR 2000 ex) using a 20 mm 4° cone geometry, gap 114 μm, at 25°C with 150 μL coacervate samples. Crosslinking of the coacervates was measured using the Oscillatory time sweep method on the Rheometer. The change in elastic (G') and viscous (G'') moduli over time was measured at a constant frequency of 1 Hz and constant strain of 1%. The coacervates were crosslinked through vinyl groups on both polymers. The coacervates were photocrosslinked using 69 μg/ml eosin-Y, and 40 mM TEA photoinitiators. The photocuring accessories were also purchased from the TA instruments. The 10 μl stock solution of photoinitators was mixed into 200 μl coacervate. The mixed coacervate was loaded onto the rheometer, and the method initiated. The samples were irradiated from below through a quartz plate for 10 s (320–500 nm, 750 mW cm^{-2}) using a liquid-filled light guide from Hg light source (Exfos S1000).

6.2.5 Mechanical Testing

The adhesion properties of complex coacervates were tested using a lap shear test on a material testing system (Instron), cured by photopolymerization. Commerically available porcine tissue Strattice (Life Cell Corp.) and a semitransparent skin graft

Dermafill (AMD-Ritmed) were used as substrates. The strattice and dermafill were cut into 2 cm x 1 cm strips, where the strattice was soaked in 150 mM NaCl salt solution and the dermafill left dry. The prepared coacervates were mixed with Eosin-Y and TEA. Two pieces of strattice were put next to each other, so the combined length is 4 cm. To each strip, 20 μl of coacervate was applied to 1 cm of each strip right next to each other, and a dry dermafill sample was placed on the two strips with the final overlay area holding the strips together be 2 cm x 1 cm. A dermafill was pressed down with a gloved finger to even out the adhesive before photocuring. The adhesive was allowed to soak into the dermafill for 1 min, while still keeping the strattice soaked within a tissue of 150 mM NaCl to prevent dehydration of the tissue. The overlapped area was photocured by irradiating each cm^2 from 5 mm above the sample using a liquid-filled light guide from Hg light source for 20 s (320–500 nm, 750 mW cm^{-2}). The photocrosslinked strattice-dermafill-strattice samples were then put into a moisture chamber to prevent dehydration for 20 min after curing. The samples were tested on the Instron, 100 N load cell, crosshead speed 10 mm min^{-1}. The substrates failed at one of the two strattice-dermafill overlaps, and that failed load was taken into account along with the overlap area to calculate the shear strength. For each condition, four specimen/measurements were made and tested.

6.2.6 Swelling Measurements

Photopolymerized complex coacervate gels were tested for swelling in 150 mM NaCl. Varied PEG-dA concentration coacervates were prepared and mixed in with the photoinitator (Eosin-Y and TEA). Each sample was photocured, with 750 mW cm^{-2} irradiance, 20 s, in a 7.72 mm disk shaped molds. After photocuring, the samples were

allowed to fully set for 20 min in a moisture chamber to prevent dehydration of the gels. Once solidified, the gels were removed from the mold and immersed in 150 mM NaCl solution in a closed chamber. The swelling dimension measurements were made from the images taken from time zero to various time points over a period of 1 month. Time zero point was measured after immersing the gel in solution after 30 s. Varied PEG-dA concentration gels were measured for two different temperatures (RT, and 37°C) and various time points (0, 4 h, 12 h, 24 h, 2 d, 3 d, 7 d, 14 d, 21 d, 28 d). An average of three measurements were taken at each set of data points.

6.2.7 Cytotoxicity[1]

Mouse osteoblasts (MC3T3-E1 subclone 4, ATCC CRL-2593, Manassas, VA, USA) were used as the cell line. The cells were maintained in essential medium supplemented with 10% fetal bovine serum, 100 U/ml penicillin, and 100 μg/ml streptomycine in a humidified 5% CO_2 and 95% air balanced incubator at 37°C. The medium was changed every other day. The direct contact cell culture test was used to evaluate cytotoxicity of the complex coacervate. To 32 μl, adhesive uncrosslinked or crosslinked, and 256 μl medium was added into a culture well plate and incubated at 37°C for 24 hours. In another plate MC3T3-E1 osteoblast cells were plated, with density of 100, 000 cells/well in the growth medium, incubated at 37°C for 48 hours. After 48 hours the medium from the MC3T3-E1 cells was removed, and from the adhesive plate the medium was added into the cell plate. After 48 hours the cell number of MC3T3 on the adhesive was determined using the MTT assay. MTT was dissolved in sterile PBS (5 mg/ml). 100 μl of the MTT stock solution was added to each well and incubated at 37°C

[1]Hui Shao carried out the cytotoxicity assay.

for 4 hours. After incubation, 1000 μl of the SDS-HCl solution (0.1 g/ml in 0.01 M HCl) was added to each well and mixed thoroughly using pipette to extract the formazan crystals. The plate was then incubated at 37°C for another 4 hours in a humidified chamber. After incubation, the extract of each sample was transferred to 96-well plate, and the absorbance intensities were measured at 570 nm using a microplate reader.

6.2.8 Sterilization of Coacervates

Sterile coacervate adhesive packets were prepared for the animal studies. In a sterile hood, all aqueous polymeric solutions were filtered through a 0.22 μm sterile filter. The sterile poly(acrylamide-co-aminopropyl methacrylamide) solution was added dropwise to the sterile poly(MOEP-co-MAA) solution under vortex. The coacervates were ripened for 24 hours. The adhesives were packed in 1 mL syringes with a tight seal cap (Qosina, Inc), sterilized by ethylene oxide sterilization (40°C). The loaded sterile syringe was then put into a sterile 50 mL centrifuge tube to be kept in a sterile packet till surgery. The PEG-dA, TEA, and Eosin-Y stock solutions were filtered through the a 0.22 μm filter to make it sterile. The photoinitators and PEG-dA were loaded into the second syringe the same way.

6.2.9 Complex Coacervate Adhesive Packets Used in Animal Studies

The adhesive and the initiator were packaged separately in two different leur-lock sterile syringes. At the animal study surgery room, a sterile mixing nozzle was connected to the two syringes by pushing all of the material of one syringe into the other, and vice versa, 5–10 times mixed in the initiator with the adhesive. Once mixed, all of the adhesive/initiators were pushed into one syringe, the empty syringe was removed, the

mixing nozzle was removed, and the cannula was attached to the leur-lock syringe adhesive and applied to the test site. The adhesive was applied within a few minutes of mixing and was photocured using a laser (Iridex, green laser 532 nm).

6.3 Results and Discussion

6.3.1 Oscillatory Rheology

Complex coaceravates of varied polyphosphates and polyamines (as shown in Chapter 5, Figure 5.1) were photopolymerized on the rheometer. In photopolymerization, the photoinitiators were dissociated with the use of light into free radicals, which react with functionalized macromers, with double or triple bonds, to propagate radical chain polymerization [23]. In this study we used photoinitiators outside the UV range, in the visible light range, to maintain the integrity of the fetal tissue. Eosin-Y (absorbance peak of 510 nm) and TEA were used as the photoinitiators to photocure the complex coacervate adhesive. Visible light source connected to the rheometer using a light guide was used to cure the glue for all rheology measurements. The crosslinking kinetics of the complex coacervates were evaluated on the rheometer by first optimizing the photoinitiators. Eosin-Y, commonly used water-soluble nontoxic photoinitiator, 69 μg/ml [24] were used throughout this study. The TEA concentration was optimized by the oscillatory rheology, time sweep, method as shown in Figure 6.1. Complex coacervates made of 40 MOEP – 4% methacrylation on the polyphosphate and 5% methacrylation on the polyamine polymer with 5 wt% PEG-dA within the coacervate, at pH 7.2 were crosslinked with fixed Eosin-Y and varied amount of TEA. Crosslinking took place in 10 seconds, with maximum modulus reaching 106 KPa at 40 mM TEA concentration. As TEA was mixed into the coacervate, the pH of the coacervate changed from initial pH of

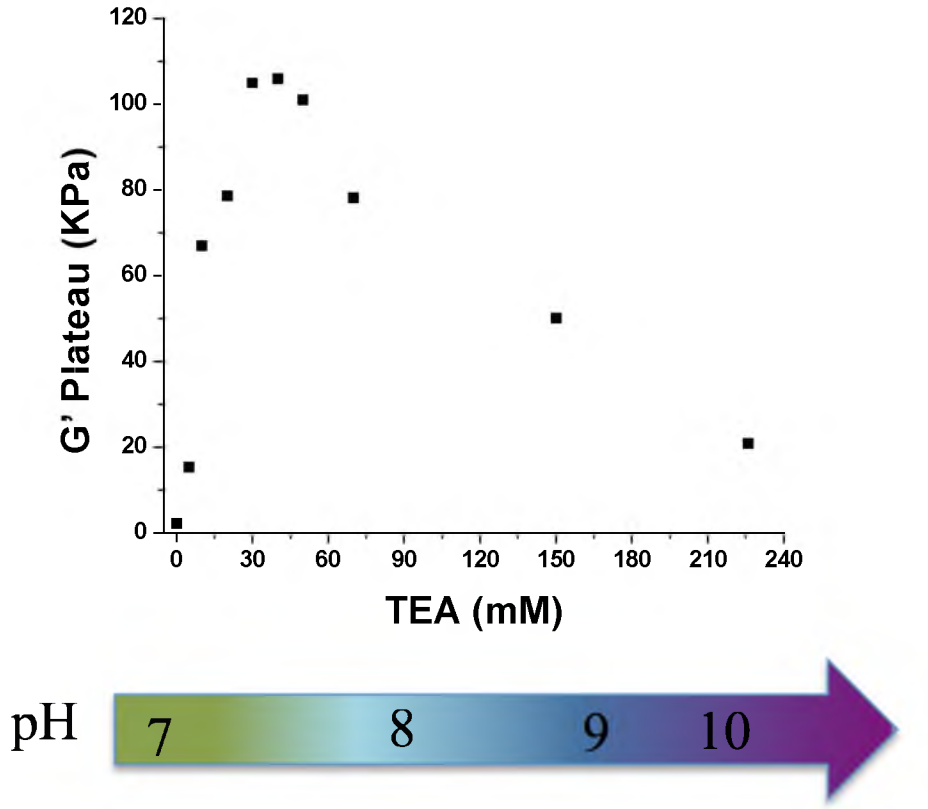

Figure 6.1 Optimizing TEA concentration vs. Elastic modulus plateau: photpolymerized complex coacervate made of 40 MOEP – 4% methacrylation on the polyphosphate polymer and 5% methacrylation on the polyamine polymer, 5 wt% PEG-dA, pH 7.2, photocrosslinked with 69µg/mL Eosin-Y, and varied TEA, at 750 mW/cm^2 irradiance for 10 sec. With an increasing amount of TEA added to the coacervate, the pH of the coacervate changed.

7.2 to an increased amount as shown in Figure 6.1. The increased pH effect of the coacervate would disrupt the coacervate phase and not be good. The maximum TEA concentration of 40 mM, however, did not change the pH of the coacervate phase. The effect of the second phase, PEG-dA, on the coacervate was also analyzed in rheology (Figure 6.2). The 40 MOEP-1% methacrylation polymer coacervate was evaluated for increasing PEG-dA concentration after photocrosslinking. As the PEG-dA concentration (wt%) increased, the plateau elastic modulus also increased tremendously for even 1% methacrylated polyphosphate within the coacervate. Within 10 seconds, we get a stiff coacervate network with increasing PEG-dA. The effect of methacrylation on modulus was difficult to measure for higher methacrylated polymers due to delamination of the samples and slippage from the geometry.

6.3.2 Mechanical Testing

The adhesion properties of the complex coacervate adhesive were tested via a lap shear test on the Instron. Commercially available soft tissue material Strattice, decellularized porcine dermis tissue, was used. Strattice is a uniform material that gave us consistent comparable bond strength data. To patch the adhesive for a photopolymerized adhesive patch Dermafil, translucent bacterial cellulose wound dressing material was used. The transparent dermafil allowed penetration of light through the patch for photopolymerization to occur. The strattice-dermafil substrates were bonded in a double lap shear method as shown in the drawing in Figure 6.3A (left). The adherends failed from one of the two overlaps, and the load at failure and the area at failure was taken into account to get a bond strength value. The tissue substrates stretched slightly before failing, as shown in Figure 6.3A (right), showing sample under tension. The lap shear

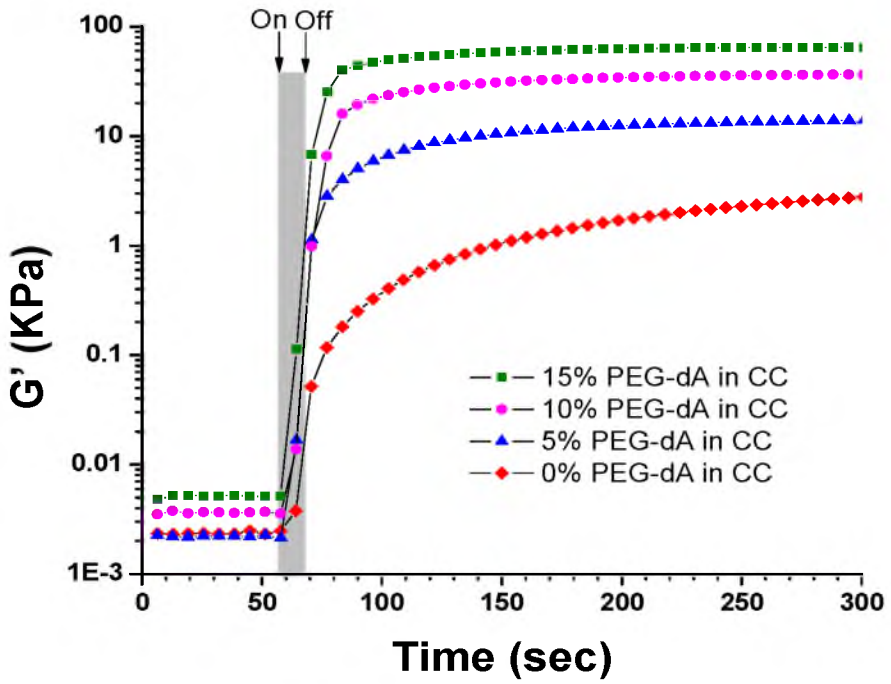

Figure 6.2 Elastic modulus of complex coacervate made of 40 MOEP – 1% methacrylation on the polyphosphate polymer and 5% methacrylation on the polyamine polymer, with varied PEG-dA (wt% concentrations), pH 7.2, photocrosslinked with 69μg/mL Eosin-Y, and 40 mM TEA, at 750 mW/cm^2 irradiance for 10 sec.

A)

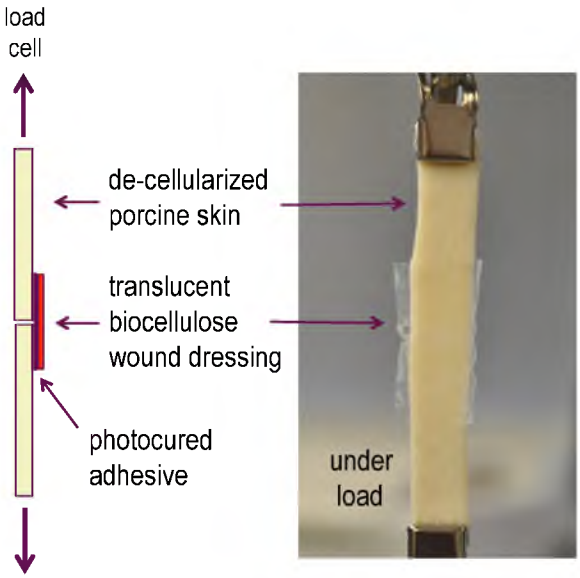

B)

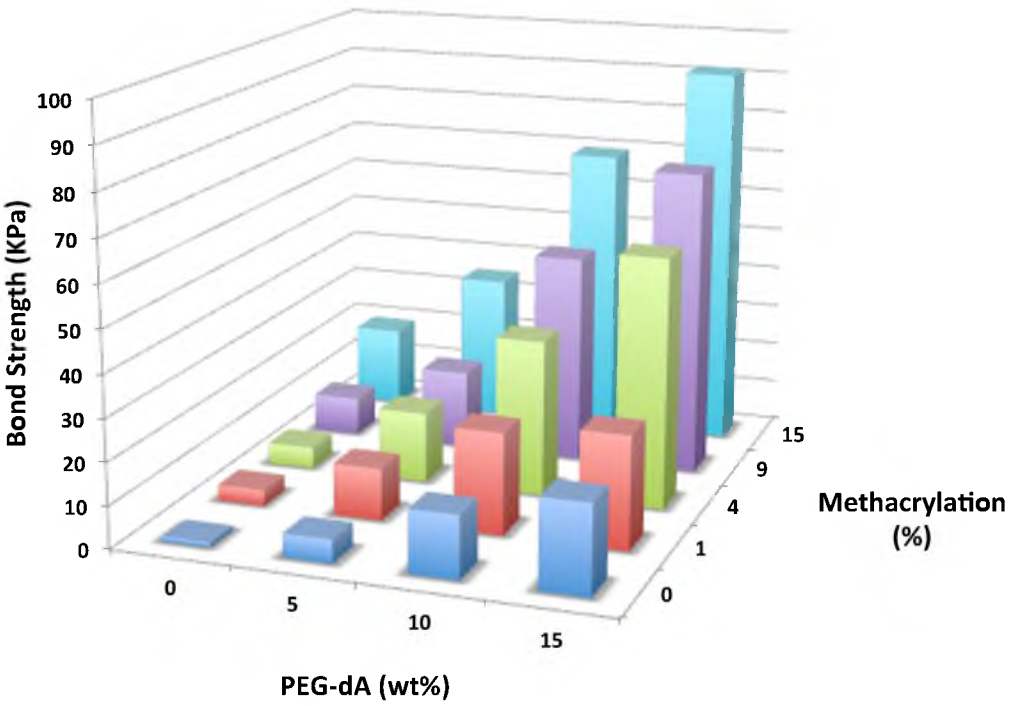

Figure 6.3 Double lap shear tissue adhesion test with stratus-dermafill-stratus: A) Drawing of the substrates under tension (left), with the image of the sample under loading (right). B) Bond strength data of 40 MOEP – varied methacrylation polymer and 5% methacrylated polyamine coacervates, with varied PEG-DA concentrations within the coacervate phase, pH 7.2. Photocrosslinked with 69μg/mL Eosin-Y, and 40 mM TEA, at 750 mW/cm^2 irradiance for 20 sec, under wet conditions, and tested after 20 min on the Instron.

bonding measurements with stratus-dermafill-stratus substrates is shown in Figure 6.3B. The bond strength data of 40 MOEP polymer with varied methacrylation and 5% methacrylation on the polyamine, with varied PEG-dA concentration coacervates at pH 7.2 were made. The samples were photocrosslinked with 20 sec exposure per cm^2 at irradiance of 750 mW/cm^2. The bonding results show an increase in bond strength over increasing PEG-dA concentration and increasing methacrylation on the polyphosphates, within the coacervates. The maximum bond strength was reached for 40 MOEP-15% methacrylated polyphosphate polymer with 15 wt% PEG-dA at 92 ± 30 KPa. The bond strength increase with increasing PEG-dA concentrations could be a result of the second polymer network within the coacervate network (Figure 6.4). Where the mechanical properties of the double network are much stronger than each individual component.

6.3.3 Swelling of Complex Coacervate Gels

The swelling behavior of the crosslinked complex coacervate adhesive is essential to the analysis of our adhesives. Whenever something is injected into the body, we do not want the material to swell in an uncontrolled manner. In terms of adhesives you do not want the adhesive to swell or shrink in an uncontrolled manner and form a interface mismatch. The swelling behavior of the photocrosslinked complex coacervate disks was evaluated and immersed in 150 mM NaCl solutions at two different temperatures (RT and 37°C) as shown in Figure 6.5. The disks hardly swelled over a month period for both coacervate gels made with 0 wt% PEG-dA and 15 wt% PEG-dA within the coacervates. Disk dimension measurements were made for coacervate gels with varied PEG-dA concentrations at two different temperatures (RT and 37°C), as shown in Table 6.1. The swelling measurements show minimal change in disk dimensions over a period of a

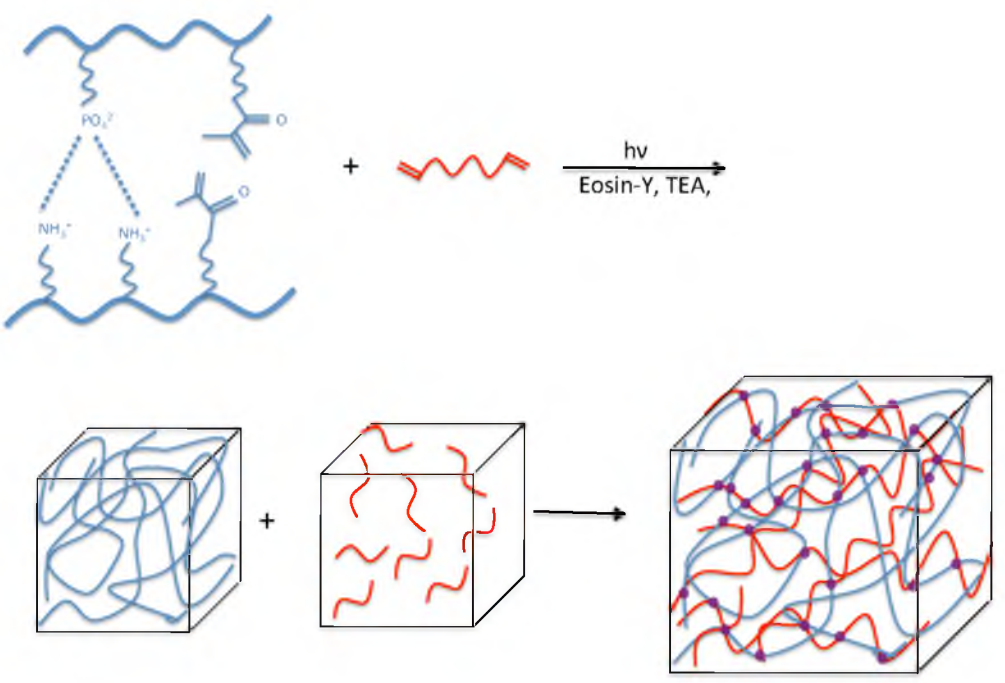

Figure 6.4 Multiphase complex coacervate PEG-dA network created by photocrosslinking.

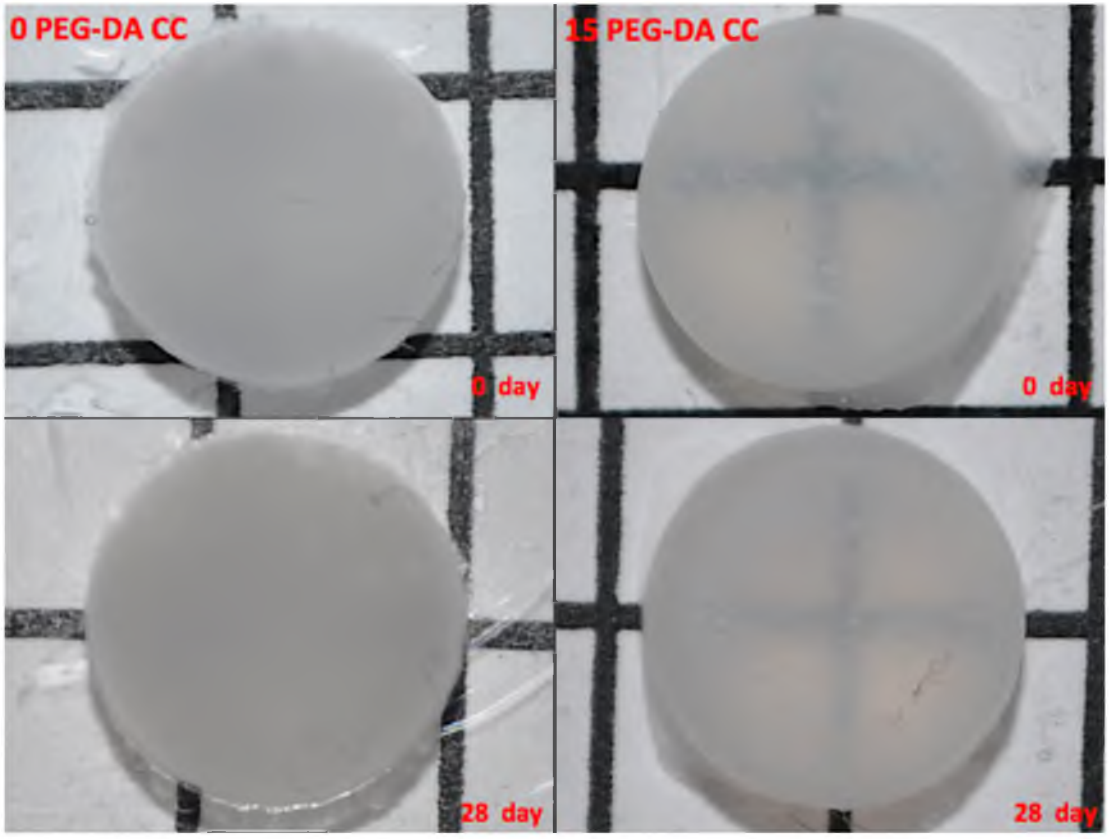

Figure 6.5 Images comparing the swelling behavior of photopolymerized disks at time zero to 28 days, made of 70 MOEP – 20% methacrylation polymer and 5% methacrylated polyamine coacervates, with 0 and 15 wt% PEG-DA concentrations within the coacervate phase, at pH 7.2, photocrosslinked with 69μg/mL Eosin-Y, and 40 mM TEA, at 750 mW/cm^2 irradiance for 20 sec, under wet conditions.

Table 6.1 Swelling measurements over time: disk diameters are compared for swelling for samples made of 70 MOEP – 20% methacrylation polymer and 5% methacrylated polyamine, with 0, 5, 10, and 15 wt% PEG-DA concentrations within the coacervate phase, at pH 7.2. Coacervates were photocrosslinked with 69μg/mL Eosin-Y, and 40 mM TEA, at 750 mW/cm^2 irradiance for 20 sec, under wet conditions.

Swelling Disk Dimensions (cm) at 25° C over time

Time (Days)	0 PEG-dA CC	5 PEG-dA CC	10 PEG-dA CC	15 PEG-dA CC
0	0.70±0.00	0.72±0.01	0.70±0.00	0.70±0.00
0.25	0.69±0.02	0.72±0.01	0.70±0.00	0.70±0.01
1	0.70±0.01	0.72±0.01	0.70±0.01	0.70±0.01
2	0.70±0.01	0.72±0.02	0.70±0.00	0.70±0.00
5	0.69±0.01	0.73±0.01	0.71±0.02	0.70±0.00
7	0.69±0.01	0.72±0.00	0.70±0.00	0.69±0.01
14	0.69±0.01	0.73±0.01	0.70±0.01	0.70±0.00
28	0.71±0.02	0.71±0.01	0.70±0.01	0.70±0.01

Swelling Disk Dimensions (cm) at 37° C over time

Time (Days)	0 PEG-dA CC	5 PEG-dA CC	10 PEG-dA CC	15 PEG-dA CC
0	0.71±0.01	0.73±0.02	0.70±0.01	0.70±0.00
0.25	0.71±0.02	0.73±0.02	0.70±0.01	0.70±0.01
1	0.70±0.01	0.73±0.01	0.70±0.00	0.70±0.00
2	0.70±0.01	0.73±0.01	0.70±0.00	0.70±0.00
5	0.71±0.01	0.72±0.01	0.70±0.01	0.70±0.00
7	0.69±0.00	0.72±0.01	0.70±0.00	0.70±0.01
14	0.71±0.02	0.73±0.01	0.71±0.01	0.70±0.00
28	0.70±0.01	0.73±0.02	0.70±0.00	0.70±0.00

month, showing dimensional stability of our crosslinked coacervates.

6.3.4 Cytotoxicity

The direct contact cytotoxicity assay was used to measure the toxicity of the photocrosslinked complex coacervate adhesive (Table 6.2). The methacrylated polymer coacervate photocrosslinked and had cell survival of 93.8%, showing minimal toxicity. Special care was used to make sure no toxins are picked up during the synthesis of all reagents and polymers to eliminate any contaminants.

6.3.5 Sterile Adhesive Complex Coacervate Packets used in Pig Animal Surgeries

Animal studies took place at the University of Texas Houston, Fetal Center. Pregnant sheep with twins were the chosen animal model to test the spina bifida adhesive patch. A normal sheep is pregnant for 147 days. To mimic the conditions of the spina bifida, a neural defect was created on the sheep fetuses on day 75. The sheep were closed up, and repair of that defect took place on day 95 with the adhesive patch. The sterile adhesive packets were used (Chapter 5) with the transparent dermafil patch to repair the neural defect. On day 135 the sheep delivered, and the animals were euthanized. The fetal membrane specimens were examined. Preliminary studies with sterile adhesive packets are being conducted at the fetal center, and are showing promising results. Making this adhesive patch work under amniotic fluid through a fetoscope is a major challenge. It will take many trials and errors to make this work.

Table 6.2 Cytotoxicity by direct contact cell assay, using mouse osteoblast cell line, was measured on 70 MOEP-20 % methacrylated polymer with 5% methacryalted polyamine coacervate.

Samples	% cell Survival	Toxicity
Medium only, 750 mW/cm^2 for 20 sec light exposure	91.8%	Not Toxic
Methacrylated Polymer CC, uncrosslinked	83.3%	Not Toxic
Methacrylated Polymer CC, Photocrosslinked	93.8%	Not Toxic

6.4 Conclusion

Biomimetics are unique because they are built on nature's concept to design a synthetic with tunable properties, for interest to a particular application. A photopolymerizable complex coacervate adhesive patch was developed for MMC repair. Photopolymerization is fast and easy and gives access to difficult spatial positions. Our complex coacervate adhesive is easily deliverable through a fine cannula and can be laser-cured in the amniotic sac. We are able to tune the elastic modulus by changing the PEG-dA concentration and % methacrylation within the coacervates. High bond strengthfor underwater adhesion was achieved by incorporating higher methacrylation and higher PEG-dA content. These coacervate adhesives did not swell, which is advantageous to the injectable system. The adhesive is not toxic and is being used in sheep animal studies using sterile adhesive packets. The preliminary results show promising results in adhering the adhesive patch to fetal tissue.

6.5 References

1. http://www.cdc.gov/ncbddd/spinabifida/data.html

2. R. M. Bowman, D. G. McLone, J. A. Gran, T. Tomita, and J. A. Ito, "Spina Bifida Outcome: A 25 year Prospective," *Pediatr. Neurosur.*, **34** [3] 114–120 (2001).

3. D. D. Cochrane, R. Adderley, C. P. White, M. Norman, and P. Steinbok, "Apnea in Patients With Myelomeningocele," *Pediatr. Neurosurg.*, **16** [4–5] 232–239 (1990).

4. S. Bouchard, M. G. Davey, N. E. Rintoul, D. S. Walsh, L. B. Rorke, and N. S. Adzick, "Correction of Hindbrain Herniation and Anatomy of the Vermis After in Utero Repair of Myelomeingocele in Sheep," *J. Pediatr. Surg.*, **38** [3] 451–458 (2003).

5. M. Michejda, "Intrauterine Treatment of Spina Bifida: Primate Mode," *Z. Kinderchir.*, **39** [04] 259–261 (1984).

6. S. Hirose, C. Meuli–Simmen, and M. Meuli, "Fetal Surgery for Myelomeningocele: Panacea or Peril?" *World J. Surg.*, **27** [1] 87–94 (2003).

7. J. P. Bruner, N. B. Tulipan, W. O. Richards, W. F. Walsh, F. H. Boehm, and E. K. Vrabcak, "In Utero Repair of Myelomeningocele: A Comparison of Endoscopy and Hysterotomy," *Fetal Diagn. Ther.*, **15** [2] 83–88 (2000).

8. D. I. Farmer, C. S. Von Koch, W. J. Peacock, M. Danielpour, N. Gupta, and H. Lee, "In Utero Repair of Myelomeningocele: Experimental Pathophysiology, Initial Clinical Experience, and Outcomes," *Arch. Surg.*, **138** [8] 872–878 (2003).

9. C. G. Fontecha, J. L. Peiro, M. Aguirre, F. Soldado, S. Anor, L. Fresno, and V. Martinez-Ibanez, "Inert Patch With Bioadhesive for Gentle Fetal Surgery of Myelomeningocele in a Sheep Model," Eu. *J. Obstet. Gynecol. Reprod. Biol.*, **146** [2] 174–179 (2009).

10. C. G. Fontecha, J. L. Peiro, J. J. Sevilla, M. Aguirre, F. Soldado, L. Fresno, C. Fonseca, A. Chacaltana, and V. Martinez, "Fetoscopic Coverage of Experimentally Myelomeningocele in Sheep Using a Patch With Surgical Sealant," *Eur. J. Obstet. Gynecol. Reprod. Biol.*, **156** [2] 171–176 (2011).

11. H. Shao, and R. J. Stewart, "Biomimetic Underwater Adhesives With Environmentally Triggered Setting Mechanisms," *Adv. Mater.*, **22** [6] 729–733 (2010).

12. H. Zhao, C. Sun, R. J. Stewart, and J. H. Waite, "Cement Proteins of the Tube-building Polychaete Phragmatopoma Californica," *J. Biol. Chem.*, **280**, 42938–42944 (2005).

13. H. Shao, K. N. Bachus, and R. J. Stewart, "A Water-borne Adhesive Modeled After the Sandcastle Glue of P. Californica," *Macromol. Biosci.*, **9** [5] 464–471 (2009).

14. S. Kaur, G. M. Weerasekare, and R. J. Stewart, "Multiphase Adhesive Coacervates Inspired by the Sandcastle Worm," *ACS Appl. Mater. Inter.*, **3** [4] 941–944 (2011).

15. H. J. Bungenberg de Jong, and H. R. Kruyt, "Coacervation (Partial Miscibility in Colloid Systems)," *Proc. K. Ned. Akad. Wet.*, **32**, 849–856 (1929).

16. H. G. Bungenberg de Jong, "Crystallization-coacervation-flocculation," *Coll. Sci.*, Elsevier Publishing Company, Amsterdam, **2,** 232–255 (1949).

17. J. N. Hunt, K. E. Feldman, N. A. Lynd, J. Deek, L. M. Campos, J. M. Spruell, B. M. Hernandez, E. J. Kramer, and C. J. Hawker, "Tunable, High Modulus

Hydrogels Driven by Ionic Coacervation," *Adv. Mater.*, **23** [20] 2327–2331 (2011).

18. L. K. Mann, R. Papanna, K. J. Moise, R. H. Byrd, E. J. Popek, S. Kaur, S. C. G. Tseng, and R. J. Stewart, "Fetal Membrane Patch and Biomimetic Adhesive Coacervates as a Sealant for Fetoscopic Defects," *Acta Biomater.*, **8** [6] 2160–2165 (2012).

19. K. T. Nguyen, and J. L. West, "Photopolymerizable Hydrogels for Tissue Engineering Applications," *Biomaterials*, **23** [22] 4307–4314 (2002).

20. W. E. Cloete, and W. W. Focke, "Fast Underwater Bonding to Polycarbonate Using Photoinitiated Cyanoacrylate," *J. Adhes. Adhes.*, **30** [4] 208–213 (2010).

21. H. Li, R. Niu, J. Yang, J. Nie, and D. Yang, "Photocrosslinkable Tissue Adhesive Based on Dextran," *Carbohydrate Polymers*, **86** [4] 1578–1585 (2011).

22. H. J. Avens, and C. N. Bowman, "Mechanism of Cyclic Dye Regeneration During Eosin-sensitized Photoinitiation in the Presence of Polymerization Inhibitors," *J. Polym. Sci. A. Polym. Chem.*, **47** [22] 6083–6094 (2009).

23. C. S. Bahney, T. J. Lujan, C. W. Hsu, M. Bottlang, J. L. West, and B. Johnstone, "Visible Light Photoinitiation of Mesenchymal Stem Cell-laden Bioresponsive Hydrogels," *Eur. Cells Mater.*, **22**, 43–55 (2011).

24. A. T. Hillel, S. Unterman, Z. Nahas, B. Reid, J. M. Coburn JM, J. Axelman, J. J. Chae, et al., "Photoactivated Composite Biomaterial for Soft Tissue Restoration in Rodents and in Humans," *Sci. Transl. Med.*, **3** [93] 67–78 (2011).

CHAPTER 7

CONCLUSION

An adhesive for sealing fetal defects, *in utero*, was developed by the method of complex coacervation. Soft tissue adhesives, and adhesives in general, are limited and pose a major challenge under wet environments. A water-borne synthetic complex coacervate adhesive, inspired by the Sandcastle worm, was developed by mimicking the basic protein chemistries of the worm for sealing fetal defects in aqueous conditions.

The synthetic analog of the sandcastle worm adhesive consisted of oppositely charged phosphate and amine copolyelectrolytes that when mixed under the right conditions formed a complex coacervate adhesive in aqueous solution at the biological pH. The liquid-liquid phase separation resulted in a dense (coacervate) and a dilute (supernatant) phase. The liquid coacervate phase can be applied underwater to various surfaces, where it stays in place, does not disperse, and is water-immiscible. The viscosity of the coacervate can be tailored to the desired application by adjusting the A/P ratio.

The complex coacervate adhesive is cured through the methacrylated sidechains on both copolyelectrolytes, polyphosphates and polyamines. The polyphosphate, Poly(MOEP-co-MAA) polymer, was methacrylated by glycidyl methacrylate (GMA) and grafted under aqueous conditions to keep the toxic solvents out. The polyamine, Poly (acrylamide-co-aminopropyl methacrylamide) was synthesized using aqueous RAFT

polymerization with methacrylated sidechain resulting from addition of MAA and EDC. The targeted methacrylation on each copolyelectrolyte resulted in tunable mechanical properties of the adhesive.

Multiphase complex coacervate adhesive resulted from the incorporation of a water-soluble PEG-dA monomer entrapped within the coacervation phase. Coacervate acted as a container for a water-soluble molecule, which could be accurately delivered to the site without losing its cargo. Upon simultaneous crosslinking of the coacervate network and PEG-dA network resulted in substantial improvement in the bond strength of the bioadhesive. The PEG-dA also made the coacervates more viscous. Despite the high viscosity, these complex coacervate adhesives could easily be ejected through a fine gauge cannula. This was due to the shear thinning behavior of this complex coacervates. This allowed highly viscous adhesives to be delivered at difficult to reach sites, making this adhesive very useful for minimally invasive procedures.

Fetal defect repair, due to iatrogenic preterm premature rupture of the fetal membrane, could greatly benefit from a good underwater adhesive to seal the ruptured membranes. An in vitro model using the complex coacervate adhesive in conjunction with a lyophilized fetal membrane patch showed an effective way to plug the iatrogenic fetal membrane defect under aqueous conditions. The toxicity of the adhesive in direct contact with human fetal membrane in organ culture setting showed no toxicity. These preliminary results were important to taking this adhesive to the next step, the animal studies.

A chemically crosslinked complex coacervate adhesive of the methacrylated polymers was developed for sealing fetal membrane rupture after a fetoscopic procedure

in twin-to-twin transfusion syndrome treatment. The coacervate was crosslinked using sodium (meta) periodate crosslinker, reaching gelation point within a minute after adding the crosslinker, and fully curing into a hard gel in less than 10 minutes. The elastic modulus of the adhesive was tailored to modulus of the fetal tissue by controlling the methacrylated groups within the coacervate. The adhesive had sufficient strength, and increased with increasing amounts of PEG-dA concentration and methacrylation within the coacervate. Direct contact cell culture of MC3T3-EI, in vitro, showed no toxicity of the methacrylated polymer complex coacervate. Sterile coacervate adhesive packets were developed to use in animal studies. Animal surgeries are showing promising results of the adhesive with the amniotic membrane patch to plug the fetal membranes after a fetoscopic defect. The adhesive adheres well to the plug patch as well as the pig fetal membranes. No toxicity in the animal after histological studies were seen.

A photocrosslinked complex coacervate adhesive patch was developed for sealing the neural spine defect in Spina Bifida. The adhesive patch is designed to cover the exposed neural tissue of the fetus under the amniotic sac through a minimally invasive fetoscope, where the adhesive is applied under amniotic fluid and photocured using a green laser diode. Photopolymerization of the complex coacervate crosslinking the adhesive through the vinyl bond of the methacrylation groups of polyelectrolytes is fast and easy and allows access of the adhesive through fine cannula to a difficult spatial position to be photocured in a controlled manner. Nontoxic visible light photoinitiators, Eosin-Y and TEA, were used. Elastic modulus of the coacervate was tuned by controlling the PEG-dA content within the coacervate. Bond strength on commercially available decellularized porcine dermis tissue (Strattice) and a translucent bacterial cellulose patch

(Dermafil) was measured on a double lap shear test. Increasing the PEG-dA content and methacrylation on the polymers within the coacervate achieved high bond strengths. The swelling measurements concluded dimensionally stable complex coacervate at biological conditions of pH, salt solution, and temperature. The photopolymerized coacervates were not toxic and were further taken to sheep animal studies. Sterile adhesive packets are being used in the animal studies. Preliminary results from the sheep studies are showing promising results.

The developed injectable complex coacervate adhesives adhere well to the fetal tissue, in utero. The complex coacervates used are very stable, up to months, when packaged in the sterile syringes. For the application of TTTS and Spina Bifida this is a huge milestone. Taking research from a concept based on the inspiration of the underwater adhesive of the sandcastle worm to a practical application in animal studies is a huge step forward. Currently there is no glue in the market that can seal fetal membrane tissue under aqueous condition with sufficient bond strength while maintaining the integrity of the fetal tissue.